SCRATCH AND WEAR BEHAVIORS OF POLYURETHANE ELASTOMERS

A Dissertation

by

SHUANG XIAO

Submitted to the Office of Graduate and Professional Studies of
Texas A&M University
in partial fulfillment of the requirements for the degree of

DOCTOR OF PHILOSOPHY

Chair of Committee,	Hung-Jue Sue
Committee Members,	Anastasia Muliana
	Bruce Tai
	Homero Castaneda
Head of Department,	Andreas A. Polycarpou

December 2018

Major Subject: Mechanical Engineering

ABSTRACT

Given the unique block copolymer structure of polyurethane (PU) elastomers, each segment of them can be modified independently to obtain a wide range of properties that meet the needs of various engineering applications. However, the susceptibility of PU elastomers to surface damages like scratch and wear significantly limits their usage in applications where surface structural integrity and aesthetic appearance are of great importance. In order to gain fundamental understanding of scratch and wear behaviors of PU elastomers, this research focuses on experimental study along with numerical analysis of scratch and wear-induced deformation in PU elastomers, leading to effective design of scratch and wear resistant PU systems.

Scratch process involves a single-pass sliding of a single-asperity across the polymer surface under the influence of an applied normal load. Wear process is more complicated, since it generally involves multi-passes and multi-asperities. Abrasive wear is one of the most common wear damages that polymers may experience during service. It is generated as the result of removal of material from polymer surface through penetration and sliding of sharp and hard asperities of the counterface, which is similar to the relatively well-establish scratch damage phenomenon.

The present research work starts with the investigation on scratch behavior of PU elastomers using a standardized scratch test, various materials characterization techniques and finite element method simulation to determine the key material properties

and surface characteristics that are related to scratch resistance of PU elastomers under two environmental conditions, i.e., dry and water-saturated.

Afterwards, abrasive wear behavior of PU elastomers is investigated using a custom built multi-axis tribometer in a pin-on-flat configuration to establish physical correlation between abrasive wear and scratch behaviors. It is found that the key material property that is responsible for scratch resistance can be extended to abrasive wear resistance of PU elastomers.

Ultimately, research effort is performed to explore the possibility of design of scratch and abrasive wear resistant PU elastomers by modifying their molecular weight, which has significant influence on the material properties of PU elastomers.

DEDICATION

To my parents

ACKNOWLEDGEMENTS

I would like to thank my committee chair, Dr. Sue, and my committee members, Dr. Muliana, Dr. Tai, and Dr. Castaneda, for their guidance and support throughout the course of this research. I would also like to acknowledge the generous support provided by Texas A&M Scratch Behavior of Polymers Consortium members in this research endeavor. Special thanks go to BASF Polyurethane Specialties (China) Co. Ltd. for providing the model polyurethane systems that made this work possible.

I would like to give my most sincere gratitude to Dr. Hung-Jue Sue, who has provided valuable guidance and served as a role model during my stay here at Texas A&M University.

Thank you to all the past and present members of the Polymer Technology Center at Texas A&M University for their help and guidance. Special thanks go to Mohammad Motaher Hossain, Peng Liu and Kevin Andrew Laux for their assistance and inspiration in this research. Thanks also to my friends and colleagues for making my time here a great experience.

Finally, I would like to sincerely thank my father, Chaoduo Xiao, my mother, Xuemei Sun, and my wife, Chuo Fang. Without your unconditional love and support, this would never have been possible.

CONTRIBUTORS AND FUNDING SOURCES

This work was supervised by a dissertation committee consisting of Professor Hung-Jue Sue, advisor and committee chair, and Professors Anastasia Muliana and Bruce Tai of the Department of Mechanical Engineering, and Professor Homero Castaneda of the Department of Materials Science & Engineering.

All work for the dissertation was completed independently by the student, and funded by Texas A&M Scratch Behavior of Polymers Consortium.

TABLE OF CONTENTS

Page

ABSTRACT ii

DEDICATION iv

ACKNOWLEDGEMENTS v

CONTRIBUTORS AND FUNDING SOURCES vi

TABLE OF CONTENTS vii

LIST OF FIGURES x

LIST OF TABLES xiv

CHAPTER I INTRODUCTION AND LITERATURE REVIEW 1

1.1 Overview of Polymer Scratch and Wear Research 1
1.2 Research Scope 7
1.3 Layout of the Dissertation 10

CHAPTER II SCRATCH BEHAVIOR OF MODEL POLYURETHANE ELASTOMERS 12

2.1 Introduction 12
2.2 Materials and Methods 14
2.2.1 Materials 14
2.2.2 Attenuated Total Reflectance-Fourier Transform Infrared Spectroscopy (ATR-FTIR) 16
2.2.3 Atomic Force Microscopy (AFM) 16
2.2.4 Coefficient Of Friction (COF) Measurement 17
2.2.5 Tensile True Stress-strain Curve Generation 17
2.2.6 Compressive True Stress-strain Curve Generation 18
2.2.7 Dynamic Mechanical Analysis (DMA) 19
2.2.8 Scratch Test 20
2.2.9 Post-scratch Analysis 21
2.3 Results 22
2.3.1 ATR-FTIR 22
2.3.2 AFM 25

Page

2.3.3 COF Measurement 28
2.3.4 Tensile True Stress-strain Behavior 29
2.3.5 Compressive True Stress-strain Behavior 33
2.3.6 Dynamic Mechanical Behavior 36
2.3.7 Scratch Behavior 39
2.4 Discussion 42
2.5 Conclusions 47

CHAPTER III MOISTURE EFFECT ON SCRATCH BEHAVIOR OF MODEL POLYURETHANE ELASTOMERS 49

3.1 Introduction 49
3.2 Materials and Methods 51
3.2.1 Materials 51
3.2.2 Environmental Conditioning 52
3.2.3 ATR-FTIR 53
3.2.4 Contact Angle Measurement 54
3.2.5 COF Measurement 54
3.2.6 Tensile True Stress-strain Curve Generation 55
3.2.7 Scratch Test 56
3.2.8 Post-scratch Analysis 57
3.3 Results and Discussion 58
3.3.1 Moisture Absorption 58
3.3.2 ATR-FTIR 60
3.3.3 Contact Angle Measurement 63
3.3.4 COF Measurement 66
3.3.5 Tensile True Stress-strain Behavior 67
3.3.6 Scratch Behavior 70
3.4 FEM Modeling 74
3.5 Conclusions 82

CHAPTER IV PHYSICAL CORRELATION BETWEEN ABRASIVE WEAR AND SCRATCH BEHAVIORS 84

4.1 Introduction 84
4.2 Materials and Methods 86
4.2.1 Materials 86
4.2.2 Wear Test 88
4.2.3 Wear Surface Imaging 92
4.2.4 Temperature Rise Measurement 92
4.2.5 Thermal Conductivity Measurement 93

Page

4.3 Results and Discussion....93
4.3.1 Sliding Wear Volume....93
4.3.2 Sliding Wear Surface....97
4.3.3 Sliding Wear Temperature Rise....99
4.3.4 Thermal and Damping Properties....101
4.3.5 Fretting Wear....104
4.4 Conclusions....111

CHAPTER V EFFECT OF MOLECULAR WEIGHT ON SCRATCH AND ABRASIVE WEAR BEHAVIORS OF THERMOPLASTIC POLYURETHANE ELASTOMERS....113

5.1 Introduction....113
5.2 Materials and Methods....116
5.2.1 Materials....116
5.2.2 AFM....118
5.2.3 Tensile True Stress-strain Curve Generation....119
5.2.4 COF Measurement....120
5.2.5 Scratch Test....120
5.2.6 Wear Test....121
5.3 Results and Discussion....123
5.3.1 AFM....123
5.3.2 Tensile True Stress-strain Behavior....126
5.3.3 COF Measurement....128
5.3.4 Scratch Behavior....129
5.3.5 Abrasive Wear Behavior....132
5.4 Conclusions....137

CHAPTER VI CONCLUSIONS AND CONSIDERATIONS FOR FUTURE RESEARCH....138

6.1 Summary and Conclusions....138
6.2 Considerations for Future Research....140
6.2.1 Improving Tensile Strength by Heat Treatment....141
6.2.2 Promoting Transfer Film Formation by the Incorporation of Nanoparticles 141
6.2.3 FEM Simulation of Tensile Tear Induced Cracking....142

REFERENCES....144

LIST OF FIGURES

Page

Figure 1. (a) Hard segment (diisocyanate): 4,4'-methylene diphenyl diisocyanate (MDI) and (b) chain extender (diol): 1,4-butane diol (BDO) of the model CPU systems. 15

Figure 2. Soft segments (polyols): (a) polytetramethylene ether glycol (PT), (b) polycaprolactone (PC), (c) ethylene oxide and propylene oxide based polyether polyol (PET) and (d) adipic anhydride based polyester polyol (PES) of the model CPU systems. 15

Figure 3. 1 mm diameter stainless steel conical scratch tip design. 21

Figure 4. ATR-FTIR spectra of the model CPU systems containing different types of soft segments. 23

Figure 5. ATR-FTIR spectra of the carbonyl C=O stretching vibration regions of the model CPU systems. 24

Figure 6. AFM phase images of the cross-sections of the model CPU systems. 27

Figure 7. Coefficient of friction of the model CPU systems. 29

Figure 8. Tensile true stress-strain curves of the model CPU systems. 30

Figure 9. Compressive true stress-strain curves of the model CPU systems. 35

Figure 10. Temperature dependence of storage modulus and tan δ of the model CPU systems. 37

Figure 11. Onset loads of scratch-induced deformation in the model CPU systems at (a) 1 mm/s and (b) 100 mm/s scratch speeds. 41

Figure 12. Optical images and height profiles of onset of cracking/material removal in the model CPU systems at 100 mm/s scratch speed. 42

Figure 13. Percent weight gain of the model CPU systems as a function of days immersed in deionized water. 59

Figure 14. Equilibrium moisture uptake of the model CPU systems. 59

Figure 15. Determination of water content in water-saturated (a) CPU-PT, (b) CPU-PC, (c) CPU-PET and (d) CPU-PES using TGA. 60

Page

Figure 16. ATR-FTIR spectra of (a) CPU-PT, (b) CPU-PC, (c) CPU-PET and (d) CPU-PES in dry, water-saturated and re-dried conditions. 61

Figure 17. Contact angle measurements of the model CPU systems in dry and water-saturated conditions. 64

Figure 18. Coefficient of friction of the model CPU systems in dry and water-saturated conditions. 67

Figure 19. Tensile true stress-strain curves of the model CPU systems in dry and water-saturated conditions. 69

Figure 20. Critical normal loads for onset of scratch damages in the dry and water-saturated model CPU systems at (a) 1 mm/s and (b) 100 mm/s scratch speeds. 71

Figure 21. (a) Bulging phenomenon of scratch groove in CPU-PT, CPU-PC and CPU-PES; (b) absence of scratch groove in CPU-PET. 73

Figure 22. Example optical image and height profile of onset of cracking/material removal in the model CPU systems (water-saturated CPU-PET tested at 100 mm/s scratch speed is shown). 74

Figure 23. Dimensions and boundary conditions of the FEM model. 76

Figure 24. von Mises stress distribution along the scratch path of (a) polypropylene and (b) the model CPU system (CPU-PES). 78

Figure 25. Evolution of von Mises stress beneath the scratch tip and maximum principal tensile stress behind the scratch tip as a function of applied normal load in (a) CPU-PET and (b) CPU-PES. 80

Figure 26. 3-D profile of hot rolled 304 stainless steel counterface scanned by violet laser scanning confocal microscope. 90

Figure 27. Schematics of linear reciprocating (a) sliding wear test and (b) fretting wear test. 91

Figure 28. Sliding wear volume of the model CPU systems (CPU-PET was measured at 100 m of traveling distance. The other systems were measured upon completion of 300 m of total travelling distance); the critical normal load for onset of tensile tear induced cracking/material removal of the model CPU systems during scratch. 94

Page

Figure 29. Abrasive wear mechanism during sliding wear test and scratch test. 96

Figure 30. VLSCM images of the sliding wear surfaces of the model CPU systems (wear volume of each model system is shown in the legend). 98

Figure 31. Sliding wear temperature rise of the model CPU systems versus travelling distance (COF and wear volume of each model system are shown in the legend). 100

Figure 32. Thermal conductivities of the model CPU systems. 102

Figure 33. Loss tangent of the model CPU systems around room temperature (COF of each model system is shown in the legend). 104

Figure 34. Fretting wear volume of the model CPU systems; the critical normal load for onset of tensile tear induced cracking/material removal of the model CPU systems during scratch. 105

Figure 35. Adhesive-fatigue wear mechanism during fretting wear test. 107

Figure 36. VLSCM images of the fretting wear surfaces of the model CPU systems (wear volume of each model system is shown in the legend). 108

Figure 37. Fretting wear temperature rise of the model CPU systems versus travelling distance (COF and wear volume of each model system are shown in the legend). 110

Figure 38. AFM modulus and adhesion maps of the model TPU systems. 125

Figure 39. Tensile true stress-strain curves of the model TPU systems. 126

Figure 40. Coefficient of friction of the model TPU systems. 129

Figure 41. Critical normal loads for onset of tensile tear-induced cracking/material removal of the model TPU systems. 130

Figure 42. VLSCM images of onset of tensile tear-induced cracking/material removal on the model TPU systems. 131

Figure 43. Abrasive wear volume of the model TPU systems. 134

Figure 44. VLSCM images of wear surfaces on the model TPU systems (wear volume of each model system is shown in the legend). 135

Page

Figure 45. (a) Abrasive wear temperature rise of the model TPU systems versus travelling distance; (b) average temperature rise in the plateau region (200 m, 250 m and 300 m).....136

LIST OF TABLES

Page

Table 1. Material information of the model CPU systems. 16

Table 2. Comparison between uniaxial tensile and compressive properties of the model CPU systems. 30

Table 3. Chemical component of the model CPU systems. 52

Table 4. Variation in uniaxial tensile properties of the model CPU systems before and after exposure to moisture. 69

Table 5. Material properties used in the FEM simulation of the scratch test. 77

Table 6. Chemical component, material properties and scratch resistance of the model CPU systems. 87

Table 7. Material information of the model TPU systems. 117

Table 8. Uniaxial tensile properties of the model TPU systems. 127

CHAPTER I

INTRODUCTION AND LITERATURE REVIEW

1.1 Overview of Polymer Scratch and Wear Research

Recent advances in polymer chemistry offer polymeric materials with enhanced physical and mechanical properties, and make them an attractive choice to replace metals and ceramics in addressing different engineering material challenges. Resistance of polymeric materials against surface damages like scratch and wear are gaining more and more attention due to the significant usage of polymeric materials in both functional and aesthetic applications.

Numerous research efforts have been pursued to establish a reliable quantitative methodology for evaluation of polymer scratch performance [1-6]. The ASTM D7027/ISO 19252 standardized scratch test [7, 8], which involves a linearly increasing normal load scratch test, has now been widely utilized to quantitatively evaluate scratch performance of polymers. By using a linearly increasing normal load test, the onset of different damage transitions, such as groove formation, cracking and plowing, along the scratch path can be determined in a straightforward fashion.

This methodology also makes it possible to relate the applied normal load or stress with the onset of these scratch-induced deformation and damage phenomena. Correlation between these damage phenomena and corresponding stresses is important for gaining fundamental knowledge of polymer scratch behavior. Recent fundamental

studies have been successfully performed on various kinds of polymeric systems by using this standardized methodology [9-16].

Hossain et al. [9] conducted an extensive study on two types of styrenic copolymers, acrylonitrile styrene acrylate (ASA) and acrylonitrile butadiene styrene (ABS), and found that the increase in coefficient of friction (COF) and damping behavior are the reasons for earlier onset of scratch damages. However, no correlation was established between the material properties and scratch resistance of the systems. In another study, Liang et al. [10] observed that for ASA with increasing rubber content, the scratch resistance of the systems generally decreases owing to the reduction of tensile and compressive yield stresses. Also, for ASA, by studying the effect of high temperature annealing, Liang et al. [11] found that the improvement in scratch performance is related to the changes in surface morphology of the systems. Browning et al. [12] carried out a study on styrene-acrylonitrile (SAN) random copolymers using the standardized test methodology and showed that the resistances to microcracking and plowing improve with increasing acrylonitrile (AN) content and molecular weight due to the increase in tensile strength.

Based on the ASTM D7027/ISO 19252 standard, numerical modeling by finite element method (FEM) analysis has also been conducted to establish quantitative correlation between material properties and the scratch behavior of polymers [16-21]. By using three-dimensional FEM, Jiang et al. [17] first found that during the scratch process, as the tip moves forward with increasing normal load, the material beneath and behind the scratch tip experiences a quick transformation of stress state from

compressive to tensile. Based on this understanding, Hossain et al. [18, 19] carried out a series of FEM parametric study and experimental work to determine the effect of asymmetric constitutive behavior on scratch-induced deformation of polymers. The results indicate that yield stress, strain at stress recovery and strain hardening slope under compression play an important role in the development of residual scratch depth and shoulder height during scratch process, while tensile strength correlates well with onset of cracking and material removal along the scratch path. Also, Hossain et al. [20] showed that since COF would affect the stress profile on and underneath the surface during scratching, the onset loads of scratch groove formation and cracking are significantly influenced by COF.

Although, significant efforts have been performed to understand and improve the scratch performances of different kinds of polymeric systems by using the ASTM D7027/ISO 19252 standardized scratch test with success, polymers also suffer from harsh environmental exposure during service, such as hot and humid conditions and UV radiation, which considerably complicate their scratch behavior. Moisture is one of the most common environmental factors that polymeric products are exposed to during service [13, 22-28].

Using the standardized scratch test, Browning et al. [13] carried out a study on a set of styrene-acrylonitrile (SAN) random co-polymers over a period of 10 days in a humid environment. They found that the scratch resistance of the SAN systems decreased in the first few days of moisture exposure, which was attributed to the plasticization effect of material by the absorbed water. However, the scratch resistance

showed some degrees of recovery upon further water exposure, which was claimed to be a result of water molecules clustering on the sample surface to serve as lubricant. Even though the mechanical properties of the SAN systems upon water exposure was not provided to demonstrate the plasticization effect, the lubrication effect of water clusters was evidenced by the scratch coefficient of friction (SCOF) of the samples that the surface friction only increased initially and then became lower with further exposure to moisture.

Thereafter, Moghbelli et al. [22] conducted a similar study on three different grades of polymethylmathacrylate (PMMA) with varying levels of polarity over a period of 28 days of exposure to a humid environment. Their results also indicated that the scratch resistance of all three systems became worse with initial exposure to moisture. However, after long-term exposure to moisture, only the two highly polar PMMA systems showed noticeable recovery of scratch resistance. They claimed that the surface polarity of polymers might play an important role in the diffusion and absorption of water within the polymer matrix. In the PMMA system with high polarity, the water molecules could aggregate on the surface and serve as lubricant. This statement was supported by the coefficient of friction (COF) measurement and contact angle measurement results of the PMMA systems investigated.

Unlike the relatively well-studied scratch behavior of polymers, wear behavior of polymers, on the other hand, is rather complex and not well understood. Wear behavior of polymers can be classified into different categories according to the surface damage mechanisms. Generally, wear damage in polymers depends on the contribution of one or

multiple of the following wear mechanisms: abrasive, adhesive and fatigue [29, 30]. Abrasive wear is generated as the result of removal of material from the polymer surface through penetration and sliding of sharp and hard asperities of the counterface. Adhesive wear is defined as the rupture of adhesive junctions between polymer and counterface during contact shearing. Fatigue wear results from the repeated impact of counterface asperities on polymer surface that leads to the propagation of cracks.

Furthermore, wear behavior of polymers can be greatly influenced by the conditions of a particular application. As a result, numerous research efforts have been made to study the wear behavior of polymers in different aspects, which include effects of loading level [31-33], velocity [34-36], wear path [29, 37], as well as environmental conditions [38-40], but only phenomenological correlation has been established, rendering it difficult to link the wear performance of polymers to their material properties. A simpler and more straightforward methodology is needed to allow for effective design of wear-resistant polymers.

To improve the scratch and wear performances of polymers, numerous research efforts have been made to look into the molecular weight effect on scratch and wear behaviors of different polymeric systems, since the molecular weights of polymers is known to have a major impact on their mechanical properties [12, 29, 41-51].

For instance, molecular weight has significant influence on the tensile properties of polymers, especially on tensile strength [41-46]. For many polymers, the effect of molecular weight on tensile strength reaches a plateau value above a sufficiently high molecular weight level, and then becomes less appreciable with further increase in

molecular weight [41]. McCormick et al. [42] examined the tensile strength of eight polystyrenes with number average molecular weight (M_n) ranging from 40,000 to 240,000 g/mol. Their result showed that the tensile strength of the specimens increased rapidly at low molecular weights, but it gradually plateaued at high molecular weights. Similarly, Perkins et al. [43] conducted tensile tests on one set of high density polyethylenes over a weight average molecular weight (M_w) range from 59,000 to 147,000 g/mol. They found that the tensile strength of the specimens increased linearly with initial increase in molecular weight, and then leveled off with further increase in molecular weight. Gardner and Martin [44] aged polycarbonate specimens in a humid environment. The hydrolysis of the specimens resulted in progressive reduction in molecular weight as a function of conditioning time. Their result showed that the tensile strength was insensitive to the decrease in molecular weight above a minimum molecular weight level. But below this level, the tensile strength dropped off quickly with decreasing molecular weight.

It is generally accepted that the density of chain entanglement increases as molecular weight increases, which serve as physical crosslinks to reinforce the polymers under tension. However, when the molecular weight is extremely high, the high density of chain entanglements and intermolecular forces reduce chain mobility and restrict the rearrangement of molecular chains to relieve the applied stress [41, 47]. As a result, the effect of molecular weight on tensile strength is generally significant at low molecular weights, but it becomes less important when the molecular weight is high.

Moghbelli et al. [48] examined the scratch behavior of polypropylene thin sheets with M_w of 305,000 and 416,000 g/mol. They found that the specimen with high molecular weight showed delayed onset of fish-scale and ploughing during scratch, which are also the result of tensile drawing and tearing on the surface induced by scratch tip. Similarly, Browning et al. [12] investigated the scratch behavior of styrene-acrylonitrile random copolymers with variation in M_w from 106,000 to 134,000 g/mol. Their results showed that increasing the molecular weight contributed to an increase in tensile strength of the specimen and a delayed onset of tensile tear-induced micro-cracking on the specimen surface during scratch.

Tervoort et al. [49] probed the abrasive wear behavior of various grades of linear polyethylenes with a wide range of M_w. They found that the abrasive wear rate decreased considerably with increasing molecular weight of the specimens. Laux et al. [29] studied the abrasive wear behavior of polyetheretherketones over a M_w range from 66,200 to 122,323 g/mol. Their results showed that the specimens with higher molecular weights possessed higher tensile strengths and exhibited lower abrasive wear volumes.

1.2 Research Scope

Polyurethane (PU) elastomers are attractive for their exceptional properties and tunability for specialty applications. They are typically composed of two different chemical constituents, i.e., hard segment and soft segment. Given this unique block copolymer structure of PU elastomers, their hard segment and soft segment can be tuned independently to obtain a wide range of properties that meet the needs of various

engineering applications. However, due to the poor resistance of PU elastomers to surface deformation and damage, the scratch and wear performances of PU elastomers remain to be a major concern.

Previous experimental and numerical scratch studies have demonstrated that material parameters will likely influence the scratch behavior of polymers in a qualitative fashion. Still, it is highly desirable to establish comprehensive fundamental knowledge on how key material parameters are related to scratch performance and their corresponding damage mechanisms. To do so, a set of well-controlled model systems is necessary for quantitative correlation between material parameters, such as COF, constitutive behavior and dynamic mechanical behavior, to the observed scratch-induced deformation mechanisms of polymers. Furthermore, it should be noted that most of the previous experimental and numerical scratch studies were performed based on rigid engineering polymers that possess elastic moduli ranging from 1.5 GPa to 4 GPa. Significant research efforts are still needed to have an in-depth understanding on the scratch behavior of elastomers, which may exhibit different scratch behavior from those of engineering polymers reported in the past. The unique block copolymer structure of PU elastomers with alternating hard and soft segments makes it possible for tailoring their morphology and mechanical properties, and thus making them an excellent candidate for systematic fundamental scratch study.

Furthermore, as in other polymers, most PU elastomers are also subjected to moisture exposure during service, which may have significant influence on their scratch behavior. It is thus of great interest to learn how the moisture content affects the material

properties, surface characteristics, and the corresponding scratch-induced deformation in PU elastomers.

As for the wear behavior of PU elastomers, as discussed earlier, due to the complex nature of wear behavior of polymers, in an effort to introduce a simpler and more straightforward approach to predict the wear performance of polymers, it is logical to first focus on the study of abrasive wear that mainly involves material removal upon sliding contact between the counterface and the polymer surface. This phenomenon is similar to the relatively well-establish scratch damage phenomenon, which can be considered as a result of an abrasive wear process with a single-pass and single-asperity scenario [30]. Consequently, it is anticipated that the scratch behavior of PU elastomers can be correlated with and provide fundamental insights into understanding of the abrasive wear behavior of PU elastomers.

Similar to other polymeric systems, for block copolymers like PU elastomers, the molecular weight of the final PU elastomers, as well as the molecular weight of each segment might play an important role on their properties and the corresponding scratch and wear behaviors. It is expected that the scratch and wear performances of PU elastomers can be improved by systematically modifying their molecular weights.

The primary objective of this research is to provide guidelines for the design of scratch and wear resistant PU elastomers. To achieve this objective, this research will start with the investigation on scratch behavior of one set of well-designed model PU elastomers using the ASTM D7027/ISO 19252 standardized scratch test, various materials characterization techniques and FEM simulation to determine the key material

properties and surface characteristics that are related to scratch resistance of PU elastomers under two environmental conditions, i.e., dry and water-saturated. Afterwards, abrasive wear behavior of the model PU elastomers will be examined using a custom built multi-axis tribometer in a pin-on-flat configuration to establish physical correlation between abrasive wear and scratch behaviors. Finally, once the correlations between material properties, scratch behavior and abrasive wear behavior of PU elastomers are determined, attempts will be made to explore the possibility of design of scratch and wear resistant PU elastomers by modifying their molecular weight.

1.3 Layout of the Dissertation

The brief review of polymer scratch and wear research presented in this chapter provides the groundwork to perform a comprehensive investigation on scratch and wear behaviors of PU elastomers. In Chapter II, extensive experimental works on one set of well-designed model PU elastomers are conducted and the results are summarized to determine the key material properties and surface characteristics that are related to scratch resistance of PU elastomers in dry condition.

The following Chapter III will investigate the changes in material properties, surface characteristics and the corresponding scratch behavior of the model PU elastomers upon exposure to moisture. In addition, FEM modeling will be employed to further understand the observed scratch-induced deformation in the model systems.

Chapter IV will focus on various experimental works related to wear behavior of the model PU elastomers. Using a custom built multi-axis tribometer in a pin-on-flat

configuration, test conditions have been designed to differentiate the abrasive wear mechanism and adhesive-fatigue wear mechanism in the model systems, so that the physical correlation between abrasive wear and scratch behaviors of PU elastomers can be identified and established.

On the basis of the knowledge we have obtained in the previous chapters, in Chapter V, the possibility of design of scratch and abrasive wear resistant PU elastomers by modifying their molecular weight is discussed based on the experimental findings on one set of model PU elastomers with different molecular weights.

In Chapter VI, conclusions that summarize the research outcome and considerations for future research will be given. Finally, the references cited in this dissertation are documented.

CHAPTER II

SCRATCH BEHAVIOR OF MODEL POLYURETHANE ELASTOMERS[*]

In this chapter, the scratch behavior of a series of model cast polyurethane elastomers (CPU) is investigated according to the ASTM D7027/ISO 19252 scratch test methodology. Four model CPU systems considered in this study are synthesized by the same hard segment, but with four different types of soft segment polyols to systematically alter their phase morphology, coefficient of friction (COF), yield stress, tensile strength and damping behavior. The objective of this chapter is to link intrinsic material properties and surface characteristics to the observed scratch-induced deformation mechanisms of the model CPU systems.

2.1 Introduction

Many investigations have been performed in the past to study the effect of type, content and length of hard and soft segments on the morphology and mechanical properties of PU elastomers [52-62]. Martin et al. [52] tried to alter the morphology and improve the tensile properties of one set of PU elastomers by increasing CH2/O ratio in the soft segment. With the changes in soft segment, an increase in the degree of microphase separation was evidenced by attenuated total reflectance Fourier transform infrared spectroscopy (ATR- FTIR), and accompanied by an increase in tensile modulus

[*] Reprinted with permission from Xiao, S., Hossain, M. M., Liu, P., Wang, H., Hu, F., & Sue, H. J. (2017). "Scratch behavior of model polyurethane elastomers containing different soft segment types." *Materials & Design*, 132, 419-429. Copyright [2017] by Elsevier.

and tensile strength. However, when the two phases became extremely immiscible, the most microphase-separated system displayed a drop in tensile strength. Korley et al. [53] found a similar result by studying a set of PU elastomers with increasing hard segment content. Their results showed that the increase in hard segment content promoted the microphase separation in PU elastomers. Unfortunately, the tensile strength only increased initially, then deteriorated with further increase in hard segment content. Rogulska et al. [54] investigated the effects of chain extender type and soft segment content on the morphology and mechanical properties of three series of thermoplastic PU elastomers. They found that the introduction of different types of chain extenders in the hard segment notably changed the morphologies and tensile properties of PU elastomers. Also, their results indicated that the degree of microphase separation and tensile strength decreased with increasing soft segment content in some of the PU elastomers studied.

Although various attempts have been made to modify PU composition to improve mechanical properties of PU elastomers, PU elastomers are still susceptible to scratch damage during service, which significantly affects their aesthetics and structural integrity. Systematical research on how the type, content and length of hard and soft segments affect the scratch behavior of PU elastomers is still lacking. Moreover, given the difficulty in the determination of true stress-strain behavior of materials, almost all the studies in the past about the mechanical properties of PU elastomers were limited to the engineering stress-strain curves generation. Thus, the correlations among morphology, surface properties, tensile and compressive true stress-strain behaviors,

dynamic mechanical behavior and the scratch resistance of PU elastomers are highly desired.

In the present study, we focus on gaining fundamental understanding of the polymer scratch behavior and their structure-property relationship by investigating a set of well-controlled model CPU systems. To achieve this objective, the model CPU systems were characterized by various microscopy, spectroscopy, and mechanical testings. Special emphasis will be placed on how the changes in soft segment type fundamentally alter the morphology, surface properties and mechanical properties of CPU, as well as the correlation between these material properties and the corresponding scratch-induced damages. Implication of the present study for designing scratch resistant PU elastomers by varying the type and/or content of their chemical constituents is discussed.

2.2 Materials and Methods

2.2.1 Materials

Four model CPU systems investigated in this study were provided by BASF Polyurethane Specialties (China) Co. Ltd. (Shanghai, China). For all the model systems, the same diisocyanate and chain extender, 4,4'-methylene diphenyl diisocyanate (MDI) and 1,4-butane diol (BDO), were utilized to form the same type of hard segment with comparable hard segment content (Figure 1). However, the four model systems contain four different types of soft segment polyols: polytetramethylene ether glycol (PT), polycaprolactone (PC), ethylene oxide and propylene oxide based polyether polyol

(PET) and adipic anhydride based polyester polyol (PES), as shown in Figure 2. Test specimens were produced into cast plaques with dimensions of 150 mm × 100 mm × 14 mm by BASF. The surface finish of the plaques was smooth with negligible difference in root mean square (RMS) roughness values measured on an area of 1.3 mm × 1 mm. Upon receipt, the plaques were dried in a vacuum oven in between two smooth glass plates at 80 ºC for 6 h to remove pre-existing moisture and residual stresses in the as-received specimens, then left to slowly cool overnight to room temperature. After drying, the plaques were placed in a desiccator before testing. For convenience, the detailed description of the model systems is summarized in Table 1.

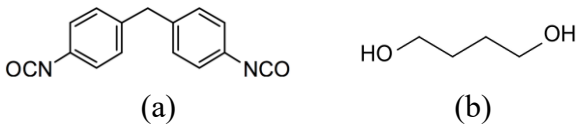

Figure 1. (a) Hard segment (diisocyanate): 4,4'-methylene diphenyl diisocyanate (MDI) and (b) chain extender (diol): 1,4-butane diol (BDO) of the model CPU systems. Reprinted with permission from Materials & Design 132 (2017) 419-429. Copyright [2017] by Elsevier.

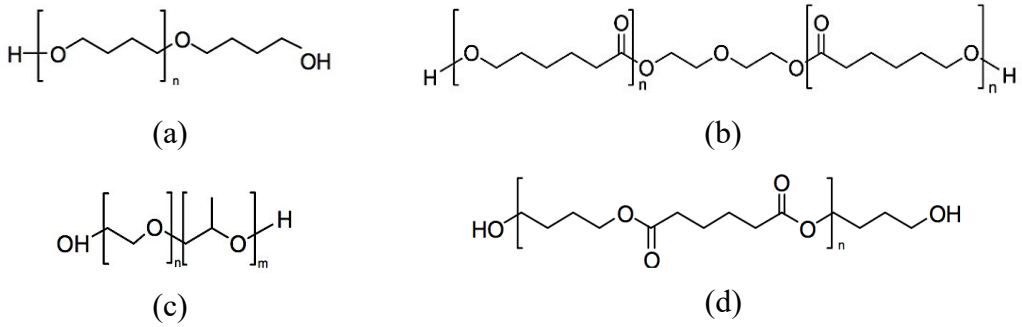

Figure 2. Soft segments (polyols): (a) polytetramethylene ether glycol (PT), (b) polycaprolactone (PC), (c) ethylene oxide and propylene oxide based polyether polyol (PET) and (d) adipic anhydride based polyester polyol (PES) of the model CPU systems. Reprinted with permission from Materials & Design 132 (2017) 419-429. Copyright [2017] by Elsevier.

Table 1. Material information of the model CPU systems. Reprinted with permission from Materials & Design 132 (2017) 419-429. Copyright [2017] by Elsevier.

	Hard Segment	Chain Extender	Hard Segment Content	Soft Segment	RMS roughness, μm
CPU-PT	MDI	BDO	37%	Polytetramethylene ether glycol (PT)	0.37 ± 0.03
CPU-PC	MDI	BDO	44%	Polycaprolactone (PC)	0.50 ± 0.04
CPU-PET	MDI	BDO	34%	Propylene oxide based polyether polyol (PET)	0.38 ± 0.03
CPU-PES	MDI	BDO	33%	Adipic anhydride based polyester polyol (PES)	0.41 ± 0.02

2.2.2 Attenuated Total Reflectance-Fourier Transform Infrared Spectroscopy (ATR-FTIR)

The FTIR spectra were recorded using a Nicolet^{TM} 380 FT-IR Spectrometer equipped with an OMNI-Sampler^{TM} ATR sampling accessory. The spectra were recorded in the spectral range of 700 - 4000 cm^{-1} with a resolution of 4 cm^{-1}. For each measurement, 128 scans were collected.

2.2.3 Atomic Force Microscopy (AFM)

The surface morphologies of the model CPU systems were characterized using AFM (Dimension Icon, Bruker) by BASF Material Physics & Analytics Lab (Shanghai, China). The phase images of the CPU surfaces were collected in tapping mode using a silicon tip (TESP, Bruker) with cantilever spring constant of 42 N/m. The smooth cross-sections close to the specimen surfaces were prepared by cryo-microtome (EM UC7

FC7, Leica) at -80ºC. The AFM measurements were done at room temperature. In order to compare the morphology of all the model systems, the imaging parameters and specimen preparation procedures were kept the same.

2.2.4 Coefficient Of Friction (COF) Measurement

A commercial scratch machine (Scratch 5, Surface Machine Systems, LLC) built according to the ASTM D7027/ISO 19252 standard was used to measure the COF between the model CPU systems and stainless steel surface. In order to prevent additional material deformation that will introduce errors to the measured COF, a stainless steel flat tip with large surface area and a low constant normal load were applied for the tests. The dimensions of the stainless steel flat surface were 10 mm × 10 mm. The tests were conducted with a 5 N constant normal load (0.05 MPa stress). Before each test, the stainless steel flat tip and the surface of the sample were cleaned by compressed nitrogen gas to remove any possible contaminants. Three tests were performed on each model system for statistical purposes.

2.2.5 Tensile True Stress-strain Curve Generation

Elastomeric materials will undergo large straining both in tensile and lateral directions, which renders the engineering stress-strain curves of elastomeric materials less meaningful and a true stress-strain curve characterization more appropriate [63]. Uniaxial tensile true stress-strain measurements were performed using a custom-built tensile test fixture with a Digital Image Correlation (DIC) video setup. This custom-built

tensile test fixture can provide necessary in-plane constraints on all edges of the specimen and prevent out-of-plane buckling during the test, so that the tensile true stress-strain behavior of the specimen can be accurately determined. The major feature of this refined tensile test fixture can be found elsewhere [64].

The tensile specimens were produced by casting them into sheets with dimensions of 180 mm × 150 mm × 2 mm, and then cut into dumbbell shape with 16 mm gauge length and 8 mm ligament length. The cutting edges were carefully polished by 4000 grit number polishing paper to remove any possible surface defects. A black ink permanent marker was used to apply random speckle patterns on the gauge section of the specimens, which are needed for the DIC analysis. A MTS Insight® universal testing machine was used to conduct the tensile tests at a crosshead speed of 5 mm/min. A Canon EOS 5D Mark II DSLR camera and VIC-2D™ DIC software package were applied to track the variation of speckle patterns on the gauge section, and hence the true strain in both tensile and lateral directions during the tests. The true stress in tensile direction was then calculated by dividing the applied load by the measured instantaneous cross-sectional area.

2.2.6 Compressive True Stress-strain Curve Generation

Uniaxial compression tests were performed according to the ASTM D695-10 standard [65] by using a MTS Insight® universal testing machine at a crosshead speed of 2.5 mm/min. The compression specimens were cut from the plaques by razor blade into prisms with nominal dimensions of 10 mm × 6 mm × 6 mm. Polishing paper with 4000

grit number was used to polish all the surfaces of the specimens to make all the surfaces flat and parallel with each other. Appropriate amount of lubricant was applied onto the contacts between the sample and compression fixture to minimize surface friction during the tests. Similar to the uniaxial tensile test of elastomers, specimens will also undergo severe deformation during compression with greatly increased cross-sectional area, which makes the engineering stress-strain curves inadequate to approximate the true compressive behavior of elastomers. A Canon EOS 5D Mark II DSLR camera and ImageJ software were applied to capture the variation of specimen width during compression to track the cross-sectional area changes. The compressive true stress was then calculated by dividing the applied load by the measured instantaneous cross-sectional area.

2.2.7 Dynamic Mechanical Analysis (DMA)

DMA was carried out using a TA Instruments ARES G2 Rheometer in torsional mode. The temperature range investigated increases from -135 °C to 180 °C at a constant ramp rate of 3 °C/min. The strain amplitude was set at 0.2% to keep the tests within the linear viscoelastic region for all the model systems. The frequency of the tests was fixed at 1 Hz. The DMA specimens were cut from the plaques by razor blade into nominal dimensions of 30 mm × 10 mm × 3 mm. Then, the surfaces of the specimens were carefully polished by 4000 grit number polishing paper to ensure the edges square and sides parallel.

2.2.8 Scratch Test

Following the ASTM D7027/ISO 19252 standard, the scratch tests were conducted using a linearly increasing normal load of 1-300 N. Two constant scratch speeds of 1 mm/s and 100 mm/s were applied for the scratch tests over the same scratch length of 100 mm. Scratch tests at 1 mm/s were used to correlate between scratch behavior and quasi-static constitutive behavior of the model CPU systems at comparable strain rates (~0.01 s^{-1}). Scratch tests at 100 mm/s were compared to the scratch tests at 1 mm/s to study the rate effect on the scratch behavior of the model CPU systems. A specially designed stainless steel conical scratch tip, which features a continuous geometry with a 1 mm diameter sphere attached to a cone, was utilized for the tests. Figure 3 shows the design of the scratch tip. Similar to the COF measurement, before each test, compressed nitrogen gas was used to remove any possible contaminants on the scratch tip surface and sample surface. By using these testing parameters, three scratch tests were performed at each speed on each model system for determining the average values of the onset loads of different damage transitions.

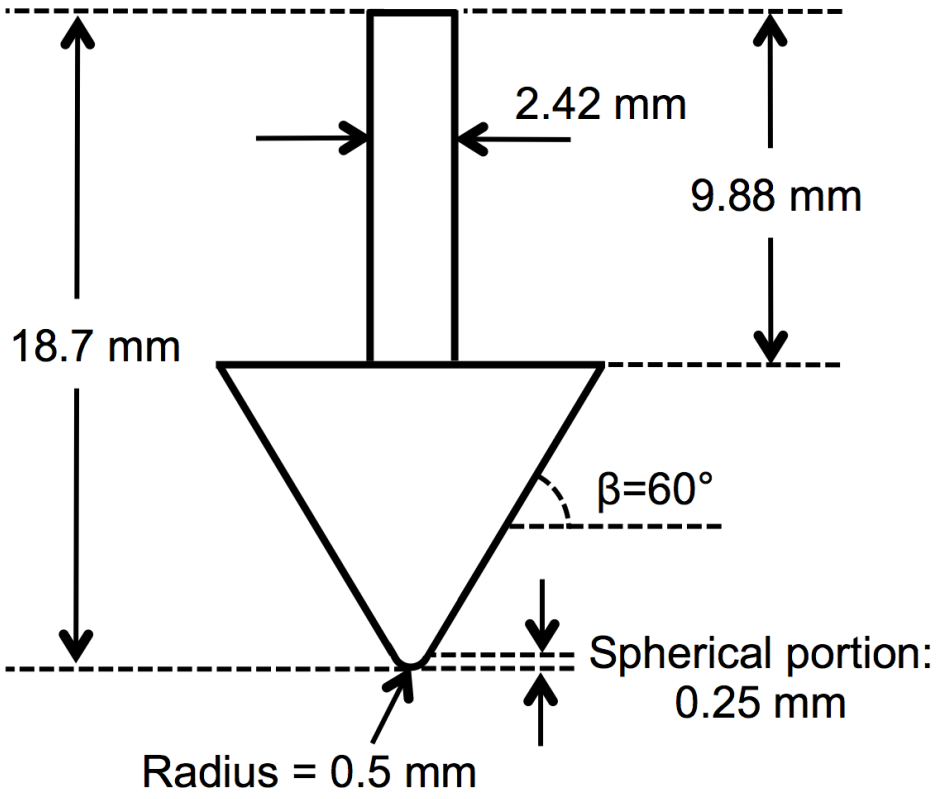

Figure 3. 1 mm diameter stainless steel conical scratch tip design. Reprinted with permission from Materials & Design 132 (2017) 419-429. Copyright [2017] by Elsevier.

2.2.9 Post-scratch Analysis

Because of the strong self-healing ability of the PU elastomers, the deformation on specimens tends to recover very quickly after each mechanical test [66, 67]. Therefore, the analyses of scratch-induced damage were performed soon after the completion of scratch tests. The onset points of groove formation and cracking/material removal damage were located by a Keyence® VK9700 violet laser scanning confocal microscope (VLSCM). Then, the corresponding critical normal loads for the onsets of groove formation and cracking/material removal damage were determined. The

geometries of the scratch grooves and damage features were observed from the topographical images taken by VLSCM.

2.3 Results

2.3.1 ATR-FTIR

Typical PU elastomers have unique block copolymer structure with alternating hard and soft segments. The microphase of PU elastomers is generally separated into hard and soft domains due to the thermodynamic incompatibility between these two components after curing. It is widely known that the hydrogen bonding between the carbonyl C=O and N–H groups in the urethane linkage is one of the key factors affecting the microphase separation in PU elastomers [68, 69]. Almost all the infrared spectroscopic studies on PU in the past have been focused on these two functional groups to characterize the hydrogen bonding state and to correlate it with the microphase separation in the systems [52, 54, 55, 59-62].

The ATR-FTIR spectra of the model CPU systems with different types of soft segments are shown in Figure 4. Since the infrared absorption peaks of hydrogen-bonded C=O and N-H emerge at lower wavenumbers than those of the groups free from hydrogen bonding [52, 62, 70], for all the model systems, only one N-H absorption peak is found at around 3300 cm^{-1}, which is an indication that most of the N-H groups are hydrogen-bonded. However, different absorption peaks in the carbonyl C=O stretching vibration regions are observed for each system. The spectra of the carbonyl stretching vibration regions of the model systems are highlighted in Figure 5. CPU-PT and CPU-

PES present two distinct carbonyl absorption peaks: 1730 cm^{-1} and 1705 cm^{-1}, which correspond to non-hydrogen-bonded and hydrogen-bonded carbonyl groups, respectively. CPU-PC has a less distinct hydrogen-bonded carbonyl peak than CPU-PT and CPU-PES. Interestingly, the hydrogen-bonded carbonyl peak in the spectrum of CPU-PET is almost absent.

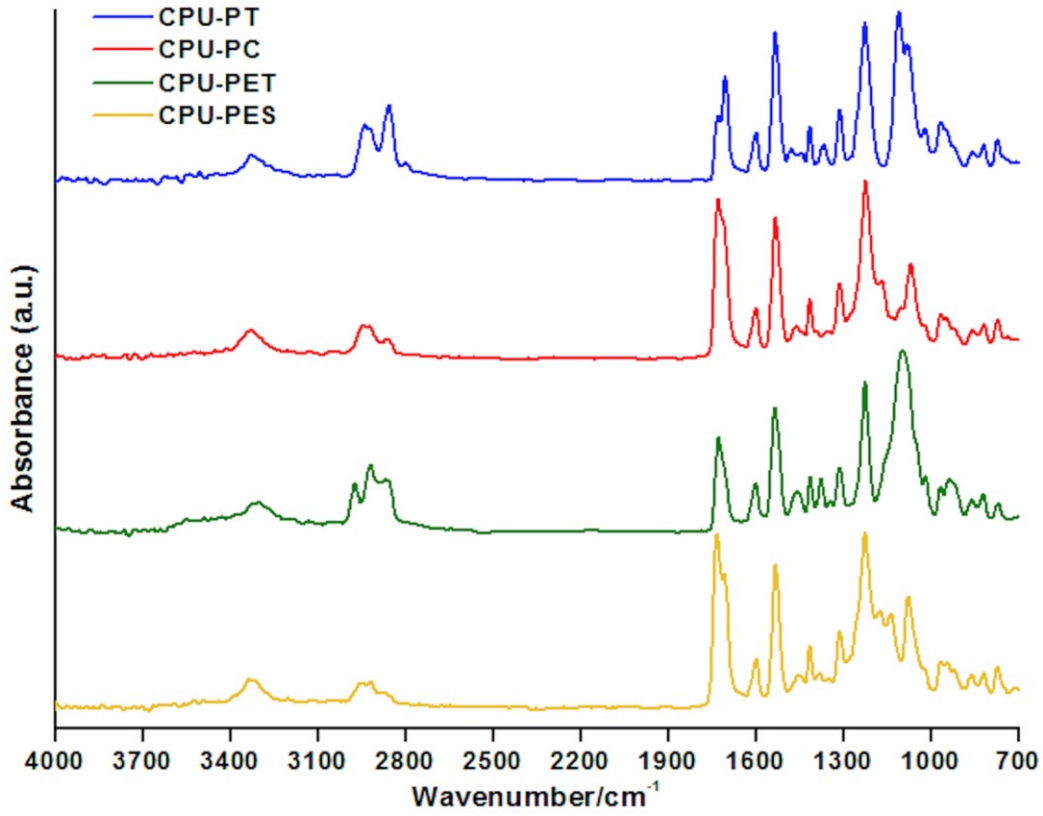

Figure 4. ATR-FTIR spectra of the model CPU systems containing different types of soft segments. Reprinted with permission from Materials & Design 132 (2017) 419-429. Copyright [2017] by Elsevier.

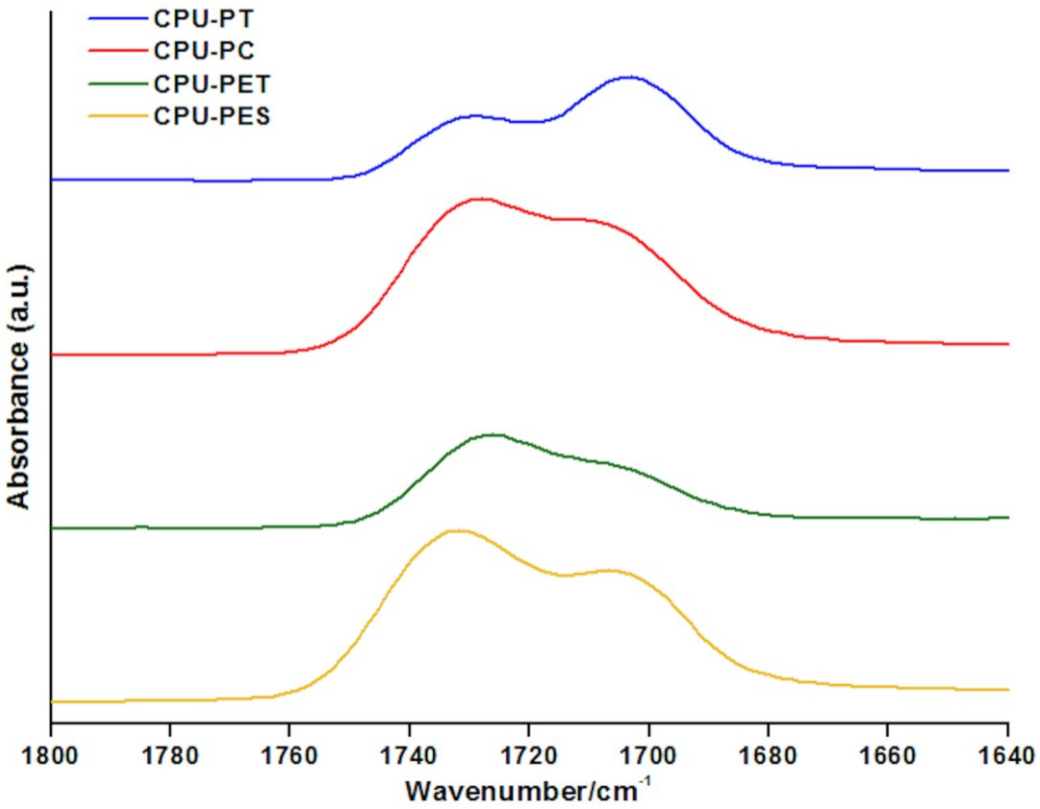

Figure 5. ATR-FTIR spectra of the carbonyl C=O stretching vibration regions of the model CPU systems. Reprinted with permission from Materials & Design 132 (2017) 419-429. Copyright [2017] by Elsevier.

The diverse absorption peak patterns in the carbonyl stretching vibration regions are a sign of different hydrogen bonding states and corresponding microphase separation among the model systems. Considering that CPU-PT and CPU-PET do not have carbonyl groups in the soft segments, the relative intensities of the carbonyl absorption peaks with and without hydrogen bonding provide direct relevance to their degree of microphase separation. As shown in Figure 5, CPU-PT has two distinct peaks for carbonyl groups with and without hydrogen bonding. However, the hydrogen-bonded

carbonyl peak of CPU-PET is almost undetectable. This directly indicates that the soft segment of CPU-PT favors hydrogen bonding between urethane linkages and offers CPU-PT a higher degree of microphase separation than that of CPU-PET.

The analysis of microphase separation in CPU-PC and CPU-PES is not as straightforward as the above two systems due to the presence of ester groups in the soft segments, which dominates the intensity of non-hydrogen-bonded carbonyl peak. As a result, both of these systems exhibit a more pronounced non-hydrogen-bonded carbonyl peak. Nevertheless, CPU-PES still shows a more distinct hydrogen-bonded carbonyl peak than CPU-PC. In addition, CPU-PC has a higher hard segment content than CPU-PES (i.e., 44% vs. 33%), which means the ester groups in the soft segment of CPU-PES contribute more to the intensity of non-hydrogen-bonded carbonyl peak. In other words, the soft segment of CPU-PES is more favorable to hydrogen bonding. Thus, the relative intensities of hydrogen-bonded and non-hydrogen-bonded carbonyl peaks of the model systems indicate that CPU-PT and CPU-PES have higher degrees of microphase separation than CPU-PC and CPU-PET. This finding is corroborated and confirmed by the phase images captured by AFM, which will be presented later.

2.3.2 AFM

In order to learn about how the soft segment type influences the microphase morphology, phase images of the model CPU systems were collected by using AFM in tapping mode. In tapping mode AFM, the cantilever is excited at or near its resonance frequency and moves across the sample surface to take the topographic image. Phase

imaging monitors the phase lag between the excitation and response oscillation of the cantilever simultaneously while the topographic image is being taken. Many different material properties may cause the phase lag, such as stiffness, adhesion and friction. The phase lag between phases is registered as bright and dark areas in the phase images. Consequently, the microphase-separated morphology of the model CPU systems with alternating hard and soft segment is captured.

The AFM phase images of the cross-sections of the model CPU systems are shown in Figure 6. The images on the left column are with 5 μm × 5 μm resolution and the images on the right column are with 10 μm × 10 μm resolution. The bright areas in these phase images refer to the regions with a higher stiffness, i.e., hard segment domains. Since the model CPU systems were prepared by casting, there is no detectable orientation of the hard segment phase in the soft segment phase or any skin-core morphology that is usually observed in injection-molded copolymers [9, 14]. This uniform morphology from surface to subsurface simplifies our fundamental understanding of the scratch behavior of the model CPU systems. The AFM investigation of the model CPU systems reveals that the incorporation of different soft segments leads to extremely different morphologies, and this difference is expected to directly impact their mechanical properties and scratch behaviors. More in-depth discussion on this matter will be further elaborated below.

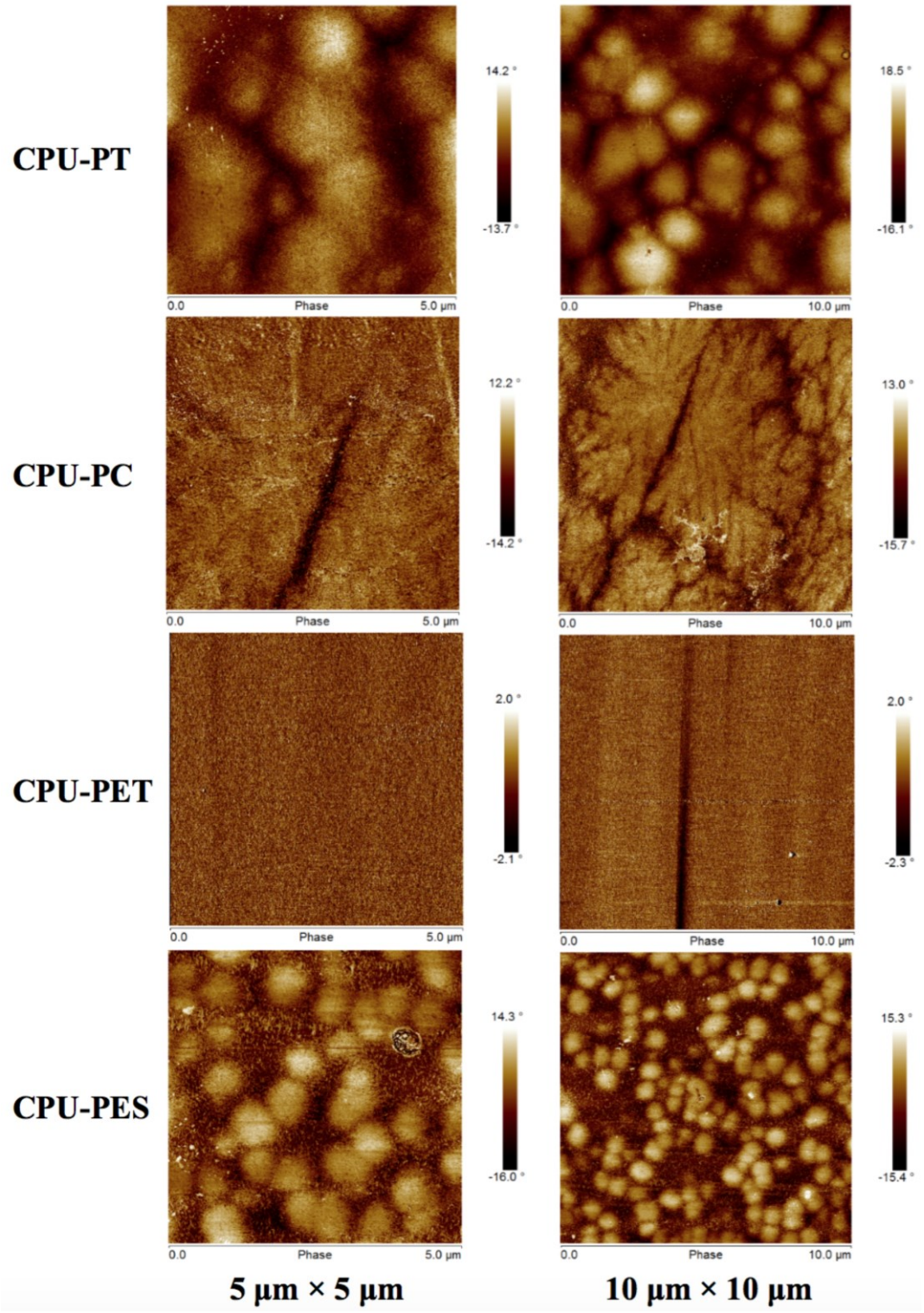

Figure 6. AFM phase images of the cross-sections of the model CPU systems. Reprinted with permission from Materials & Design 132 (2017) 419-429. Copyright [2017] by Elsevier.

2.3.3 COF Measurement

COF cannot be regarded as a material property because it depends on many external variables like environment and surface conditions of the two contacting counterfaces. Since the conical scratch tip used in the scratch test is made of stainless steel, so the material pair studied in this case are the model CPU systems and stainless steel. As the flat stainless steel tip used in the COF measurement has large dimensions (10 mm × 10 mm) and the applied load is small (5 N = 0.05 MPa), any frictional force due to material deformation is minimal, if any. The COF is defined by the ratio of the tangential force that the tip experienced to the normal load applied to the sample. These two forces were simultaneously recorded during the measurement. The COF between the model CPU systems and stainless steel are calculated and shown in Figure 7. Under the above-mentioned testing conditions, CPU-PET shows the highest COF value among the four model systems, followed by CPU-PC, CPU-PES, and CPU-PT sequentially. As the following discussion will reveal, the different damping behaviors among the model systems may contribute to the variation in frictional behaviors, and the frictional behavior has a significant influence on scratch damages to the model CPU systems.

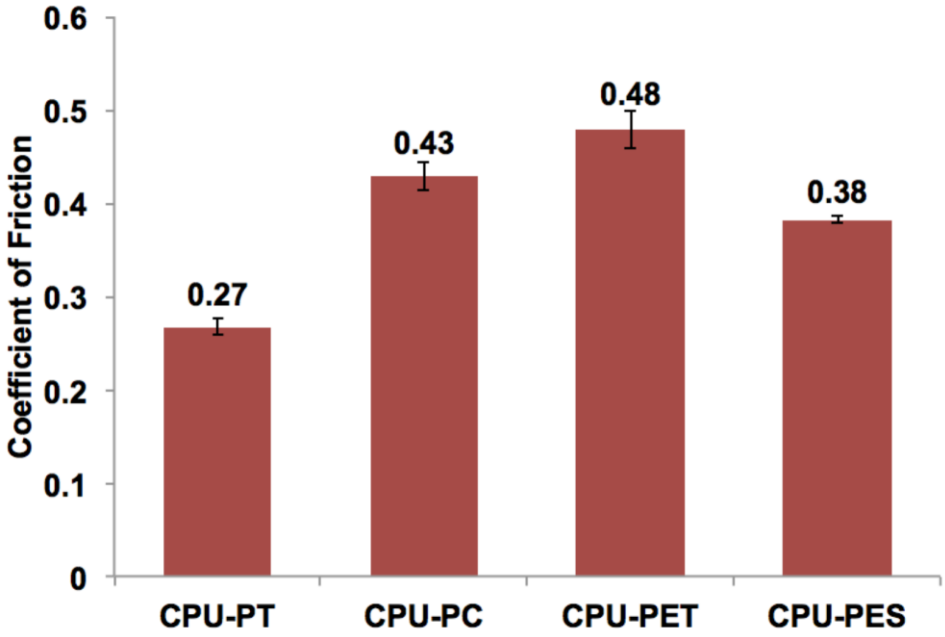

Figure 7. Coefficient of friction of the model CPU systems. Reprinted with permission from Materials & Design 132 (2017) 419-429. Copyright [2017] by Elsevier.

2.3.4 Tensile True Stress-strain Behavior

By employing the custom-built tensile test fixture along with DIC setup, the uniaxial tensile true stress-strain curves of the model systems were generated and compared in Figure 8. All the model systems exhibited yielding phenomenon and the dumbbell shape specimens could not recover to their original dimensions after unloading. The maximum rate of cross-sectional area reduction was used to determine onset of yielding. All the samples were stretched to break to determine their tensile strengths. The key uniaxial tensile properties of the model CPU systems are listed in Table 2. It is apparent that the introduction of different types of soft segments results in significantly different tensile true stress-strain behaviors among the model systems.

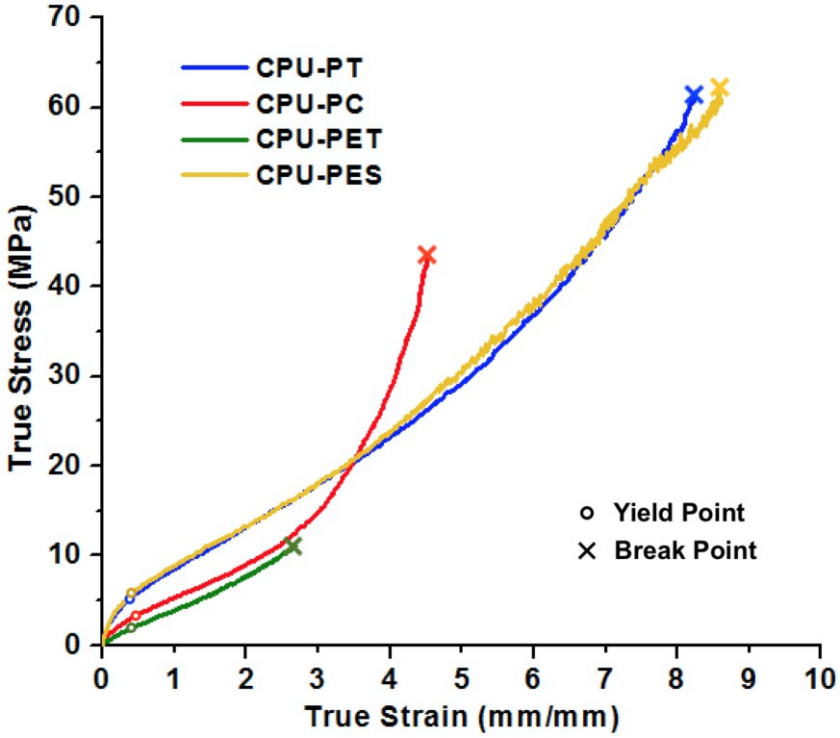

Figure 8. Tensile true stress-strain curves of the model CPU systems. Reprinted with permission from Materials & Design 132 (2017) 419-429. Copyright [2017] by Elsevier.

Table 2. Comparison between uniaxial tensile and compressive properties of the model CPU systems. Reprinted with permission from Materials & Design 132 (2017) 419-429. Copyright [2017] by Elsevier.

	CPU-PT	CPU-PC	CPU-PET	CPU-PES
Tensile modulus (MPa)	16.2 ± 1.2	9.4 ± 0.7	6.0 ± 0.4	17.0 ± 0.8
Tensile yield stress (MPa)	5.0 ± 0.3	3.0 ± 0.1	1.9 ± 0.2	5.3 ± 0.2
Tensile strain at break (%)	854.2 ± 40.1	460.6 ± 16.0	259.7 ± 12.1	881.8 ± 29.0
Tensile strength (MPa)	63.7 ± 2.7	45.5 ± 3.3	10.3 ± 1.3	65.2 ± 4.1
Compressive modulus (MPa)	18.0 ± 0.3	12.5 ± 0.3	7.3 ± 0.3	18.2 ± 0.7
Compressive yield stress (MPa)	7.0 ± 0.2	5.5 ± 0.3	4.3 ± 0.1	7.5 ± 0.3

The tensile properties of PU elastomers are greatly influenced by their morphology. A higher degree of microphase separation results in a better development of the reinforcing hard segment domain within the soft segment matrix and improves the tensile properties of the system [60, 62]. Moreover, a more uniform hard segment domain size and a better ordering of the hard domain further strengthen the PU system during deformation by dissipating the mechanical energy more effectively [53, 55]. As shown in Figure 6, CPU-PT and CPU-PES exhibit a distinct two-phase morphology, and thus leading to better tensile properties than CPU-PC and CPU-PET. The clear microphase-separated morphology of CPU-PES shows ordered hard segment domains with a more uniform hard segment domain size, which contributes to the best tensile properties of CPU-PES among all the model systems.

The hard segment domain sizes of CPU-PT are generally larger than those of CPU-PES, which is due to the polyol properties and slightly higher hard segment content in CPU-PT. The increase in hard segment domain size with increasing hard segment content has been observed by others, as well [53, 55]. It should be noted that the hard segment domain sizes in CPU-PT are not uniform, with the larger ones to be over ten times larger than the smaller ones. The non-uniformity of the hard domain sizes may cause non-uniform distribution of local stresses that promotes localized stress concentration during deformation, and hence compromise the mechanical properties [55]. Consequently, CPU-PT exhibits slightly lower tensile properties than CPU-PES.

On the other hand, the soft segments of CPU-PC and CPU-PET cause difficulty in microphase separation. In CPU-PC, the hard segment domains are tightly packed

together to form large blocks and the soft segment spreads out within the hard segment domains. The high hard segment content in CPU-PC may also contribute to the less distinctive two-phase morphology. Other researchers have found that it is difficult to observe microphase separation by AFM in systems containing high hard segment contents [55, 71]. The lower degree of microphase separation in CPU-PC leads to deterioration in tensile properties compared to CPU-PT and CPU-PES. Similarly, the two-phase morphology is almost indistinguishable in CPU-PET where the soft segment domain is hard to detect, and thus leading to a noticeable drop in its tensile properties, especially in tensile strength. Therefore, based on the model systems study, it is evident that an increase in the degree of microphase separation will lead to improvement in tensile properties of PU elastomers. This finding is also supported by previous studies [52-55].

It should also be pointed out that the tensile true stress-strain curves of all the model CPU systems show different degrees of upturn after yielding, i.e., different degrees of strain hardening. This steep increase in stress after yielding has been demonstrated to be related to the stress-induced crystallization of the soft segment [52, 72]. It has also been shown that the chemical structure and regularity of the soft segment polyols in the PU elastomer determine the degree of stress-induced crystallization [73]. This crystallization of soft segment during stretching can, to some extent, improve the tensile strength of the system. Among all the model CPU systems, CPU-PC displays the most pronounced strain hardening after yielding that results in the observed increase in tensile strength of the system even if it possesses a relatively lower degree of microphase

separation. Another study has found that the application of crystallizable polycaprolactone as the soft segment in PU elastomer can enhance the tensile strength and tensile strain at break of the system owing to the stress-induced crystallization effect [74]. Accordingly, the presence of moderate crystallinity in the soft segment of PU elastomer should improve its tensile strength and tensile strain at break. Moreover, the variation in post-yielding behaviors of the model CPU model systems signifies the importance of true stress-strain curve generation of PU elastomers. Since the gauge section of the tensile specimens of PU elastomers undergoes localized deformation after yielding, the engineering stress-strain curve is inadequate for accurate characterization of post-yielding behavior.

As discussed in the previous FEM investigations [18, 19], tensile strength correlates well with onset of cracking/material removal during scratch process. The significant variation in uniaxial tensile properties among the model CPU systems makes them ideal for validation of the above findings in numerical studies.

2.3.5 Compressive True Stress-strain Behavior

In general, polymeric materials are known to behave differently when being loaded under tension and compression. During scratching, when the tip moves with increasing normal load, the stress state near the scratch tip can be quite complex, as it involves both tensile and compressive stresses, as well as transitions between these two stress states [17]. Thus, it is also critical to determine compressive behaviors of the model systems.

The uniaxial compressive true stress-strain curves of the model CPU systems were generated and compared in Figure 9. Not surprisingly, the model CPU systems exhibit different true stress-strain curves in compression from those in tension. The asymmetric tension-compression behavior of the model CPU systems is evidenced. The stress value corresponding to the intersection of the extensions of the initial linear region and the plateau region is generally assigned as the compressive yield stress of elastomers that do not exhibit a distinct yield point under compression [75, 76]. This tangential intercept method was used to calculate the compressive yield stress of each model system. Since compressive strength, which is the stress at compressive failure, is not relevant to scratch-induced damage [18, 19], compressive strength was not measured here and the compression tests were stopped before compressive failure took place (loaded the samples to 80% of engineering strain). The key uniaxial compressive properties of the model CPU systems are also listed in Table 2.

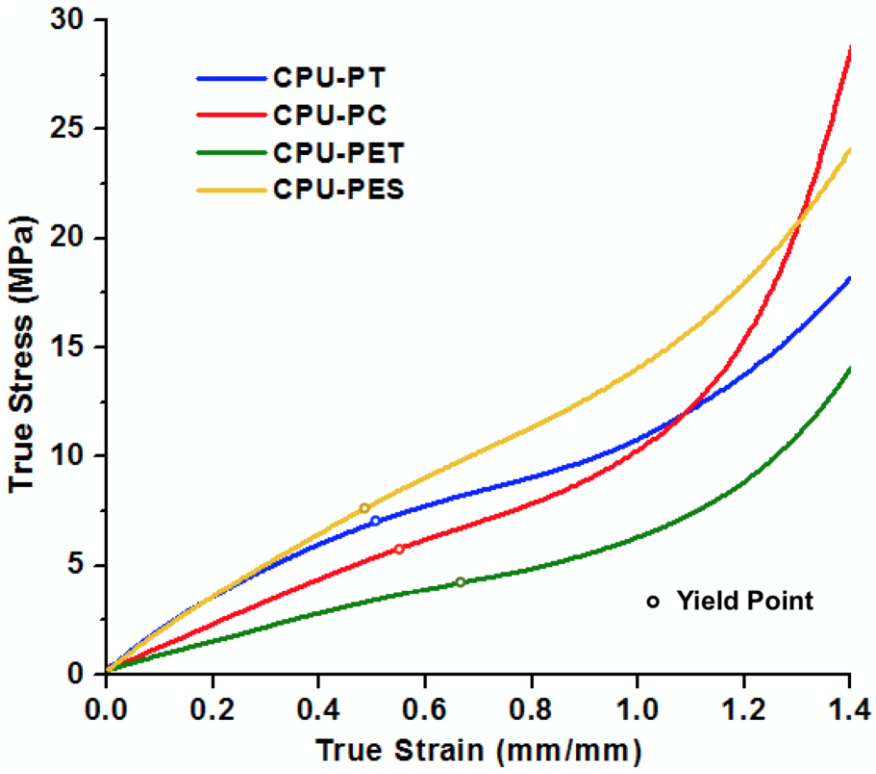

Figure 9. Compressive true stress-strain curves of the model CPU systems. Reprinted with permission from Materials & Design 132 (2017) 419-429. Copyright [2017] by Elsevier.

As expected, all the model systems show slightly higher yield stress values under compression than tension. However, similar to the trend of the yield stress magnitudes in tension, CPU-PT and CPU-PES still possess higher yield stresses than the other two model systems in compression. It is noted that considerable research has been devoted to linking morphology to tensile properties of PU elastomers. Little information is available for correlation between morphology and compressive properties. As demonstrated in the current study, the compressive behaviors of the model systems follow the same trend as their tensile behaviors. Therefore, it can be presumed that the development of microphase-separated morphology in PU elastomers offers a similar improvement in

compressive properties as those found in tensile properties. Knowledge on the asymmetric tension-compression behavior of the model CPU model systems can help elucidate the scratch-induced deformation and damage in a more straightforward fashion, as will be discussed below.

2.3.6 Dynamic Mechanical Behavior

The viscoelastic behaviors of the model CPU systems were studied by DMA. The temperature dependence of storage modulus and tan δ of the model systems in semi-log scale is shown in Figure 10. Within the temperature range investigated, all the model CPU systems exhibit one prominent T_g peak at relatively higher temperatures and the secondary peak found at around -85 °C, which are labeled as α and β peaks, respectively. The α relaxation is attributed to the T_g of the soft segment. As expected, the presence of different types of soft segments among the model systems leads to different α relaxation peaks at various temperatures. The soft segment of CPU-PT has the lowest T_g of all the model systems, followed by the soft segment of CPU-PES. The T_g of the soft segments of CPU-PC and CPU-PET occurs at around 22 °C, which is near room temperature. The secondary β relaxation is associated with the local motions in the hard segment domains [77]. Since all the model systems contain the same type of hard segment with comparable hard segment content, the β relaxation peaks of the model systems reside at the same temperature.

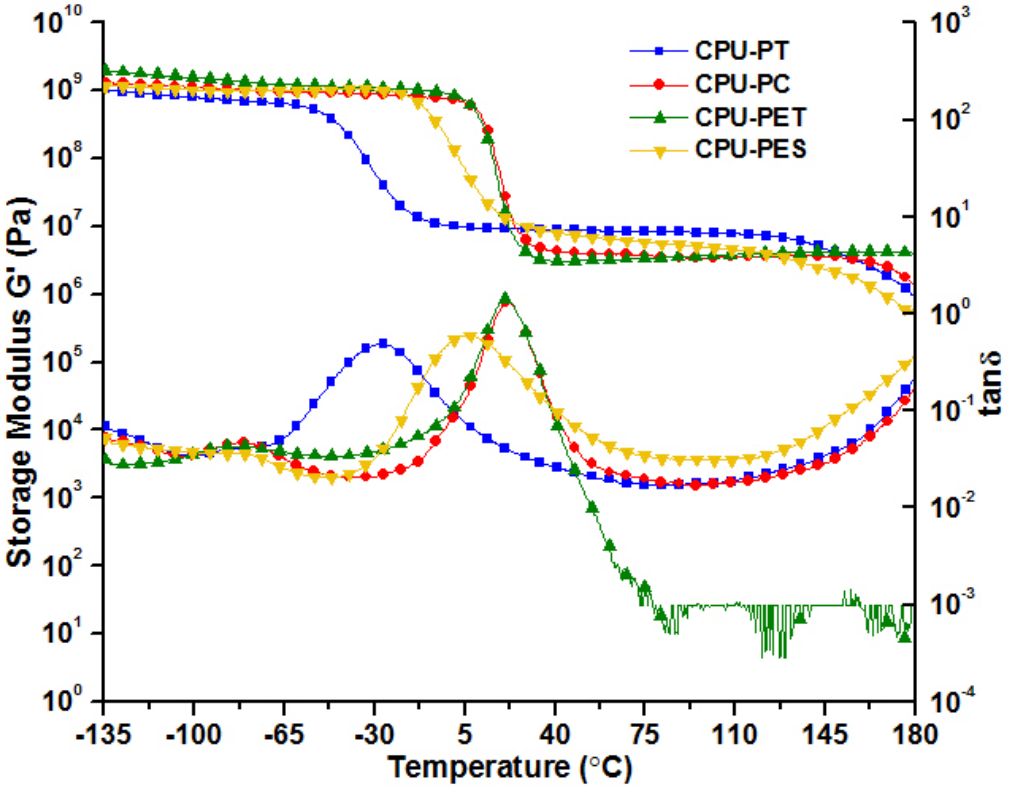

Figure 10. Temperature dependence of storage modulus and tan δ of the model CPU systems. Reprinted with permission from Materials & Design 132 (2017) 419-429. Copyright [2017] by Elsevier.

When the temperature rises above approximately 60 °C, CPU-PET begins to show noise for the tan δ values. This is due to the phase angle of CPU-PET above this temperature has exceeded the lowest phase angle that DMA can detect. In other words, CPU-PET has a strong elastic response when the temperature rises above 60 °C. As the temperature rises above the T_g of each system, all the systems display an extensive rubbery plateau. The presence of the rubbery plateau region above T_g suggests sufficient levels of crosslinking of the model CPU systems. Since all the model systems contain

similar amount of hard segment, the variation in the magnitudes of rubbery plateau moduli is indicative of the different crosslink densities among the model systems.

Most importantly, the introduction of different types of soft segments not only affects the T_g of the model systems but also significantly alters their damping behaviors at room temperature, where most mechanical tests as well as scratch test were carried out. As can be seen from the tan δ curves, since CPU-PC and CPU-PET have T_g near room temperature, these two model systems have more pronounced damping characteristics at room temperature. As the T_g of CPU-PES and CPU-PT are 6 °C and -27 °C, respectively, the magnitudes of the damping keep decreasing as temperature increases, which result in weaker damping characteristics than CPU-PC and CPU-PET around room temperature. Among all the model systems, CPU-PT shows the lowest damping characteristic around room temperature. The greatly varied damping behaviors of the model CPU systems are expected to affect their strain rate dependencies in mechanical properties and corresponding scratch performance. This can be explained by the fact that as strain rate increases, the amount of heat dissipated increases faster for a polymer with a higher damping. As a result, polymers with a higher damping experience a higher temperature rise, causing more deterioration in mechanical properties during increased strain rate of testing. In other words, a higher damping of a polymer makes it more sensitive to testing rate.

In addition, research has found that the frictional behavior of polymers sliding against another surface is closely related with the damping behaviors [78-80]. It has been shown that polymers with high damping will experience a noticeable softening

accompanied by a drop in shear strength during sliding, which is due to the large amount of heat dissipated, and thus causing an increase in friction [78]. As shown earlier, CPU-PET has the most pronounced damping at around room temperature, followed by CPU-PC and CPU-PES. CPU-PT shows a much lower magnitude of damping near room temperature among the model systems. The measured COF between the model CPU systems and stainless steel surface follow the same trend as their damping characteristics. Therefore, the different damping characteristics among the model systems are at least partially responsible for the differences in COF among the model CPU systems when sliding against stainless steel scratch tip.

2.3.7 Scratch Behavior

To study the effect of soft segment on the scratch behavior of the model CPU systems, scratch tests were performed according to the ASTM D7027/ISO 19252 standard. The critical normal loads for the onset of scratch-induced deformation, which includes groove formation and cracking/material removal, at 1 mm/s and 100 mm/s scratch speeds were determined and compared in Figure 11(a) and 11(b), respectively. As linearly increasing normal load was used for the scratch tests, the formation of scratch groove first appeared along the scratch path, and then turned into more severe cracking/material removal damage as load further increased. The onset of groove formation was located by the height profile of the topographical images. The onset of cracking/material removal was determined by the location where the first sign of cracking on the surface occurred. Since the damage features at 1 mm/s and 100 mm/s

scratch speeds are similar, Figure 12 shows the optical images and height profiles obtained from VLSCM at the onset of cracking/material removal in the model CPU systems at 100 mm/s speed as an example. The onset point of each model system is marked by a dash line, and the onset load is shown in the figure. All the model systems display a clear onset for cracking/material removal. Even though the features of the cracking/material removal damage in the four model systems are slightly different, all of them involve continuous parabolic cracks formation with slight amount of materials displaced from the middle portion of the cracks.

The model CPU systems containing different soft segments exhibit dramatically different onsets of scratch-induced deformation. Except for CPU-PET, which does not form scratch groove before onset of cracking/material removal, CPU-PC shows the earliest onset of groove formation, followed by CPU-PES and CPU-PT. The absence of groove formation in CPU-PET, which is due to its noticeable low tensile strength with respect to its compressive yield stress, will be discussed in more details in the discussion session. Even though CPU-PET does not have a scratch groove formation, it shows a noticeably early onset of cracking/material removal. For instance, at 1 mm/s scratch speed, the onset load is only around 63 N. All the other systems show much higher onset loads of cracking/material removal than CPU-PET. It is readily apparent that if the applications of the model CPU systems only involve low scratching loads, CPU-PET will have the best scratch performance due to the absence of any scratch-induced deformation below 63 N. However, CPU-PET will become the worst system against cracking/material removal if the scratching load is above 63 N. The onsets of scratch-

induced deformation in the model CPU systems at 100 mm/s scratch speed follow the same trend with those at 1 mm/s scratch speed. The scratch testing rate dependency of the model systems will be further discussed below.

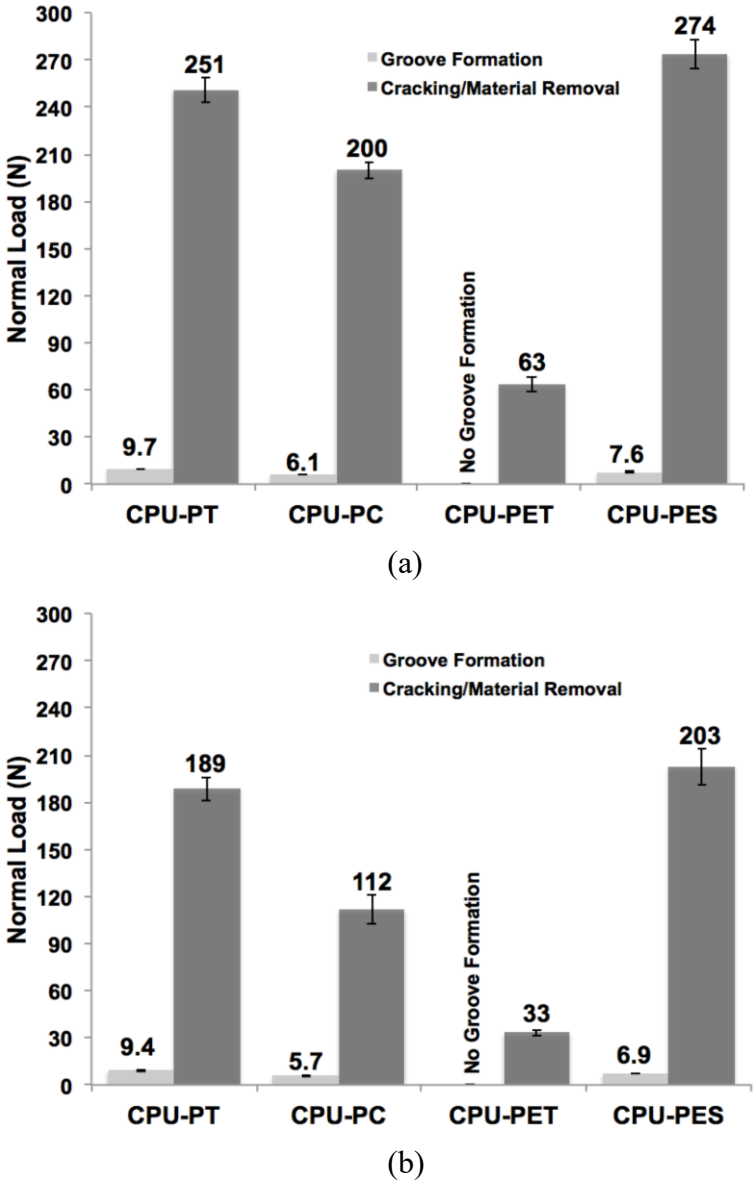

Figure 11. Onset loads of scratch-induced deformation in the model CPU systems at (a) 1 mm/s and (b) 100 mm/s scratch speeds. Reprinted with permission from Materials & Design 132 (2017) 419-429. Copyright [2017] by Elsevier.

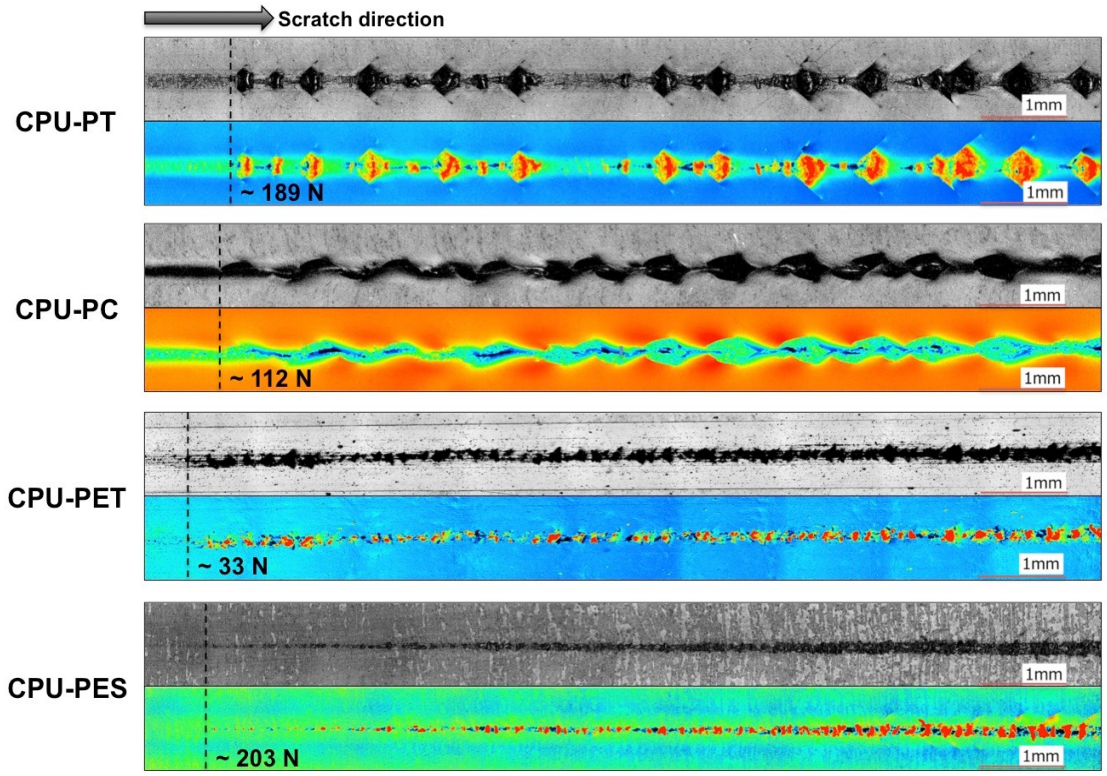

Figure 12. Optical images and height profiles of onset of cracking/material removal in the model CPU systems at 100 mm/s scratch speed. Reprinted with permission from Materials & Design 132 (2017) 419-429. Copyright [2017] by Elsevier.

2.4 Discussion

Given the detailed knowledge on the chemical, morphological, surface and mechanical properties of the model CPU systems described above, which is resulted from the four different soft segment polyols, it is now possible to fundamentally learn how they influence the scratch behavior in a systematic, straightforward fashion.

As mentioned in the introduction, our previous numerical studies [17-20] have shown that the onset of groove formation of a polymer is dominated by its compressive yield stress, which is strongly influenced by COF. Hossain et al. [20] carried out

experimental work on neat and Teflon coated PC and SAN systems to validate their FEM findings. They found that both increase in compressive yield stress and decrease in COF delayed the onset of groove formation. In the case of the model CPU systems, except for the absence of groove formation in CPU-PET, which will be discussed later, CPU-PC shows the earliest onset of groove formation. CPU-PES and CPU-PT both exhibit delayed onsets than CPU-PC. The onsets of groove formation of the model CPU systems match well their corresponding compressive yield stress values. Since the significant influence of COF on the onset of groove formation has been demonstrated in literature [20], the much lower COF of CPU-PT makes it most resistant to groove formation among the model systems. It is noted that since polymer beneath the scratch tip generally experiences a multi-axial compressive stress state during scratch process [20, 21], the application of uniaxial compressive properties to correlate with the onset of groove formation may oversimplify the situation, especially when dealing with soft PU elastomers that undergo deep penetration of scratch tip into the sample during scratching.

In terms of the cracking/material removal in the model CPU systems during scratch tests, numerical studies [17-19] have revealed that the material behind the scratch tip experiences a high magnitude of tensile stress during scratching. The direction of the tensile stress is the same with the scratch direction and parallel to the sample surface. As such, the stress state along the scratch direction on the surface region of the sample is dominated by uniaxial tension. As the normal load increases, the magnitude of the tensile stress behind the scratch tip will eventually reach and exceed the tensile strength

of the sample, thus causing cracking damage to develop. Due to the elastomeric nature of PU, crack tearing is likely to happen soon after the formation of cracks, which may result in material removal from the middle portion of the cracks. Thus, the onset of cracking/material removal of the model CPU systems is mainly dependent on their tensile strength values.

As the tensile true stress-strain curves have revealed, CPU-PET has the lowest tensile strength among all the model systems. For CPU-PC, CPU-PT and CPU-PES, they all possess much higher tensile strengths than CPU-PET. It is evident that the tensile strengths of the model CPU systems correspond well with their resistances to cracking/material removal damage. This finding indicates that the scratch resistance of PU elastomers to cracking/material removal can be improved by increasing their tensile strengths. It should be noted that the scratch process is complex, which depends on many factors, including the constitutive behavior of the material, surface roughness, COF, processing-induced anisotropy and others. For example, a higher COF can greatly increase the magnitude of tensile stress along the scratch path to cause premature cracking [20]. Therefore, it is necessary that the surface conditions among the material systems be kept the same for a meaningful structure-property relationship to be established.

Among all the model systems, CPU-PET is the only system that does not have scratch groove formation before onset of cracking/material removal. This is likely due to its low tensile strength, which is relatively close to its compressive yield stress. According to the FEM simulation performed by Jiang et al. [17], it can be seen that the

magnitude of the tensile stress behind the scratch tip develops faster than the magnitude of compressive stress beneath the scratch tip as the tip moves with an increasing normal load. In addition, the hydrostatic tension behind the scratch tip, which promotes brittle damage, is dramatically increased with increasing normal load, thus further facilitating cracking during scratch process. Furthermore, CPU-PET has a much lower elastic modulus than the other model systems that leads to a larger contact area between scratch tip and CPU-PET during scratching. The increase in contact area significantly decreases the compressive stress beneath the scratch tip for CPU-PET. Therefore, given the small difference between the tensile strength and compressive yield stress of CPU-PET, the tensile stress magnitude behind the scratch tip would reach its tensile strength limit first before the compressive stress magnitude beneath the scratch tip has a chance to reach its compressive yield stress value for groove formation. Consequently, this results in the absence of groove formation prior to the onset of cracking/material removal in CPU-PET. An in-depth analysis and discussion of this phenomenon will be subsequently reported using our FEM modeling study in the near future.

In the previous study of polymer scratch deformation [21], it has been shown that the scratch test at 100 mm/s speed can induce a strain rate as high as 1000 s^{-1} on or near the sample surface during scratching. Therefore, scratch tests at 100 mm/s speed were also performed on the model CPU systems to further validate the correlations found above between 1 mm/s speed scratch results and the quasi-static mechanical testing results. The critical normal loads for the onsets of groove formation and cracking/material removal at 100 mm/s scratch speed are shown in Figure 11(b). The

onsets of scratch-induced deformation in the model CPU systems at 100 mm/s scratch speed follow the same trend with those at 1 mm/s scratch speed, which confirms the validity of the correlations mentioned above. Scratch speed seems to have some influence on the onset of cracking/material removal where all the model systems exhibit earlier onsets of damages at a higher speed. This can be attributed to the fact that polymers generally behave in a more brittle fashion with increased scratch speed, thus facilitating the onset of brittle cracking damage. As scratch speed increases, the changes in the onset loads among the model systems appear to be related to their different damping behaviors and corresponding strain rate dependencies. The model system with a higher damping near room temperature tends to be more sensitive to testing rate, and thus a higher percent of change in the onset load with increased scratch speed. The damping behaviors have been reported to be responsible for the strain rate dependency in the mechanical properties of styrenic copolymers [9] and block copolymer modified epoxy [81], as well. Overall, the present correlation holds true for both scratch tests carried out at low speed and high speed.

The present study provides fundamental understanding on the polymer scratch process and offers fundamental insights into the design of scratch resistant PU elastomers. In addition, it highlights the importance of true stress-strain curve generation in determining the constitutive behaviors of soft elastomers. However, the constitutive behaviors of elastomers under multi-axial loading and high strain rate loading as high as 1000 s^{-1} could also play a significant role in influencing their scratch behavior. The temperature rise due to frictional heating during scratch process appears to be another

factor that can affect the scratch behavior of PU elastomers. These aspects of studies will be subjected to our future investigation.

2.5 Conclusions

The scratch behavior of a series of model CPU with variation in soft segment type was investigated. The incorporation of different kinds of soft segments in PU elastomers significantly alters their morphologies, surface properties, mechanical properties and the corresponding scratch behaviors. The fundamental structure-property relationships have been established by studying the model CPU systems. By varying the type and/or content of the chemical constituents in PU elastomer, it is possible to design scratch resistant PU elastomers that meet the needs of various engineering applications. Furthermore, the correlation between material properties and onsets of scratch-induced deformation has been quantitatively assessed based on the model CPU systems investigated. Once the relationship between applied load and stress value during scratch process is determined, the onsets of scratch-induced deformation can be quantitatively predicted without carrying out scratch test. The following conclusions can be drawn based on this study:

- PU elastomers with a higher degree of microphase separation, a more uniform hard segment domain size and a better ordering of hard segment domain possess improved tensile and compressive properties.
- The presence of moderate crystallinity in the soft segment of PU elastomers improves their tensile strength and tensile strain at break.

- Increasing the compressive yield stress and decreasing the COF of PU elastomers can delay the onset of scratch groove formation.
- Increasing the tensile strength and decreasing the COF of PU elastomers can enhance scratch resistance against cracking/material removal.
- PU elastomers with a more pronounced damping characteristic exhibit a higher COF when sliding against stainless steel and tend to be more sensitive to strain rate of testing.

CHAPTER III

MOISTURE EFFECT ON SCRATCH BEHAVIOR OF MODEL POLYURETHANE ELASTOMERS[†]

Most PU elastomers are subjected to moisture exposure during service, which may have significant influence on their scratch behavior. In this chapter, the effect of moisture exposure on scratch behavior of the model CPU systems is investigated. Since two model CPU systems contain less polar ether groups and the other two contain more polar ester groups in the soft segment polyols, it is expected that the absorbed moisture alters their surface characteristics, mechanical properties and the corresponding scratch behaviors in different fashions. Furthermore, a 3-D FEM modeling is conducted to further understand the observed scratch-induced deformation in the model systems.

3.1 Introduction

Numerous investigations have been carried out in the past to study the effect of moisture on the mechanical properties of different PU systems [82-87]. Huacuja-Sanchez et al. [82] conducted a water immersion study on a crosslinked PU system over a period of 15 days. They found that water caused a noticeable plasticization in the PU system as the shear modulus decreased and glass transition shifted to a lower temperature. Based on the IR spectra, they proposed that the plasticization effect was a

---

[†] Reprinted with permission from Xiao, S., Wang, H., Hu, F., & Sue, H. J. (2018). "Effect of moisture exposure on scratch behavior of model polyurethane elastomers." *Polymer*, 137, 209-221. Copyright [2018] by Elsevier.

result of substitution of urethane-urethane hydrogen bonds by water-urethane hydrogen bonds after exposure to water. A similar plasticization effect was observed in a study on a PU shape memory polymer done by Yang et al. [83]. With increasing period of immersion in deionized water, the uniaxial tensile behavior of the PU system shifted from a rigid ductile behavior to a rubber-like behavior, which was attributed to the increased mobility of molecular chains. Boubakri et al. [84] investigated the changes in mechanical properties of a thermoplastic polyurethane (TPU) system upon immersion in distilled water at different temperatures. Their results indicated that the equilibrium water uptake of TPU was increased accompanied by a significant reduction in tensile properties when the TPU system was immersed in water at high temperature. This degradation in properties was corroborated by scanning electron microscopy (SEM) observation on the tensile fracture surface that small voids and cracks formed in the matrix with increasing water immersion temperature. However, the field of PU elastomers is still mostly unexplored. Namely, fundamental understanding on how the moisture exposure affects the material properties and the corresponding scratch behavior of PU elastomers is still lacking.

The present study focuses on gaining fundamental insight into the effect of long-term moisture exposure on structure-property relationships and on scratch behavior of PU elastomers by investigating a set of well-controlled model CPU systems under dry and water-saturated conditions. To achieve this objective, the water-saturated model CPU systems were characterized by various spectroscopy, microscopy and mechanical testings, and compared with the dry model systems, which was reported earlier. In

addition, 3-D FEM modeling was employed to further understand the observed scratch-induced deformation in the model systems. It is anticipated that fundamental understanding can thus be gained on how moisture exposure influences the scratch behavior of polymers.

3.2 Materials and Methods

3.2.1 Materials

BASF Polyurethane Specialties (China) Co. Ltd. (Shanghai, China) provided four well-controlled model CPU systems for this study (Table 3). The four model systems were designed to contain four different types of soft segments: polytetramethylene ether glycol (PT), polycaprolactone (PC), ethylene oxide/propylene oxide based polyol (PET) and adipic anhydride based polyol (PES). However, the hard segment of the model systems was kept the same to consist of the same diisocyanate and chain extender, 4,4'-methylene diphenyl diisocyanate (MDI) and 1,4-butane diol (BDO). The chemical structures of the soft segments and hard segment are given elsewhere [88]. It should be noted that CPU-PT and CPU-PET were polyether-based PU systems, while CPU-PC and CPU-PES were polyester-based PU systems. The presence of the more polar ester groups in the backbones of polycaprolactone and adipate soft segments was intended to increase the polarity of CPU-PC and CPU-PES, respectively. The model CPU systems were prepared into cast plaques with dimensions of 150 mm × 100 mm × 14 mm by BASF. To remove pre-existing moisture and residual stresses in the as-received plaques, all the specimens were dried in a vacuum oven (30 mm Hg of vacuum

pressure) in between two smooth glass plates at 80 ºC for 6 h, then left to slowly cool overnight to room temperature. The detailed physical information of the model systems is also listed in the literature [88].

Table 3. Chemical component of the model CPU systems. Reprinted with permission from Polymer 137 (2018) 209-221. Copyright [2018] by Elsevier.

	Hard Segment		**Soft Segment**
	Diisocyanate	**Chain Extender**	
CPU-PT	4,4'-methylene diphenyl diisocyanate (MDI)	1,4-butane diol (BDO)	Polytetramethylene ether glycol **(Polyether-based)**
CPU-PC			Polycaprolactone **(Polyester-based)**
CPU-PET			Ethylene oxide/propylene oxide based polyol **(Polyether-based)**
CPU-PES			Adipic anhydride based polyol **(Polyester-based)**

3.2.2 Environmental Conditioning

Thin sheets of specimens with nominal dimensions of 30 mm × 10 mm × 3 mm were cut from the plaques by razor blade for the study of water absorption and diffusion behaviors of the model systems. After cutting, all the sides of the specimens were carefully polished by 4000 grit number polishing paper to remove any attached debris and to make the surfaces smooth. Thereafter, the specimens were firstly dried in a vacuum oven according to the procedure described above and weighed using a high precision analytical balance (Sartorius Research R200D, 0.01 mg readability). The

specimens were then immersed in a sealed container with deionized water at 30 °C to accelerate water uptake. Over a period of 3 weeks, the specimens were removed from the deionized water and weighed periodically. The percent weight gain was used to monitor the water absorption behavior until saturation. The amounts of equilibrium moisture uptake for the model CPU systems were determined when the specimens reached water saturation, i.e., the percent weight gain leveled off and reached a plateau value as a function of time at 30 °C.

The specimens for the following experiments were also environmentally conditioned in the same fashion. To confirm if the specimens have reached water saturation, thermogravimetric analysis (TGA) was utilized to measure the water content in the specimens before experimentation. A TGA test (TA Instrument Q500) was carried out on each of the specimens in air. A small piece of the specimen (~10 mg) was heated from 30 °C to 900 °C at a rate of 10 °C/min. The stabilized weight loss of the water-immersed model systems at around 250 °C was used to determine the amount of absorbed water in the specimens.

3.2.3 ATR-FTIR

A Nicolet^{TM} 380 FT-IR Spectrometer equipped with an OMNI-Sampler^{TM} ATR sampling accessory was used to record the FTIR spectra of the model systems under each environmental condition. A spectral range of 700-4000 cm^{-1} with a resolution of 4 cm^{-1} was employed for the measurement. A total of 128 scans were collected for each specimen.

3.2.4 Contact Angle Measurement

All the model CPU systems under dry and water-saturated conditions were evaluated to assess the changes in contact angle before and after exposure to moisture. The specimens were placed on a flat and even surface with minimal vibration under ambient conditions and 50% relative humidity. A 1 ml syringe fitted with a 27.5 gauge needle was used to deposit several single droplets of deionized water on the specimen surface. The gauge needle was maintained a fixed distance (3 mm) from the specimen surface to deposit the water droplets. Each droplet was positioned at least 20 mm away from the others to prevent interference.

Using a digital microscope (Dino-Lite AM-311S), images of the droplets on the specimen surface were captured. The captured images were then processed (grayscaled, sharpened and inverted colors) using ImageJ software (https://imagej.nih.gov/ij/) for the contact angle measurement. The DropSnake plugin [89] in ImageJ was employed to measure the contact angles on both sides of each droplet with respect to the specimen surface. To obtain an average value of the contact angle, five droplets were measured for each specimen. The changes in contact angle of all the model systems before and after exposure to moisture were then evaluated.

3.2.5 COF Measurement

The COF between the water-saturated model CPU systems and stainless steel surface were determined using a commercial scratch machine (Scratch 5, Surface Machine Systems, LLC) built according to the ASTM D7027/ISO 19252 standard. A

stainless steel flat tip with large surface area (10 mm × 10 mm) and a low constant normal load (5 N = 0.05 MPa) were applied for the tests to prevent additional material deformation that will compromise the COF measurements. Compressed nitrogen gas was used to remove any possible contaminants on the stainless steel flat tip and specimen surfaces before each test. Three tests were performed on each water-saturated model system to obtain an average value of the COF.

3.2.6 Tensile True Stress-strain Curve Generation

As it has been demonstrated in the previous study of the model CPU systems in dry condition [88], true stress-strain curve generation is necessary to precisely characterize the tensile behavior of the model systems due to the large straining both in tensile and lateral directions of the specimens during stretching. Therefore, the same setup for the measurement of dry specimens, which features a custom-built tensile test fixture [64] with a Digital Image Correlation (DIC) video system, was utilized to generate the uniaxial tensile true stress-strain curves of the water-saturated model CPU systems.

The test specimens were thin sheets of CPU with dimensions of 180 mm × 150 mm × 2 mm. A dumbbell shape with 16 mm gauge length and 8 mm ligament width was then cut from the sheets by razor blade, and the cutting edges were carefully polished by 4000 grit number polishing paper to remove any possible surface defects. The random speckle patterns required for the DIC analysis were applied on the gauge section of the specimens using a black ink permanent marker. Afterwards, the specimens were

environmental conditioned in deionized water according to the above-mentioned procedure until saturation.

The custom-built tensile test fixture was loaded onto a MTS Insight® universal testing machine to perform the tensile tests at a crosshead speed of 5 mm/min. During the test, the variation of speckle patterns on the gauge section was tracked by a Canon EOS 5D Mark II DSLR camera, and then the true strains in both tensile and lateral directions were generated by a VIC-2D™ DIC software package. Subsequently, by dividing the applied load by the measured instantaneous cross-sectional area, the true stress in tensile direction was calculated. From the measured true strain in lateral direction, the cross-sectional area reduction rates were tracked throughout the test. The maximum rate of cross-sectional area reduction was used to determine the onset of yielding during stretching. And the specimen was stretched to break to determine the tensile strength.

3.2.7 Scratch Test

Scratch tests were conducted according to the ASTM D7027/ISO 19252 standard by using a linearly increasing normal load of 1-300 N over a scratch length of 100 mm at two constant scratch speeds of 1 mm/s and 100 mm/s. The correlation between scratch behavior and quasi-static constitutive behavior of the water-saturated model CPU systems was investigated based on the scratch tests at 1 mm/s. The strain rate effect on the scratch behavior of the water-saturated model CPU systems was studied by comparing the scratch tests at 100 mm/s to the scratch tests at 1 mm/s. A stainless steel

conical scratch tip [88], which features a continuous geometry with a 1 mm diameter sphere attached to a cone, was used for the tests. Compressed nitrogen gas was used to remove any possible contaminants on the scratch tip and specimen surfaces before each test. Three scratch tests were performed at each speed on each water-saturated model system to obtain the average values of the onset loads of damage transitions.

3.2.8 Post-scratch Analysis

The scratch-induced damages on all the water-saturated model CPU systems were analyzed by a Keyence® VK9700 violet laser scanning confocal microscope (VLSCM). Since PU elastomers exhibit instantaneous elastic recovery on the recoverable portion of deformation upon scratching, the timing for observing the scratch-induced damages is not critical. The topographical images of the model systems taken by VLSCM under 20 × magnification were used to observe the geometries of the scratch grooves and damage features. The onset points of scratch groove formation and cracking/material removal damage were located by the VLSCM, and then the corresponding critical normal loads for the onsets of groove formation and cracking/material removal damage were determined through the applied normal load-travel distance curves.

3.3 Results and Discussion

3.3.1 Moisture Absorption

The absorption of moisture for all the model CPU systems as a function of days immersed in deionized water is shown in Figure 13. The percent weight gains indicate that the majority of moisture uptake occurred within the first few days of immersion. This is most likely due to the gradual diffusion of absorbed moisture from surface to the core. The moisture absorption was conducted until water saturation was reached for all the model systems, which took approximately 2 weeks. After that, the percent weight gain leveled off and reached a plateau. The amounts for the equilibrium moisture uptake of the model CPU systems are summarized in Figure 14. Careful analysis suggests that the incorporation of different soft segments in PU elastomers has direct influence on the amount of moisture uptake at equilibrium. This finding also sheds some light on the different moisture absorption and diffusion mechanisms of PU elastomers resulted from their greatly varied polarities. And, this difference is expected to affect their material properties and scratch behaviors in different fashions upon exposure to moisture.

TGA was used as a complementary tool to confirm if all the immersed specimens have reached water saturation, i.e., equilibrium moisture uptake, before conducting further characterization. A typical TGA curve of each water-saturated model CPU systems is shown in Figure 15. The water content was determined and shown in the figure that it had a similar value with the equilibrium moisture uptake measured in the moisture absorption study for all the model systems. The water contents of the water-saturated model CPU systems determined by TGA were also summarized in Figure 14.

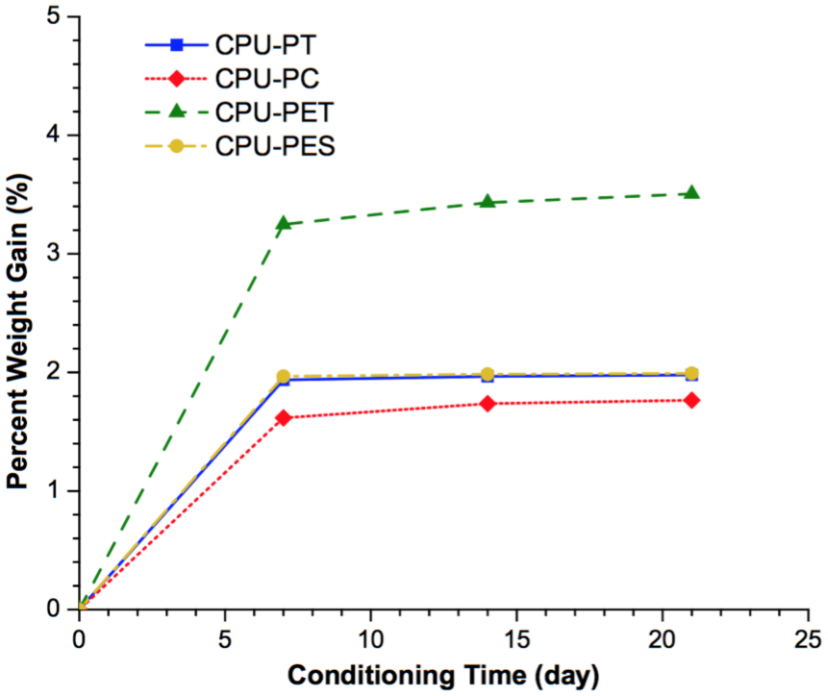

Figure 13. Percent weight gain of the model CPU systems as a function of days immersed in deionized water. Reprinted with permission from Polymer 137 (2018) 209-221. Copyright [2018] by Elsevier.

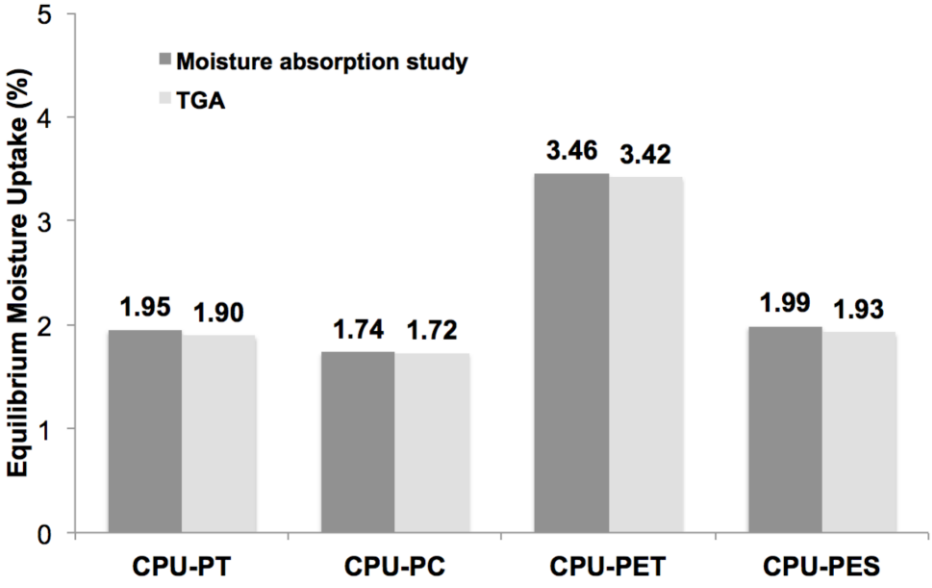

Figure 14. Equilibrium moisture uptake of the model CPU systems. Reprinted with permission from Polymer 137 (2018) 209-221. Copyright [2018] by Elsevier.

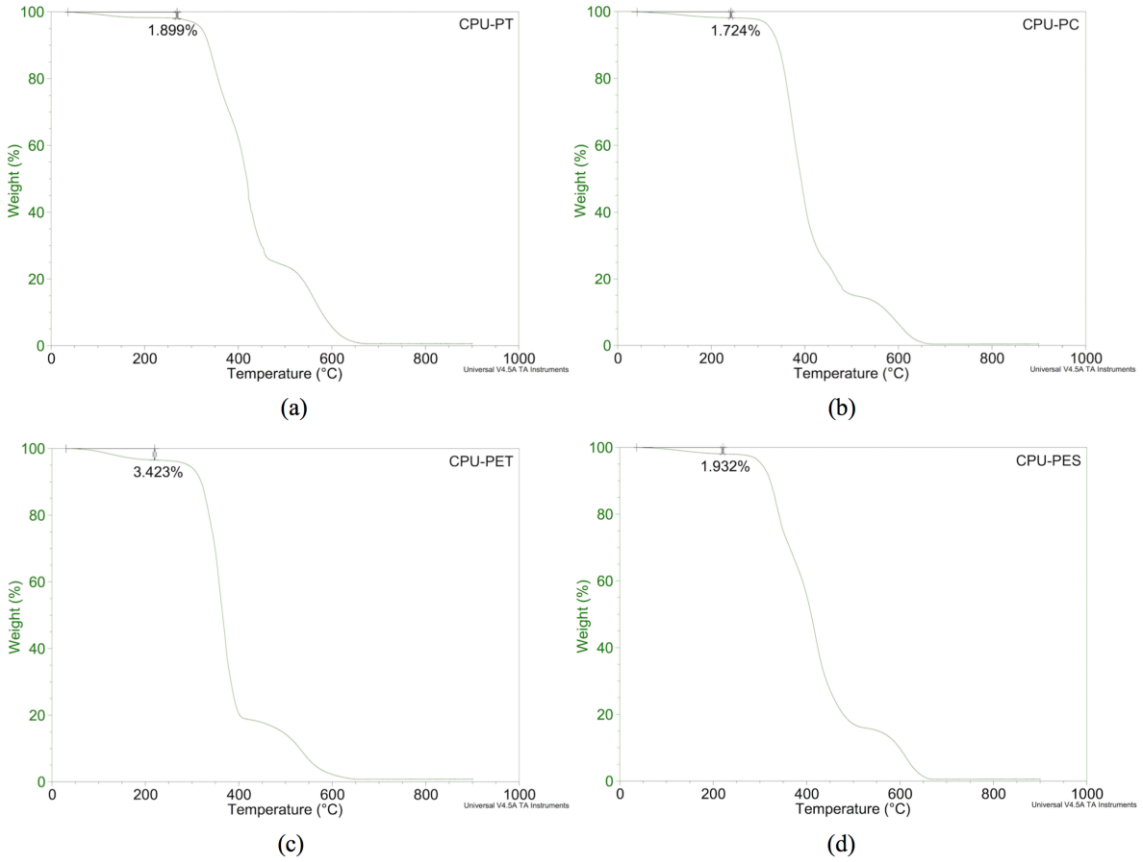

Figure 15. Determination of water content in water-saturated (a) CPU-PT, (b) CPU-PC, (c) CPU-PET and (d) CPU-PES using TGA. Reprinted with permission from Polymer 137 (2018) 209-221. Copyright [2018] by Elsevier.

3.3.2 ATR-FTIR

To detect if the absorbed moisture lead to any changes of the functional groups in the model CPU systems, ATR-FTIR spectra of all the model systems after exposure to moisture were obtained and compared with the spectra of the dry model systems. Any new appearance or disappearance of the absorption peaks can be an evidence of chemical structure changes in the system. In addition, to investigate if the moisture-induced changes in CPU structure are reversible, IR spectroscopic analysis was also

performed on the re-dried model systems. To achieve the re-dried condition, the water-saturated specimens were dried in a vacuum oven (30 mm Hg of vacuum pressure) at 80 ºC for 48 h, then left to slowly cool overnight to room temperature. The ATR-FTIR spectra of all the model CPU systems in dry [88], water-saturated and re-dried conditions are shown in Figure 16.

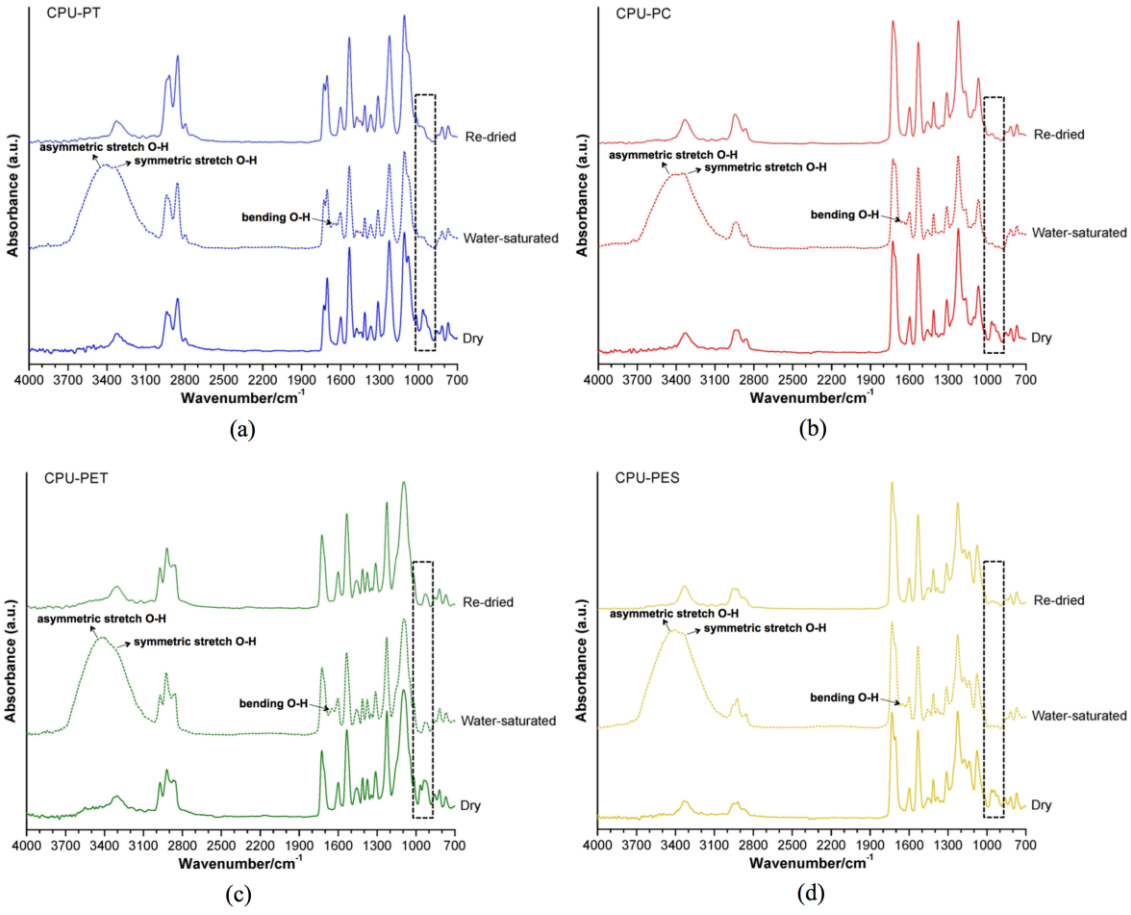

Figure 16. ATR-FTIR spectra of (a) CPU-PT, (b) CPU-PC, (c) CPU-PET and (d) CPU-PES in dry, water-saturated and re-dried conditions. Reprinted with permission from Polymer 137 (2018) 209-221. Copyright [2018] by Elsevier.

As shown in the figure, under water-saturated condition, the absorption peaks due to asymmetric stretching, symmetric stretching and bending of O-H groups in free water were detected. Meanwhile, a missing or diminished peak was observed at around 940 cm^{-1} of the spectrum. After re-dry of the specimens, all the peaks due to free water were removed. However, the missing or diminished peak was not recovered. As this absorption peak is found in the fingerprint region of IR spectrum, which contains a series of very complicated absorption peaks, limited research has been done in the past related to the fingerprint region of the IR spectrum of PU elastomers. Zhou et al. [90] proposed that the decrease in intensity or disappearance of this peak at around 940 cm^{-1} was due to the crosslinking reaction of unsaturated C=C double bonds during environmental conditioning. Thomas et al. [91] also examined the stability of this double bonds absorption peak to demonstrate the stability of PU in oxidative and lipid environments. However, the chemical composition of different PU elastomers varies significantly and any subtle vibration or deformation of the molecule may cause peak changes within the fingerprint region, detailed analysis of the peak changes in this region is beyond the scope of this study and should be addressed separately. To sum up, the ATR-FTIR spectra of the model CPU systems showed that irreversible changes had occurred in the CPU matrix upon exposure to moisture. The following studies will investigate how these moisture-induced changes in the structure influence the material properties of different model CPU systems.

3.3.3 Contact Angle Measurement

The contact angles of deionized water droplets on all the model CPU systems under dry and water-saturated conditions were determined and shown in Figure 17. The difference in contact angles among the model systems is a good indicator of their relative surface polarity, since a lower contact angle implies greater wettability and higher surface polarity. As shown in Figure 17, under both conditions, CPU-PC shows the lowest contact angle among the four model systems, followed by CPU-PES, CPU-PT, and CPU-PET sequentially. This indicates that CPU-PC has the highest surface polarity among the model CPU systems. As the CPU specimens absorbed moisture, the contact angles of all the model systems were decreased due to the increased wettability of the surface. However, different model CPU systems showed different degrees of reduction in contact angle upon exposure to moisture. The model systems with higher polarity exhibited more reduction in contact angle. This is attributed to the formation of water clusters on the surface of more polar model CPU systems that facilitated the increase in wettability. Similar phenomenon was also observed in PMMA with different polarities that the effect of moisture on contact angle was maximized in the most polar PMMA grade [22].

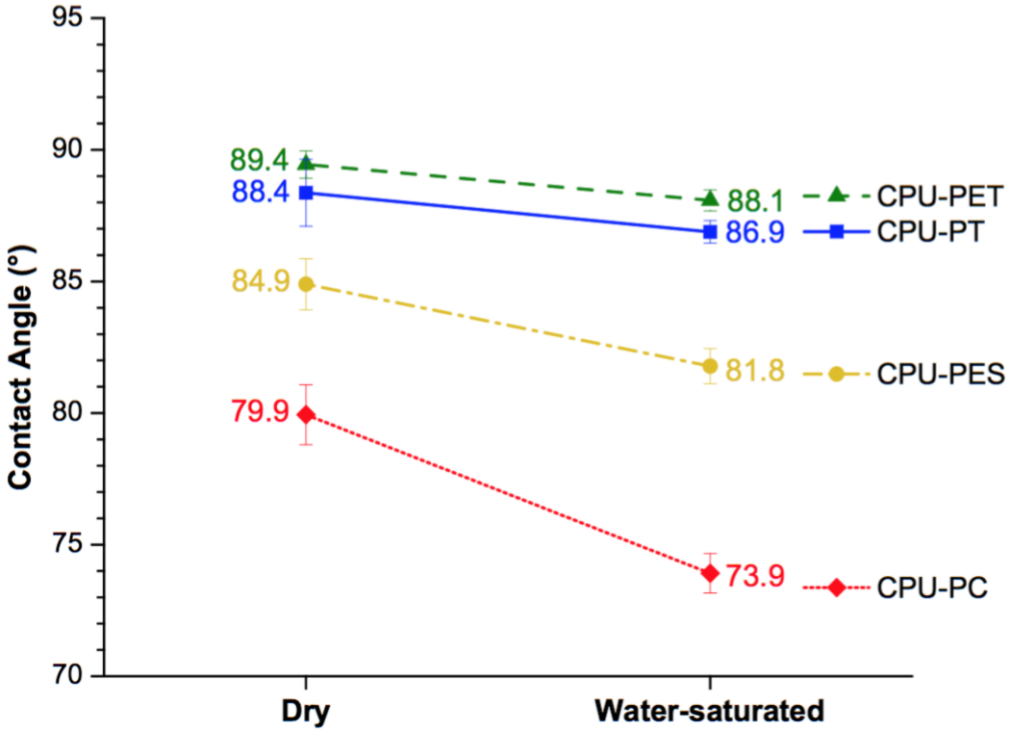

Figure 17. Contact angle measurements of the model CPU systems in dry and water-saturated conditions. Reprinted with permission from Polymer 137 (2018) 209-221. Copyright [2018] by Elsevier.

The effect of polarity on the moisture absorption and diffusion mechanisms of various polymers has been quite extensively investigated in the past [23-28]. Depending on the polarity of the polymer, the absorption and diffusion of water molecules in the polymer matrix will be dominated by either free volume or polar bonding sites in the matrix [22]. For polymers with low polarity, water molecules have a tendency to distribute uniformly throughout the free volume within the polymer matrix and serve as plasticizer to weaken the mechanical properties. But for polymers with high polarity, the interaction between water molecules and polar sites is preferred that leads to the formation of hydrogen bonding and prompts the formation of water clusters on the

surface. The water clustering phenomenon has been demonstrated in many PU systems when the environmental water activity is high [92-96]. Water activity is a measurement of humidity. The multiplication of water activity by 100% gives the equilibrium relative humidity of the environment. In the current study, since the CPU specimens were immersed in deionized water during conditioning, which provided the highest water activity and made the formation of water clusters possible.

The study conducted by Mondal et al. [97] found that due to the presence of polar ester groups in polycaprolactone soft segment, strong interaction between polymer chains occurred that restricted the movement of segmental structure and hindered the free volume size and concentration in this kind of polyester-based PU systems. In contrast, polyether-based PU systems, which had polytetramethylene ether glycol as soft segment, showed much higher free volume size and concentration. Therefore, it can be presumed that in the present study, the moisture absorption and diffusion of the polyether-based PU systems, CPU-PT and CPU-PET, were dominated by the abundant of free volume in the matrix. However, due to the existence of polar ester groups in the soft segments of CPU-PC and CPU-PES, the moisture absorption and diffusion of these two polyester-based systems were governed by the polar bonding sites in the matrix. Consequently, CPU-PC and CPU-PES showed more reduction in contact angle than the other two model systems upon exposure to moisture, since the interaction between water molecules and polar sites promoted water clustering on the surface and further increased the wettability. This assumption is in agreement with the equilibrium moisture uptake of

the model CPU systems that the polyether-based systems showed generally higher moisture uptake as a result of their high free volume content.

This different water diffusion and absorption mechanisms among the model CPU systems may result in different changes in their material properties and scratch behaviors upon exposure to moisture.

3.3.4 COF Measurement

The COF of all the model CPU systems after the specimens achieved water saturation were determined and shown in Figure 18. For comparison with the previously obtained results in dry condition, the COF of the dry model CPU systems [88] were also presented in the same figure. After exposure to moisture, CPU-PT and CPU-PET exhibited noticeable increases in COF. On the contrary, CPU-PC showed a big drop and CPU-PES showed almost no change in COF. This finding suggested that the absorbed moisture provided more significant lubrication effect on the surface of the model CPU system with a higher polarity. The early discussion in contact angle measurement supported this argument. Due to the interaction between water molecules and polar bonding sites, clustering of water occurred on the surface that resulted in more reduction in contact angle for the model systems with higher polarity. The aggregated water molecules also acted as lubricant to reduce the surface friction of the model systems. This lubrication effect of absorbed moisture in high polar systems was found in the studies of SAN [13] and PMMA [22], as well. However, for the model CPU system with a lower polarity, as the subsequent section will reveal, the uniformly distributed water

molecules in the free volume of the matrix served as plasticizer to degrade the mechanical properties and surface mechanical integrity, and thus leading to the increase in surface friction.

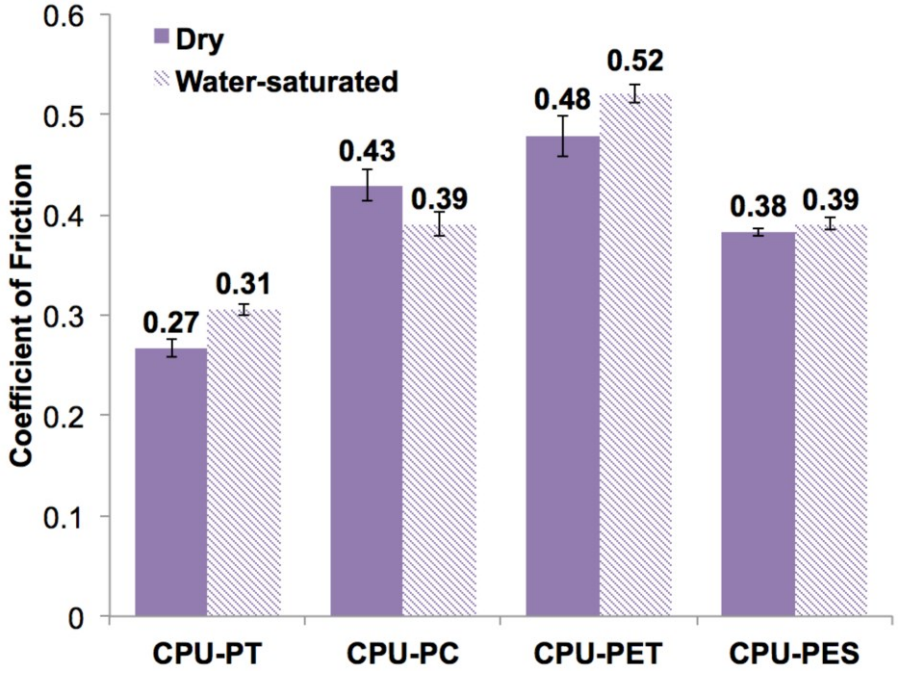

Figure 18. Coefficient of friction of the model CPU systems in dry and water-saturated conditions. Reprinted with permission from Polymer 137 (2018) 209-221. Copyright [2018] by Elsevier.

3.3.5 Tensile True Stress-strain Behavior

The uniaxial tensile true stress-strain curves and some key uniaxial tensile properties of the water-saturated model CPU systems obtained in this study are shown in Figure 19 and Table 4, respectively, and compared with those of the dry model systems found in the previous study [88]. As shown in the figure and table, different model CPU systems exhibited different degrees of changes in uniaxial tensile properties upon

exposure to moisture. The two polyether-based model systems, CPU-PT and CPU-PET, showed significant deterioration in tensile strengths, yield stresses and moduli upon absorption of moisture in the matrix. In comparison, the two polyester-based model systems, CPU-PC and CPU-PES, retained their uniaxial tensile properties after water saturation with a slight increase in ductility. This finding further supported the early argument that the moisture absorption and diffusion of the polyether-based PU systems with low polarity tended to be dominated by the high free volume content in the matrix. The water molecules throughout the free volume plasticized the matrix and contributed to the formation of defects, and thus resulting in the deterioration in tensile properties, particularly in tensile strength. As a result of the degradation, surface mechanical integrity was also affected and surface friction increased as demonstrated in the former section. By contrast, owing to the limited free volume in the polar polyester-based PU systems [97], the plasticization effect of absorbed moisture was minimized.

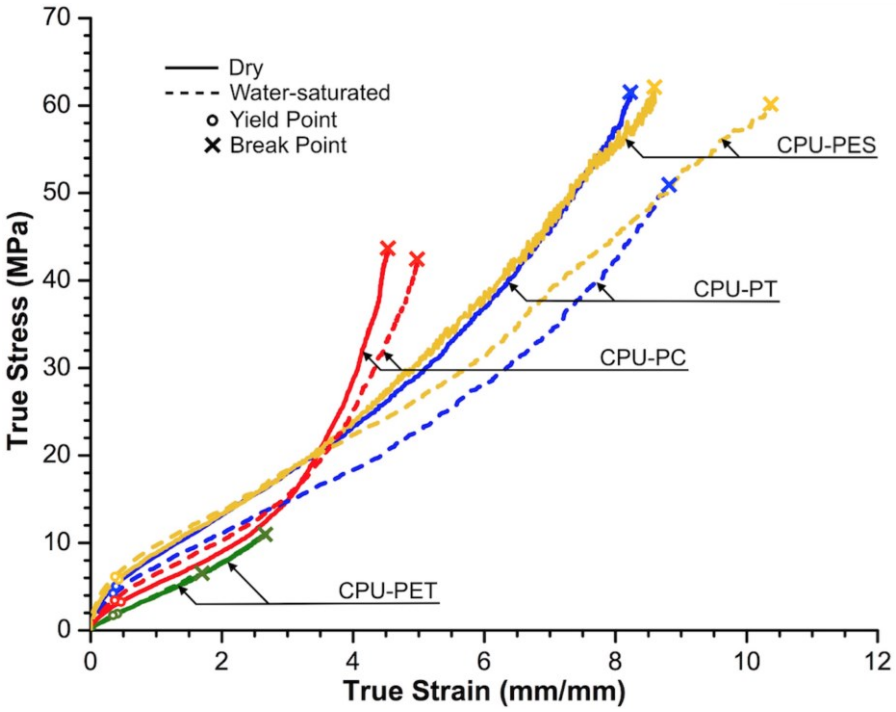

Figure 19. Tensile true stress-strain curves of the model CPU systems in dry and water-saturated conditions. Reprinted with permission from Polymer 137 (2018) 209-221. Copyright [2018] by Elsevier.

Table 4. Variation in uniaxial tensile properties of the model CPU systems before and after exposure to moisture. Reprinted with permission from Polymer 137 (2018) 209-221. Copyright [2018] by Elsevier.

		Polyether-based		**Polyester-based**	
		CPU-PT	**CPU-PET**	**CPU-PC**	**CPU-PES**
Dry	Tensile modulus (MPa)	16.2 ± 1.2	6.0 ± 0.4	9.4 ± 0.7	17.0 ± 0.8
	Tensile yield stress (MPa)	5.0 ± 0.3	1.9 ± 0.2	3.0 ± 0.1	5.3 ± 0.2
	Tensile strength (MPa)	63.7 ± 2.7	10.3 ± 1.3	45.5 ± 3.3	65.2 ± 4.1
Water-saturated	Tensile modulus (MPa)	14.5 ± 0.8	5.9 ± 0.3	9.7 ± 0.8	17.1 ± 0.8
	Tensile yield stress (MPa)	4.4 ± 0.6	1.8 ± 0.1	3.1 ± 0.3	5.3 ± 0.4
	Tensile strength (MPa)	53.6 ± 3.6	6.3 ± 0.3	44.3 ± 5.1	64.1 ± 5.5

3.3.6 Scratch Behavior

As the scratch normal load increased linearly during the tests of the model CPU systems, scratch groove formed along the scratch path first. With further increase in normal load, scratch damage transited from scratch groove to periodic cracking along with material removal. The critical normal loads for the onsets of these scratch-induced damages in the water-saturated model CPU systems at two scratching speeds, 1 mm/s and 100 mm/s, were determined and shown in Figure 20(a) and 20(b), respectively, and compared with those of the dry model systems obtained in the previous study [88].

For the groove formation during scratching, it has been shown that the increase in compressive yield stress and decrease in COF improve the resistance of PU elastomers to this kind of scratch-induced deformation [88]. However, as shown in Figure 20, since the onsets of groove formation for all the model systems at both low and high speeds did not exhibit big changes after water saturation, it was presumed that the compressive properties of the model systems were not affected by the moisture significantly, and thus not investigated in the present study. The variation in COF of the model systems upon exposure to moisture was sufficient to account for the minor changes in the onsets of groove formation of the model systems after water saturation, such as the decrease in the COF of CPU-PC contributed to a slightly delayed onset of scratch groove at both speeds.

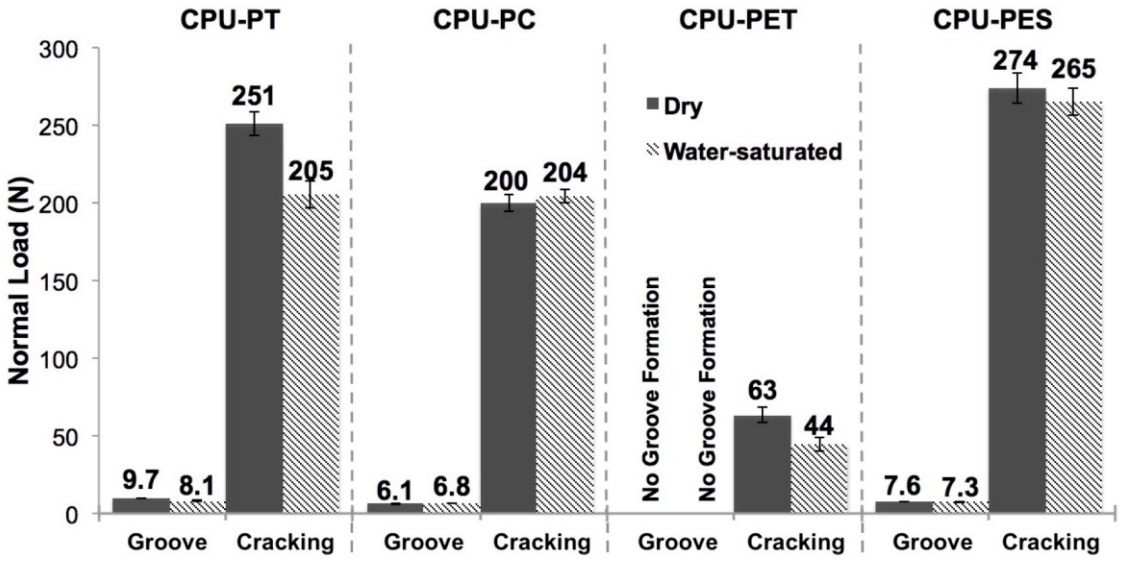

(a)

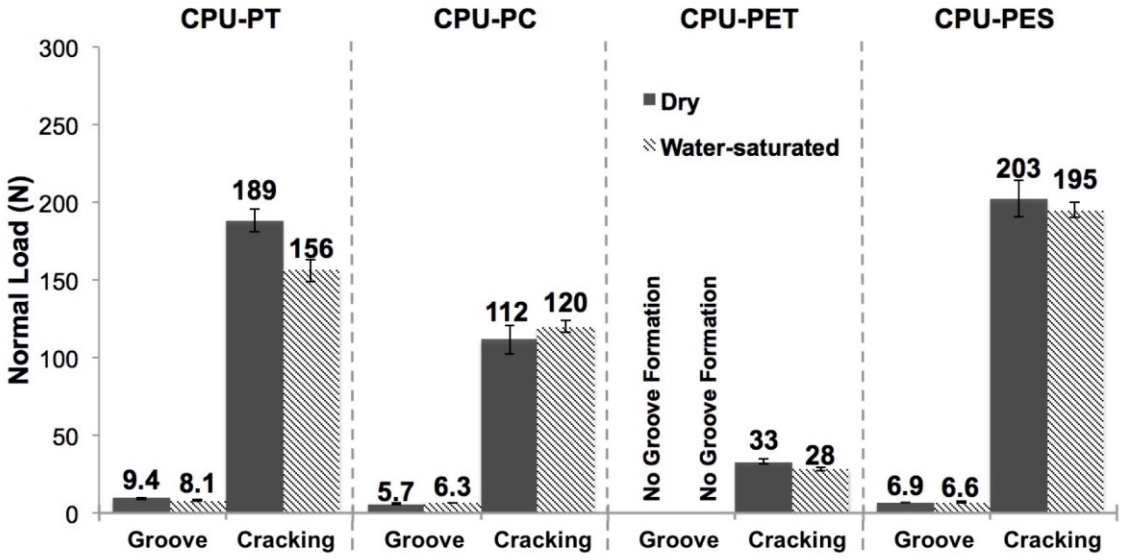

(b)

Figure 20. Critical normal loads for onset of scratch damages in the dry and water-saturated model CPU systems at (a) 1 mm/s and (b) 100 mm/s scratch speeds. Reprinted with permission from Polymer 137 (2018) 209-221. Copyright [2018] by Elsevier.

It is noted that the surface topography of the scratch grooves of the model CPU systems showed two interesting phenomena. For CPU-PT, CPU-PC and CPU-PES, regardless of the environmental condition or scratching speed, scratch groove formed along the scratch path. Moreover, with increasing normal load, a slight surface bulging appeared in the mid-portion of the scratch groove, as shown in Figure 21(a). This bulging phenomenon of scratch groove is unique to the scratch behavior of PU elastomers, as it has never been observed in the scratch studies of other commonly known polymers in the past. On the contrary, CPU-PET did not show any scratch groove formation before the onset of cracking/material removal disregarding the environmental condition or scratching speed, as shown in Figure 21(b). Nonetheless, it did exhibit a much earlier onset of cracking/material removal compared to the other three model systems. These two distinct scratch-related phenomena in the scratch groove region of the model CPU systems will be further discussed based on the findings obtained from FEM modeling.

For the cracking/material removal during scratching, the optical image and 2-D height profile of the onset of cracking/material removal in water-saturated CPU-PET is shown in Figure 22 as an example. Similar type of cracking/material removal damage was detected among the model CPU systems irrespective of environmental condition or scratching speed. It has been shown that the increase in tensile strength and decrease in COF enhance the scratch resistance of PU elastomers against cracking/material removal [88]. As shown in Figure 20, it is apparent that in the present study, upon exposure to moisture, the deterioration in tensile strength and increase in COF of the two polyether-

based model systems, CPU-PT and CPU-PET, resulted in earlier onset of cracking/material removal during scratch of them at both speeds. The relatively stable tensile strengths of the two polyester-based model systems, CPU-PC and CPU-PES, before and after water saturation led to nearly identical onset loads for cracking/material removal in dry and water-saturated conditions. Furthermore, the decrease in COF of CPU-PC upon exposure to moisture even made its scratch resistance against cracking/material removal slightly improved, which was similar to its slightly improved resistance against groove formation in water-saturated condition. It should be noted that the absorbed moisture had the same effect on the scratch behavior of the model systems at low and high speeds of scratching, which indicated that the absorbed moisture did not influence the strain rate dependency of the model systems significantly, if any.

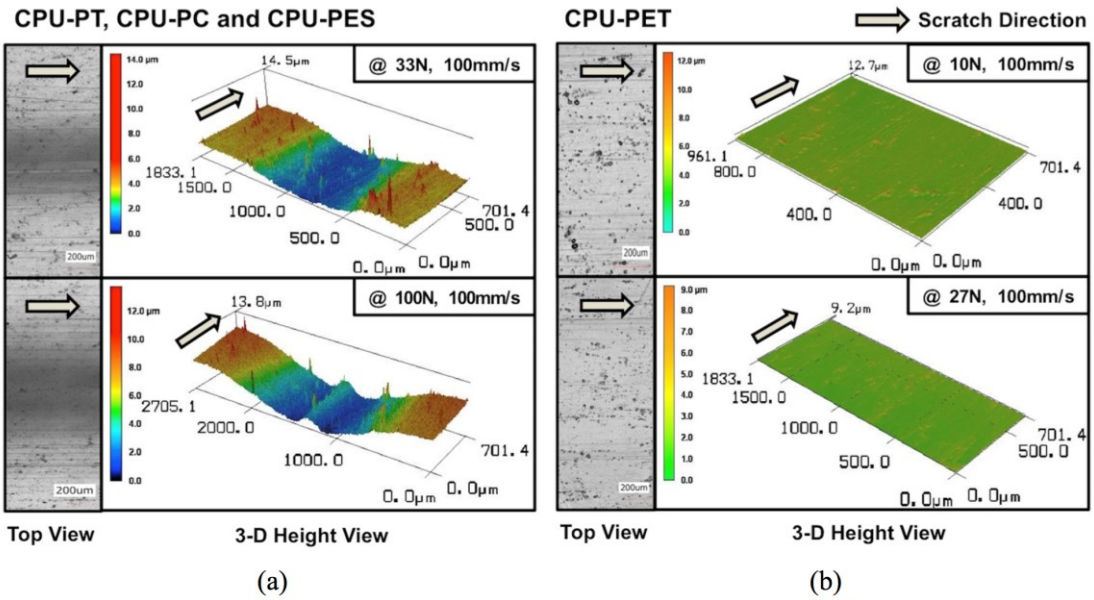

Figure 21. (a) Bulging phenomenon of scratch groove in CPU-PT, CPU-PC and CPU-PES; (b) absence of scratch groove in CPU-PET. Reprinted with permission from Polymer 137 (2018) 209-221. Copyright [2018] by Elsevier.

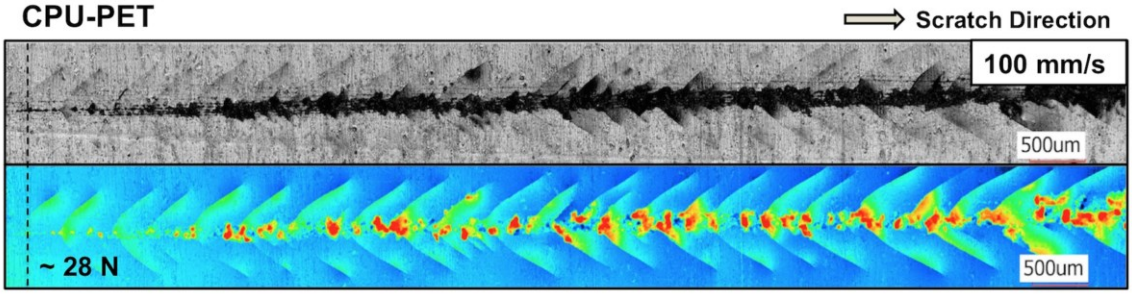

Figure 22. Example optical image and height profile of onset of cracking/material removal in the model CPU systems (water-saturated CPU-PET tested at 100 mm/s scratch speed is shown). Reprinted with permission from Polymer 137 (2018) 209-221. Copyright [2018] by Elsevier.

The above findings revealed that moisture had different influences on the scratch behaviors of PU elastomers if they had different chemical compositions, such as the varied soft segment types investigated in the present study. In addition, these findings further confirmed the correlations between intrinsic material properties and scratch behaviors of PU elastomers found in the previous study.

3.4 FEM Modeling

To better understand the unique bulging phenomenon of scratch groove and the absence of scratch groove observed in the scratch tests of the model CPU systems, 3-D FEM modeling of the scratch process was conducted using a commercial finite element package ABAQUS® 6.14 [98]. Extensive FEM modeling efforts have been carried out in the past to gain in-depth understandings on the scratch behaviors of different polymeric systems through the analysis of stress and plastic strain profiles [16-18, 20, 21, 99-101].

The dimensions and boundary conditions of the model used in this study are shown in Figure 23. A plane of symmetry along the scratch path direction was employed

and half of the model was simulated to save the computational time. The nodes on the two ends of the model were restrained in all directions to simulate the clamping condition at the boundaries. The nodes on the symmetry plane and bottom surface were restrained in the normal direction (x) and vertical direction (z), respectively, to prevent model translation. Eight-node 3D linear brick elements (C3D8R) were applied for the modeling. A fine meshing with 256 elements was utilized only across a critical distance between points A and B shown in Figure 23 to obtain sufficient accuracy of the results within a reasonable computational time. Distortion control was used to prevent elements from inverting or distorting excessively during the simulation. The scratch tip was modeled as a rigid body with a 1 mm diameter sphere attached on the bottom. Dynamic stress analysis of ABAQUS/Explicit was employed to simulate the dynamic scratching process. The heat generation during scratching and time-dependent viscoelastic response of polymeric materials were found to be insignificant for our purposes and were not considered in this study for simplification of the simulation [20, 21].

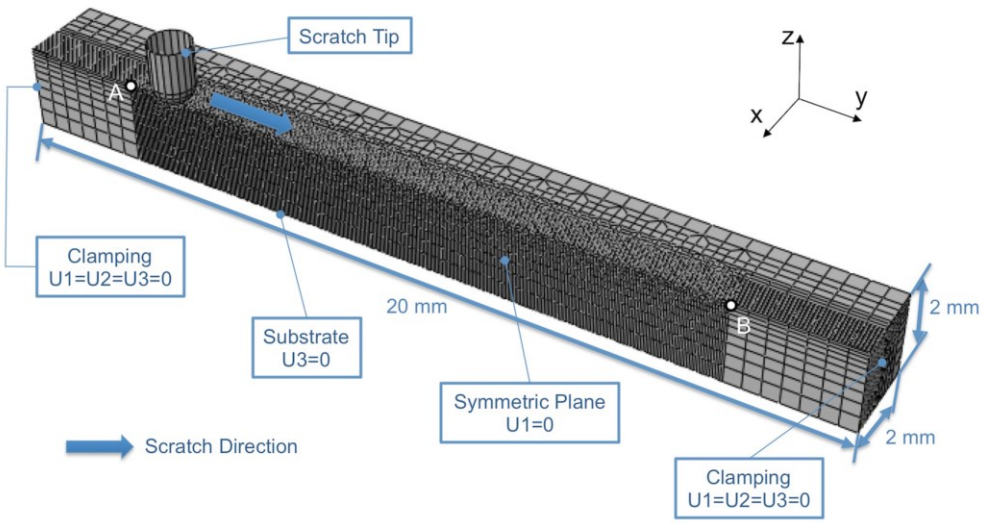

Figure 23. Dimensions and boundary conditions of the FEM model. Reprinted with permission from Polymer 137 (2018) 209-221. Copyright [2018] by Elsevier.

To model the ASTM/ISO standard scratch test, the simulation was performed by applying a linearly increasing normal load along the scratch path. The rigid tip moved over a distance of 12 mm at a constant speed of 100 mm/s during the scratching process to reduce computational time of the simulation. As the time-dependent response of the model was not considered in the simulation, the modeling at 100 mm/s scratching speed was adequate to represent the observed scratch behavior of the model CPU systems at both low and high speeds of the experiments. Isotropic Coulomb friction model was applied to define the frictional behavior of the two contacting surfaces.

Since the scratch groove formation is known to be dominated by the compressive stress beneath the tip and the COF during scratching [88], the constitutive properties of the model CPU systems were obtained from the uniaxial compressive true stress-strain generation [88], and the frictional properties were obtained from the COF measurement mentioned above. Representative constitutive and frictional properties of CPU-PES and

CPU-PET were selected from those of the model CPU systems and introduced in the FEM model to investigate the observed bulging phenomenon of scratch groove and the absence of scratch groove during experiments, respectively. It is noted that CPU-PES has the highest elastic modulus while CPU-PET has the lowest elastic modulus among the model CPU systems. For comparison, the scratch simulation was also carried out on polypropylene (PP) [18, 101] to learn the difference in scratch behaviors between PU elastomers and other commonly known polymers. For clarity, the material properties used in the simulation are listed in Table 5.

Table 5. Material properties used in the FEM simulation of the scratch test. Reprinted with permission from Polymer 137 (2018) 209-221. Copyright [2018] by Elsevier.

	CPU-PES	**CPU-PET**	**Polypropylene**
Elastic modulus	18.2 MPa	7.3 MPa	1.5 GPa
Yield stress	7.5 MPa	4.3 MPa	30 MPa
Strain hardening slope	45 MPa	50 MPa	50 MPa
Poisson's ratio	0.48	0.48	0.4
COF	0.38	0.48	0.3

The distribution of von Mises stress, which is known to be responsible for plastic deformation in polymers, along the scratch path of PP and CPU-PES from 1-10 N from the top view of the model is shown in Figure 24. It is observed that for PP, the stress concentration is always located along the centerline (black dashed line) of the scratch path throughout the scratch process. This result suggests that the most severe

deformation always happens along the centerline of the scratch path for PP, thus leading to the formation of a simple concave shape scratch groove. However, for CPU-PES, it is found that the stress concentration gradually shifts away from the centerline with increasing normal load. This can be attributed to the nearly incompressible nature of PU elastomers that alters the stress state beneath the scratch tip during scratching. This shift in stress concentration with increasing normal load indicates that for the model CPU systems, the most severe deformation would shift away from the centerline of the scratch path, thus explaining the bulging phenomenon observed in the mid-portion of the scratch groove. The FEM simulation results are in good agreement with the experimental findings that the bulging phenomenon of scratch groove, which has never been observed in the past scratch studies of other commonly known polymers, is unique to the scratch behavior of PU elastomers that possess high Poisson's ratios.

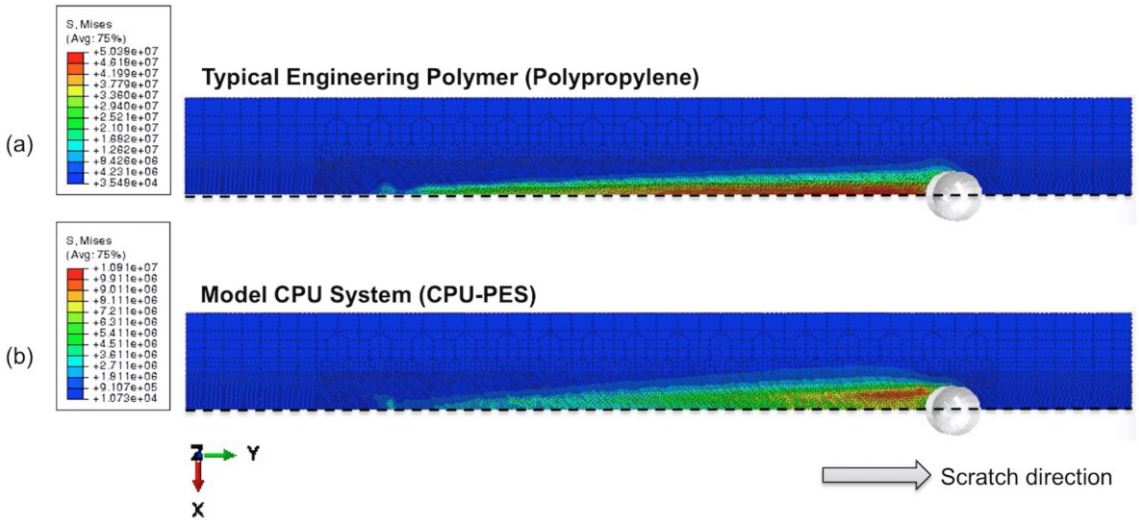

Figure 24. von Mises stress distribution along the scratch path of (a) polypropylene and (b) the model CPU system (CPU-PES). Reprinted with permission from Polymer 137 (2018) 209-221. Copyright [2018] by Elsevier.

During the scratch process with increasing normal load, the material beneath and behind the scratch tip experiences a compressive stress state and a tensile stress state, respectively [17]. It has been shown that the compressive yield stress of PU elastomers correlates well with the onset of scratch groove formation, while the tensile strength of PU elastomers is responsible for the onset of cracking/material removal [88]. Once the von Mises stress magnitude beneath the scratch tip reaches the compressive yield stress value of the material, plastic deformation of the material occurs, i.e., the formation of scratch groove. When the tensile component of the maximum principal stress magnitude behind the scratch tip reaches the tensile strength value of the material, cracking/material removal takes place. Therefore, to investigate the absence of scratch groove formation before cracking in CPU-PET, the evolution of both the von Mises stress beneath the scratch tip and the maximum principal tensile stress behind the scratch tip were monitored during the simulation and shown in Figure 25(a). For comparison, the evolution of these two stress values in CPU-PES where scratch groove would form before cracking were also monitored and shown in Figure 25(b). Due to the poor mechanical properties of CPU-PET, excessive deformation occurred during FEM modeling of the scratch process, which made the simulation computationally expensive. Consequently, the simulation for CPU-PET was performed from 1-5 N to reduce computational time. Fortunately, the simulation in this load range is sufficient for demonstrating the observed phenomenon, as the stresses show steady trends of evolution as shown in the figure, and thus the stress values at higher loads can be safely predicted.

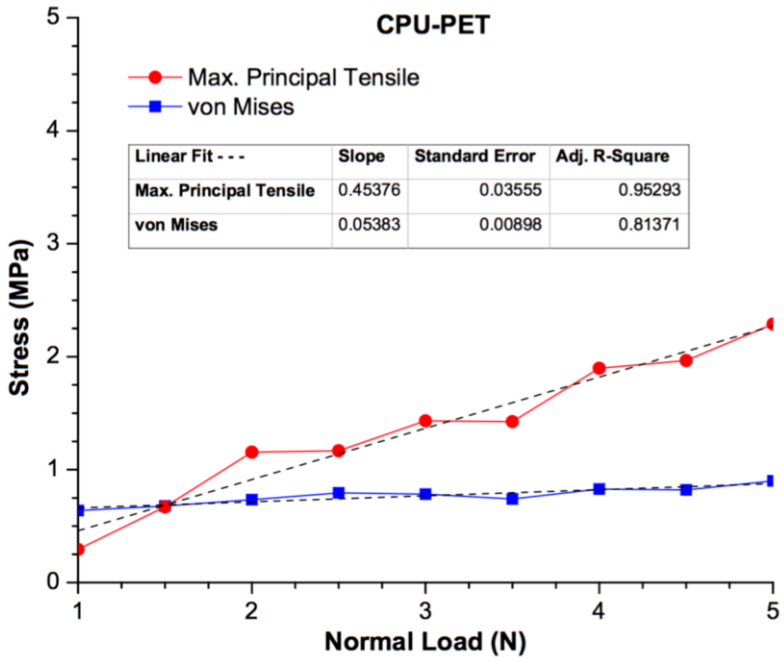

(a)

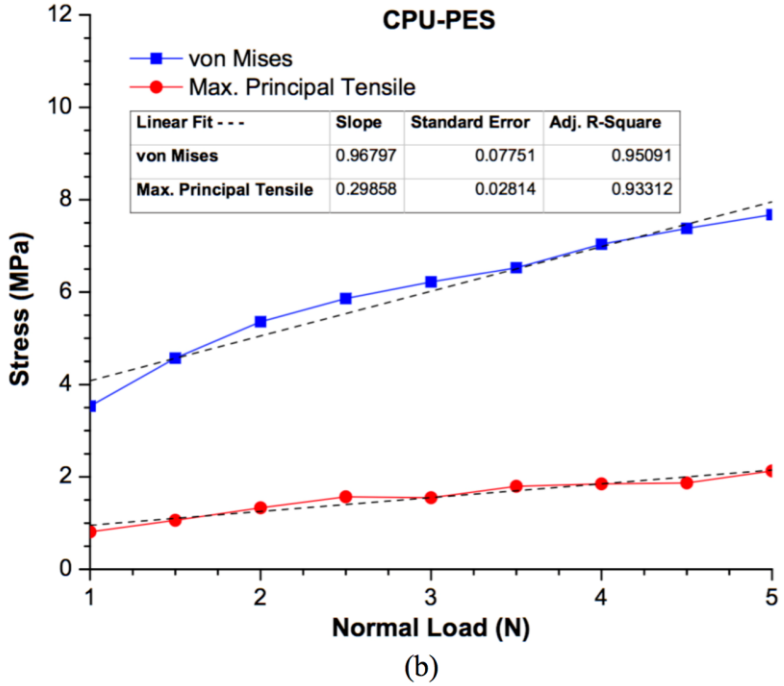

(b)

Figure 25. Evolution of von Mises stress beneath the scratch tip and maximum principal tensile stress behind the scratch tip as a function of applied normal load in (a) CPU-PET and (b) CPU-PES. Reprinted with permission from Polymer 137 (2018) 209-221. Copyright [2018] by Elsevier.

For CPU-PES, the von Mises stress beneath the scratch tip increases much faster than the maximum principal tensile stress behind the tip. As a result, the von Mises stress magnitude reaches the compressive yield stress value of CPU-PES quickly and leads to plastic deformation of the material, i.e., the formation of scratch groove. Thereafter, the tensile stress magnitude increases gradually until it approaches the tensile strength value of CPU-PES and causes cracking/material removal. In contrast, for CPU-PET, the maximum principal tensile stress behind the scratch tip increases faster than the von Mises stress beneath the tip. It is noted that even with increasing normal load, the von Mises stress keeps fluctuating around one value and increases slowly. This can be due to the extremely low elastic modulus of CPU-PET that contributes to a deep penetration of tip into the model and leads to a large contact area between the scratch tip and the matrix during scratching, thus slowing down the rise in stress magnitude. This deep penetration of scratch tip also facilitates the tensile dragging of material behind the tip and results in the fast increase in tensile stress. Given that CPU-PET has small difference between its tensile strength (10.3 MPa) and compressive yield stress (4.3 MPa), the tensile stress magnitude reaches the tensile strength value of CPU-PET first and causes cracking/material removal to occur before the scratch groove has a chance to develop.

The FEM modeling results provide evidences for the unique bulging phenomenon of scratch groove and absence of scratch groove observed in the model CPU systems. It is conceivable that the present scratch test methodology and FEM modeling approach can be utilized as an effective tool to develop highly scratch resistant

polymers and coatings for a variety of engineering and microelectronic display applications. Additional effort is now underway to establish guidelines for developing scratch and mar resistant self-healing polymers.

3.5 Conclusions

Effect of moisture exposure on scratch behavior of a series of model CPU systems was investigated. It is found that the water absorption and diffusion mechanisms in PU elastomers depend on their chemical constituents, e.g., different soft segment types in the present study. As a result, the absorbed moisture alters their surface characteristics, mechanical properties and the corresponding scratch behaviors in different fashions. The FEM modeling results show good agreement with the experimental findings and help elucidate the observed scratch-induced deformation phenomena. The present study provides guidelines for preparing scratch-resistant PU elastomers that are exposed to humid environment during service. The following conclusions can be drawn based on this study:

- The water absorption and diffusion of the less polar polyether-based PU elastomers are dominated by the abundant of free volume in the matrix, while those of the more polar polyester-based PU elastomers are governed by the polar bonding sites in the matrix.
- The homogeneously absorbed water molecules serve as plasticizer to degrade the tensile strength of polyether-based PU elastomers, thus deteriorating the resistance against cracking/material removal. The plasticization effect also

contributes to an increase in COF and results in earlier onset of groove formation and cracking/material removal.

- Due to the interaction between water molecules and the polar bonding sites, clustering of water occurs on the surface and acts as lubricant to decrease the COF of polyester-based PU elastomers, thus improving the resistance to groove formation and cracking/material removal.
- The shift in stress concentration away from the centerline of scratch path leads to a bulging phenomenon found in the mid-portion of the scratch groove of PU elastomers.
- PU elastomer with small differences in compressive yield stress and tensile strength can result in an absence of scratch groove formation before onset of cracking/material removal.

CHAPTER IV

PHYSICAL CORRELATION BETWEEN ABRASIVE WEAR AND SCRATCH BEHAVIORS

In this chapter, wear behaviors of the model CPU systems under linear reciprocating sliding and fretting conditions are investigated and physically compared with their corresponding scratch behavior. Using a custom built multi-axis tribometer in a pin-on-flat configuration, test conditions have been designed to differentiate the abrasive wear mechanism and adhesive-fatigue wear mechanism in the model systems, so that the physical correlation between abrasive wear and scratch behaviors of PU elastomers can be identified and established. Temperature rise measurement of the model CPU systems during wear is also performed to further understand the observed wear behaviors. It is anticipated that the results of this chapter can provide fundamental insights into understanding of complex abrasive wear behavior of polymers through their corresponding simpler scratch behavior.

4.1 Introduction

Wear behavior of polymers can be classified into different categories according to the surface damage mechanisms. Generally, wear damage in polymers depends on the contribution of one or multiple of the following wear mechanisms: abrasive, adhesive and fatigue [29, 30]. Abrasive wear is generated as the result of removal of material from the polymer surface through penetration and sliding of sharp and hard asperities of the

counterface. Adhesive wear is defined as the rupture of adhesive junctions between polymer and counterface during contact shearing. Fatigue wear results from the repeated impact of counterface asperities on polymer surface that leads to the propagation of cracks. In an effort to introduce a simpler and more straightforward approach to predict the wear performance of polymers, it is logical to first focus on the study of abrasive wear that mainly involves material removal upon sliding contact between the counterface and the polymer surface. This phenomenon is similar to the relatively well-establish scratch damage phenomenon, which can be considered as a result of an abrasive wear process with a single-pass and single-asperity scenario [30].

Limited research has been performed in the past to look into the correlation between scratch and wear resistances of polymers. Friedrich et al. [30] tried to find the relationship between the depth of scratch groove and the loss in volume of the material after one scratch test. They proposed that the loss in volume from the scratch groove after scratch test could be associated with the wear volume after wear test. However, scratch groove formation of polymers during scratching is only contributed by plastic deformation on polymer surface. Most of the materials are either compressed or piled up on the two sides of the scratch groove, and almost no material is removed from the scratch groove [17].

In the previous scratch studies on the model CPU systems, it has been shown that in addition to scratch groove formation, the model systems also exhibit tensile tear induced cracking along with material removal with increasing scratch normal load [88, 102]. Therefore, it is expected that the scratch resistance to tensile tear induced

cracking/material removal can be related with the volume loss during abrasive wear, and thus the abrasive wear resistance.

The present study focuses on establishing fundamental correlation between abrasive wear resistance and scratch resistance of CPU. To achieve this objective, the wear behaviors of a series of model CPU systems under linear reciprocating sliding and fretting conditions were investigated and physically compared with their corresponding scratch behavior. In addition, temperature rise of the model systems during wear was also investigated to determine how it influences the observed wear behaviors. Key material properties related to the abrasive wear resistance are discussed.

4.2 Materials and Methods

4.2.1 Materials

A total of four well-designed model CPU systems used in this study were prepared by BASF Polyurethane Specialties (China) Co. Ltd. (Shanghai, China). CPUs are block copolymers composed of alternating hard and soft segments. In this study, the model CPU systems were synthesized by the same type of hard segment that consisted of the same diisocyanate and chain extender. However, to obtain sufficiently different material properties among the model systems, each CPU was synthesized using different soft segment. The hard segment and soft segments of the model systems are listed in Table 6 along with the distinct tensile true stress-strain properties and COF of the model systems that resulted from the different soft segments incorporated. The chemical structures of each component are provided elsewhere [88].

Table 6. Chemical component, material properties and scratch resistance of the model CPU systems. Reprinted from [88].

	CPU-PT	CPU-PC	CPU-PET	CPU-PES
Hard segment	4,4'-methylene diphenyl diisocyanate (MDI) + 1,4-butane diol (BDO)			
Soft segment	Polytetramethyl-ene ether glycol	Polycaprolacto-ne	Ethylene oxide/propylen-e oxide based polyol	Adipic anhydride based polyol
RMS roughness (μm)	0.37 ± 0.03	0.50 ± 0.04	0.38 ± 0.03	0.41 ± 0.02
Tensile modulus (MPa)	16.2 ± 1.2	9.4 ± 0.7	6.0 ± 0.4	17.0 ± 0.8
Tensile yield stress (MPa)	5.0 ± 0.3	3.0 ± 0.1	1.9 ± 0.2	5.3 ± 0.2
Tensile strain at break (%)	854.2 ± 40.1	460.6 ± 16.0	259.7 ± 12.1	881.8 ± 29.0
Tensile strength (MPa)	63.7 ± 2.7	45.5 ± 3.3	10.3 ± 1.3	65.2 ± 4.1
Coefficient of friction	0.27 ± 0.01	0.43 ± 0.02	0.48 ± 0.02	0.38 ± 0.01
Critical normal load for onset of cracking/materi-al removal during scratch (N)	188.6 ± 7.5	111.6 ± 9.2	33.2 ± 1.8	202.5 ± 11.7

The scratch performance of these model CPU systems was investigated previously [88]. The critical normal loads for the onset of tensile tear induced cracking/material removal of the model systems at 100 mm/s speed of scratch test are

shown in Table 6. The critical normal load for the onset of damage is a metric to evaluate the resistance of polymers to scratch-induced damage during scratch process, with a higher value refers to a later onset of damage and thus a better scratch resistance [7, 8]. These critical normal loads will be utilized later on to establish correlation between scratch resistance against cracking/material removal damage and abrasive wear resistance of the model systems.

The specimens were cast into plaques with 14 mm in thickness by BASF. The surfaces of the specimens were smooth with similar root mean square (RMS) roughness measured on an area of 1.3 mm × 1 mm. To remove pre-existing moisture and residual stresses in the as-received specimens, all the specimens were dried in a vacuum oven with a vacuum pressure of 30 mm Hg in between two smooth glass plates at 80 ºC for 6 h, then left to slowly cool overnight to room temperature. After drying, the specimens were machined into pins with 25.4 mm in diameter and 14 mm in thickness for wear testing.

4.2.2 Wear Test

Wear tests in this study were conducted by a custom built multi-axis tribometer in a pin-on-flat configuration. In this setup, the CPU pin specimens were pneumatically loaded against a planar counterface. The counterface was mounted on two stacked-up programmable linear stages (Aerotech) that were capable of producing two axis of motion at a specified velocity. During the wear test, the CPU pin specimen remained stationary while the counterface moved according to the programmed wear path and

velocity, and thus wear was generated as a result of the relative motion between the pin and the counterface. This pin-on-flat configuration has been successfully employed to investigate the wear behaviors of polyaryletherketone (PAEK) family of thermoplastics in the past [29, 37, 103].

A hot rolled 304 stainless steel sheet with a RMS roughness of 8.19 μm was chosen as the counterface in the present study. As depicted in the 3-D profile in Figure 26, the hot rolled stainless steel surface is rough with many irregular asperity tips, and the dimensions of these asperity tips are small. In other words, these asperity tips are much shaper than the 1 mm diameter conical scratch tip described in the previous scratch study [88, 102]. Since the asperity tips on the stainless steel counterface are non-uniform without directionality, wear path direction has minimal impact on the wear behavior of the model systems [29, 37]. Therefore, a linear reciprocating wear path is adequate and thus utilized to perform the wear tests.

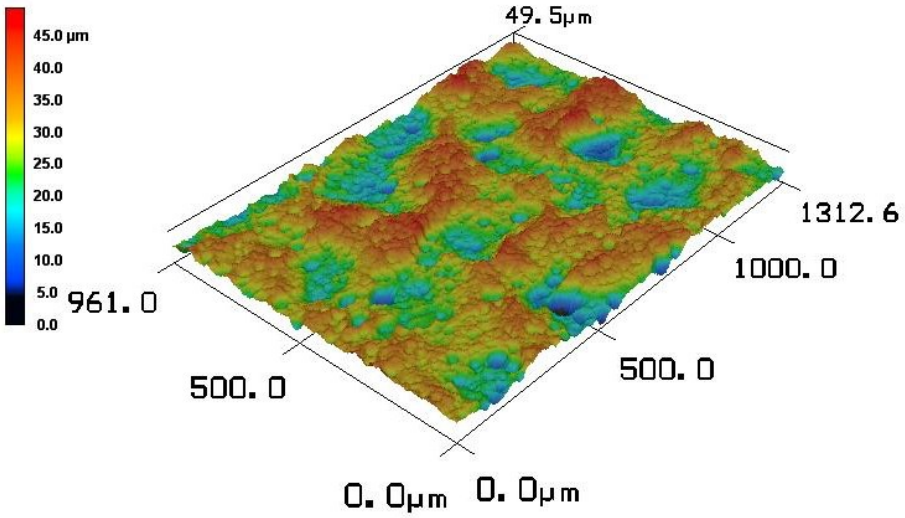

Figure 26. 3-D profile of hot rolled 304 stainless steel counterface scanned by violet laser scanning confocal microscope.

Sliding wear tests were first carried out on the model CPU systems. Sliding wear is accomplished by continuously moving the counterface relative to the vertically loaded specimen surface [29]. To ensure the two mutually loaded surfaces have sufficient distance to continuously slide against each other, a 50 mm long stroke distance, which is close to the length of a scratch test [88], was used for the reciprocation, as shown in Figure 27(a). A long stroke distance also allows most debris to be expelled so that a fresh pin surface is constantly moving across counterface asperities during the reciprocation. A normal load of 250 N, which achieved a nominal contact pressure of 0.5 MPa for the 25.4 mm diameter pins, was applied to run the tests at a constant velocity of 100 mm/s. Each test was run for 300 m of total traveling distance to generate measurable quantity of wear debris. Compressed nitrogen gas was used to clean the specimen surface before and after each test. The weight loss was measured by weighing the

specimen before and after each test using an analytical balance with 0.01 mg resolution. The wear volume was then calculated by the weight loss and density of each model CPU system. Three tests were done for each model CPU system to obtain an average value of the wear volume.

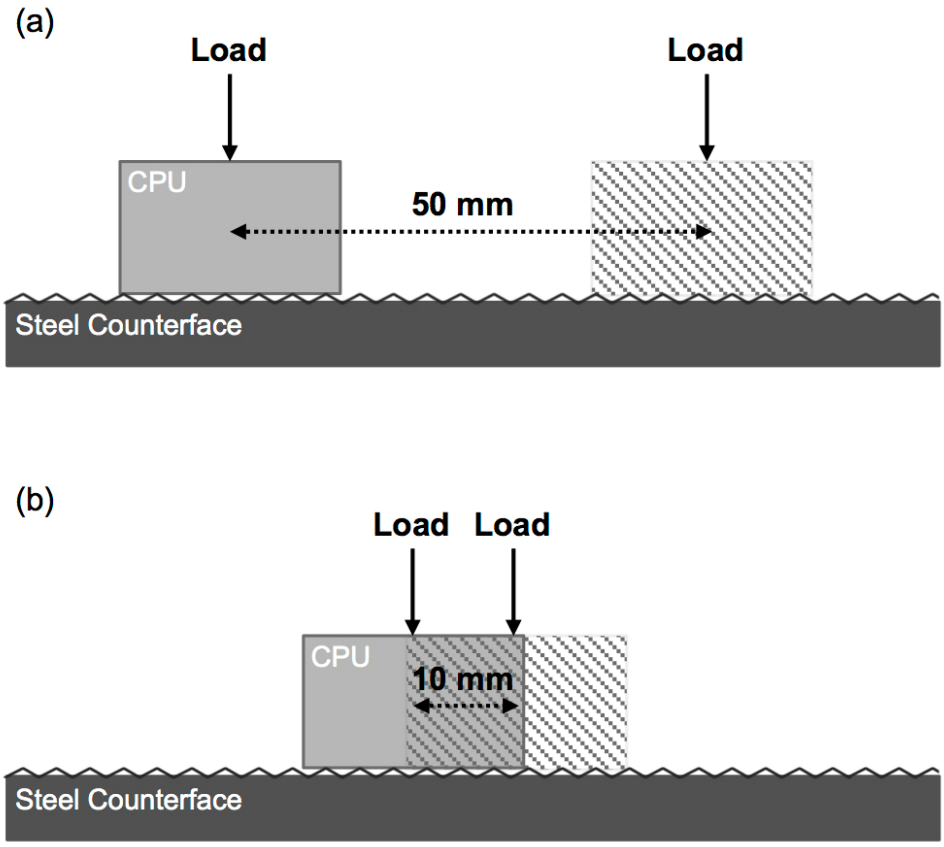

Figure 27. Schematics of linear reciprocating (a) sliding wear test and (b) fretting wear test.

In addition to sliding wear behavior, fretting wear behavior of the model systems was also investigated as a comparison. Unlike sliding wear that the two mutually loaded surfaces have sufficient distance to continuously slide against each other, fretting wear is

characterized as intermittent sticking and slipping between the two surfaces at the two ends of reciprocation [29]. In other words, the stroke distance is minimized that only enough to break the adhesive sticking between the two surfaces. Therefore, a 10 mm short stroke distance was used for the reciprocation in fretting wear tests, as shown in Figure 27(b). All the other testing conditions were kept the same with those of sliding wear tests.

4.2.3 Wear Surface Imaging

Following the wear tests, wear surfaces of the model CPU systems were examined by a Keyence® VK9700 violet laser scanning confocal microscope (VLSCM) at 20 × magnification. Multiple images were taken at random locations of the wear surface to check the consistency of wear damage feature throughout the wear surface for each model system. One image of each model system at each testing condition was selected and shown.

4.2.4 Temperature Rise Measurement

Wear tests were carried out at room temperature in the present study. Due to the relative motion between the two contacting surfaces, frictional heat was generated and temperature of the specimens increased. As the specimens heated up, infrared (IR) radiation was emitted. A Fluke® Ti45FT IR camera was positioned 0.3 m from the specimen to detect the IR radiation emitted from the specimen and track the temperature rise of the specimen during wear test. For each specimen, an IR image was first taken

before the test started to record the initial temperature. Subsequently, an IR image was taken at every 50 m of travelling distance from the beginning of the test. The detector of the IR camera had a 160 × 120 focal plane array with a temperature sensitivity down to 0.08 ºC. Before taking every image, an automatically internal calibration was performed by the IR camera to maintain high quality of each captured image.

4.2.5 Thermal Conductivity Measurement

Thermal conductivities of the model CPU systems were measured by a Hot Disk® Transient Plane Source 2500 S instrument (ISO 22007-2.2). Two of each CPU wear specimens were used for the measurement. During a measurement, a nickel double-spiral sensor was sandwiched between two specimens and a current passed through the spiral that generated heat. Heat dissipated into the specimens at a rate depending on the thermal transport properties of the specimens. The resulting temperature increase versus time at the sensor was recorded to calculate the thermal conductivity of the specimen. Three measurements were done for each model CPU system for statistical purposes.

4.3 Results and Discussion

4.3.1 Sliding Wear Volume

The amounts of volumetric wear of the model CPU systems from the linear reciprocating sliding wear test are plotted in Figure 28. All the model systems started to generate wear debris immediately from the first cycle of test. Under the same testing conditions, different model CPU systems showed significantly different wear volumes

from each other. It is noted that severe wear damage and volume loss were found in CPU-PET before completing the entire 300 m of sliding wear test, so only 100 m of travelling distance was performed on this system. Even though the tests were stopped at 100 m of travelling distance, CPU-PET still showed the highest wear among the model systems. For the other three model systems that completed the entire 300 m of sliding wear test, CPU-PC had a higher wear volume, followed by CPU-PES and CPU-PT sequentially.

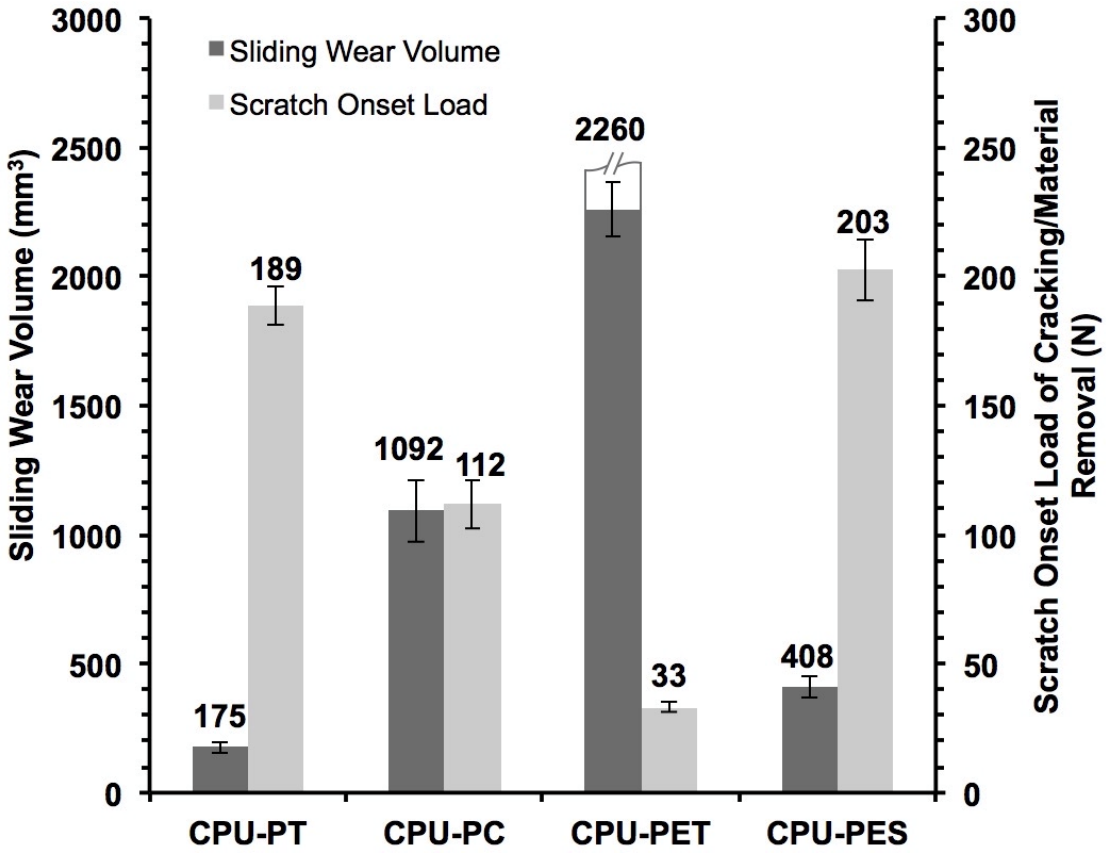

Figure 28. Sliding wear volume of the model CPU systems (CPU-PET was measured at 100 m of traveling distance. The other systems were measured upon completion of 300 m of total travelling distance); the critical normal load for onset of tensile tear induced cracking/material removal of the model CPU systems during scratch.

In examining the sliding wear results, a good correlation was found between the sliding wear volume measured in the present study and the scratch resistance against tensile tear induced cracking/material removal investigated in the previous study [88], which are also shown in Figure 28 for comparison. The model systems with a later onset (higher onset load) of tensile tear induced cracking/material removal during scratch also showed a lower wear volume during sliding wear. For instance, CPU-PES has 81% later onset of cracking/material removal than CPU-PC during scratch (203 N vs. 112 N), and it also has 63% less wear volume than CPU-PC during sliding wear (408 mm^3 vs. 1092 mm^3). As scratch involves a single-pass sliding abrasion of a single-asperity under the influence of an applied normal load [30], sliding wear can be considered a multi-passes and multi-asperities abrasion process. Because of the presence of many irregular asperity tips on the steel counterface, each of them can act as a sharp scratch tip that scratches the CPU specimens simultaneously during the sliding wear process. The linear reciprocating motions of these asperities over the long stroke distance of sliding wear test serve as repetitive scratch tests conducting on the specimen surface. The long stroke distance also allows most debris to be expelled so that the asperities can remain in direct contact with the specimen surface during each wear cycle. Therefore, the sliding wear and scratch damages of the model systems are both governed by abrasive wear mechanism as illustrated in Figure 29.

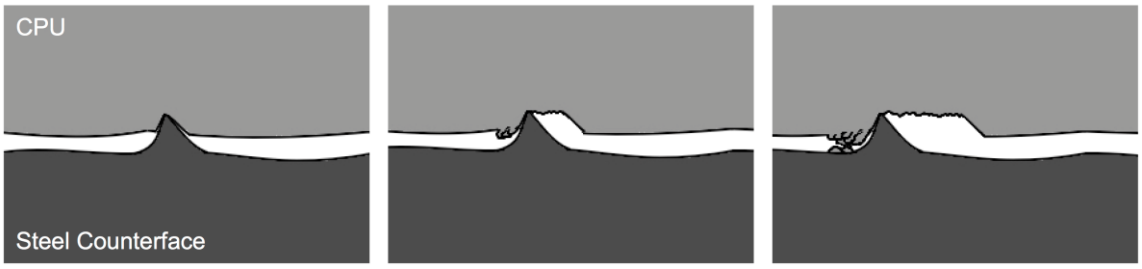

Figure 29. Abrasive wear mechanism during sliding wear test and scratch test.

From the experimental and numerical scratch studies [16, 18, 19, 88, 102], it has been shown that during scratch process, as the scratch tip penetrates the specimen surface and slides, the material behind the scratch tip suffers from a high magnitude of tensile stress. As the scratching normal load increases, the magnitude of the tensile stress will gradually approach and then exceed the tensile strength of the specimen and result in cracking along with material removal. Tensile strength has been demonstrated to be the key material property that determines the scratch resistance against tensile tear induced cracking/material removal of the model CPU systems [88, 102]. Since sliding wear and scratch are both dominated by abrasive wear mechanism, tensile strength can also be closely related with the sliding wear volume, and thus the abrasive wear resistance of the model systems.

Based on the wear studies of different polymeric systems, other researchers also proposed that tensile strength might have significant influence on the abrasive wear resistance of polymers [29, 39, 103, 104]. However, for instance, due to the development of transfer film during wear or incorporation of fillers in the polymers that complicated the wear behaviors, a direct correlation between tensile strength and abrasive wear

resistance could not be established. In the present study, all the model CPU systems did not show transfer film formation on the stainless steel counterface after the sliding wear tests. The model CPU system with a higher tensile strength showed a later onset of tensile tear induced cracking/material removal during scratch, as well as a lower wear volume during sliding wear. Therefore, tensile strength can be the major material property that determines the abrasive wear resistance of the model systems. The extraordinarily low sliding wear volume of CPU-PT will be discussed later on based on the temperature rise measurement during wear.

4.3.2 Sliding Wear Surface

The sliding wear surface images of the model CPU systems taken by the VLSCM are shown in Figure 30. The most apparent features are the irregular cracking damages on the surfaces of CPU-PC and CPU-PET. Under the loading condition used in the present study, only these two model systems with lower tensile strengths exhibited this kind of irregular cracking damages. Owing to the presence of many non-uniform asperity tips on the steel counterface, the local stresses at these asperities resulted from the applied normal load can be quite high during the tests. If the local stresses exceed the tensile strength of the model system at most of the asperities on the counterface, tensile tear induced cracking along with material removal will be the dominant damage feature. These cracking damages overlap each other during the reciprocating tests and finally result in the fracture-like wear surface and large amount of wear volume.

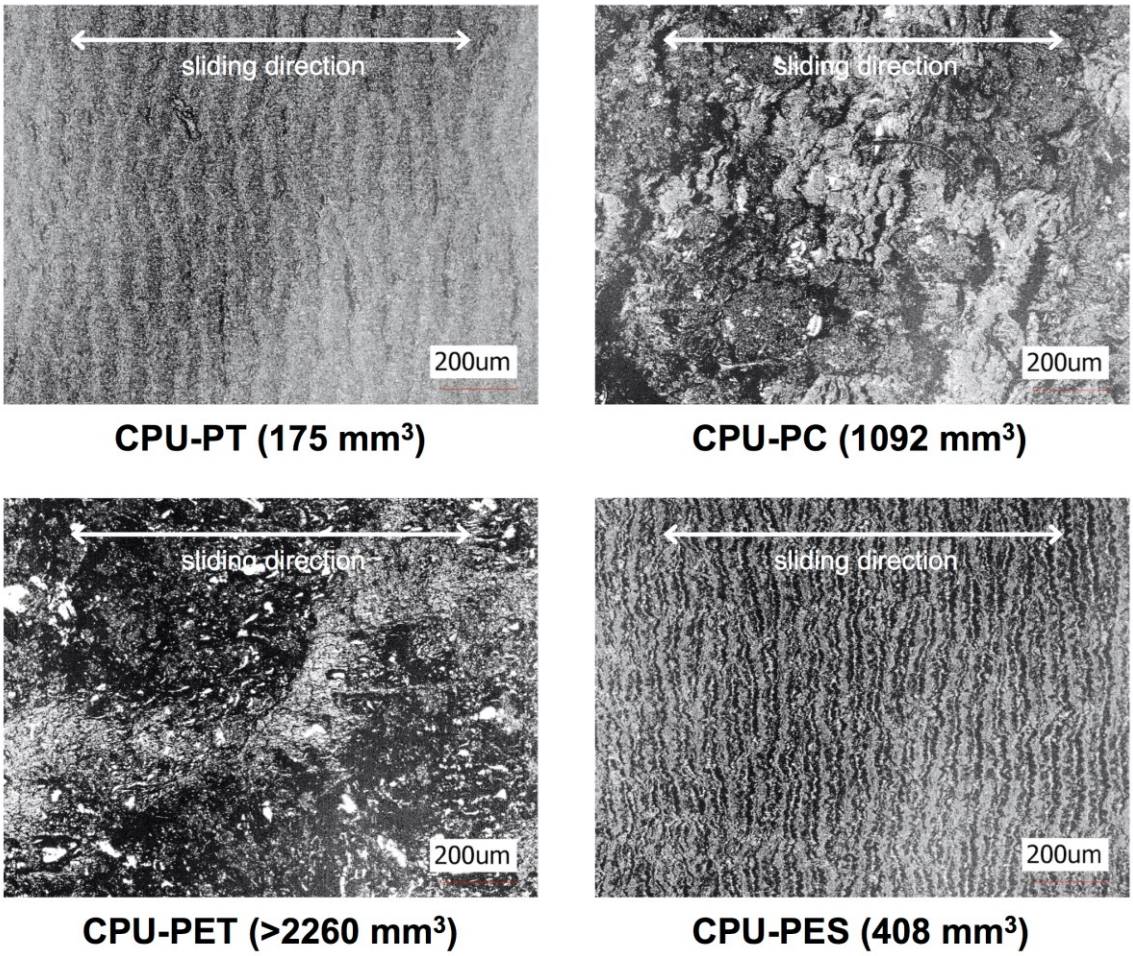

Figure 30. VLSCM images of the sliding wear surfaces of the model CPU systems (wear volume of each model system is shown in the legend).

On the contrary, for the other two model systems with higher tensile strengths, no appreciable cracking damage can be observed on the wear surfaces. Instead, parallel wave pattern was generated throughout the wear surfaces perpendicular to sliding direction. This kind of wave or ripple-like feature on the wear surface has been observed in the wear studies of many polymeric systems, and numerous explanations have been proposed to account for the formation of this feature [31, 34, 105-107]. It is generally

accepted that the accumulation of plastic deformation can be the reason for the waves formation on wear surfaces. Owing to the high tensile strengths of CPU-PT and CPU-PES, under the loading condition used in the present study, the local stresses might only exceed the tensile strengths of them at a few asperities with sufficient sharpness and contribute to a small amount of material removal. Most of the specimen surface is just plastically deformed and buckled during the slide-stop reciprocating motion. Consequently, the parallel wave is the dominant damage feature on the wear surfaces of these two model systems, and the cracking damage is barely detectable.

Considering the measured wear volume being consistent with the observed wear surfaces, it can be presumed that most sliding wear debris is generated through tensile tear induced cracking damage on the wear surfaces. The observation of sliding wear surfaces further support the earlier argument that tensile strength plays the most important role in the abrasive wear resistance of the model systems.

4.3.3 Sliding Wear Temperature Rise

The temperature rises of the model CPU systems versus travelling distance during sliding wear test are plotted in Figure 31. At the first 50 m of sliding wear test, the temperatures of all the model CPU systems increased rapidly. As the subsequent section will reveal, due to the low thermal conductivities of the model CPU systems, heat cannot be dissipated away easily from the specimens. As a result, frictional heat accumulated quickly within the specimens and led to the rapid temperature rises. However, since the steel counterface is a good thermal conductor with a thermal

conductivity (~14-17 W/mK) almost a hundred times higher than those of the model CPU systems, the accumulated heat quickly reached thermal equilibriums and the temperature rises approached their plateaus.

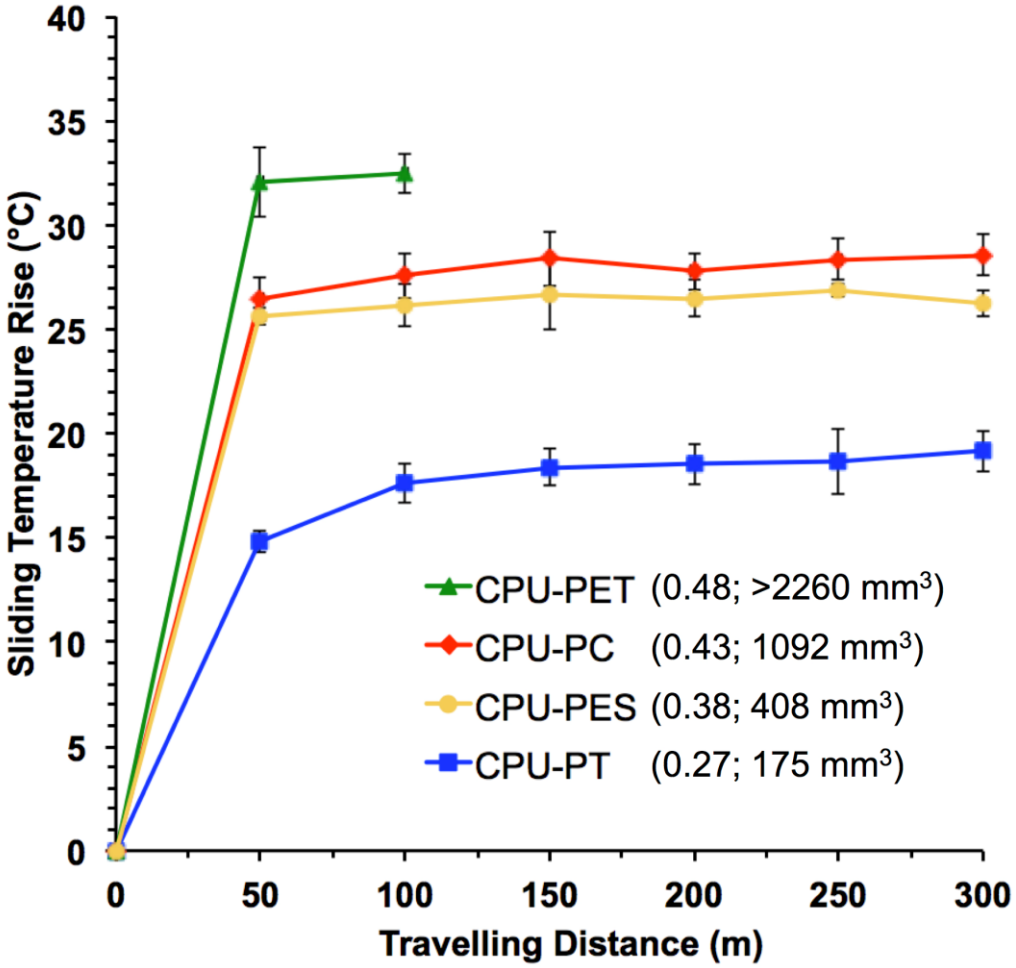

Figure 31. Sliding wear temperature rise of the model CPU systems versus travelling distance (COF and wear volume of each model system are shown in the legend).

It should be noted that different model CPU systems generated significantly different amounts of heats and contributed to greatly varied temperature rises during

sliding wear tests. CPU-PET exhibited the highest sliding wear temperature rise among the model systems, even if the tests were stopped at 100 m of travelling distance, followed by CPU-PC and CPU-PES sequentially. CPU-PT experienced a considerably lower sliding wear temperature rise than the other model systems. Many studies have found that the temperature rise resulted from frictional heat during wear can be high enough to soften or even melt the polymer surface and result in augmented wear damages [108-110]. It appears that the temperature rises of the model CPU systems during wear might also have impact on their wear performances. The high temperature rise of CPU-PET during sliding wear tests might further degrade its poor mechanical properties and exaggerated the cracking damage. As a consequent, CPU-PET showed the highest volume loss among the model systems. In contrast, the low temperature rise of CPU-PT along with its high tensile strength contributed to its extraordinarily low sliding wear volume. Therefore, a higher temperature rise accelerates the wear damage of the model systems.

The influence of temperature rise during wear on the wear resistance of the model CPU systems cannot be ignored. The root cause for the different sliding wear temperature rises among the model systems deserves further investigation.

4.3.4 Thermal and Damping Properties

The measured thermal conductivities of the model CPU systems are shown in Figure 32. As expected, four model systems possess different thermal conductivities. However, the differences are not significant. Numerous research efforts have been done

in the past to look into the effect of thermal conductivity on temperature rise during wear [111-113]. The results of these studies showed that an increase in thermal conductivity resulted in a decrease in temperature rise during wear. But the polymeric systems used in these studies were typically modified by mineral fillers or carbon nanotubes. The thermal conductivities of the filled systems were several times higher than those of the neat systems. In the present study, the minor differences in thermal conductivities among the model CPU systems do not seem to have a substantial influence on their temperature rises during wear. Other properties, such as damping characteristic and COF, should also be considered to account for the observed temperature rises.

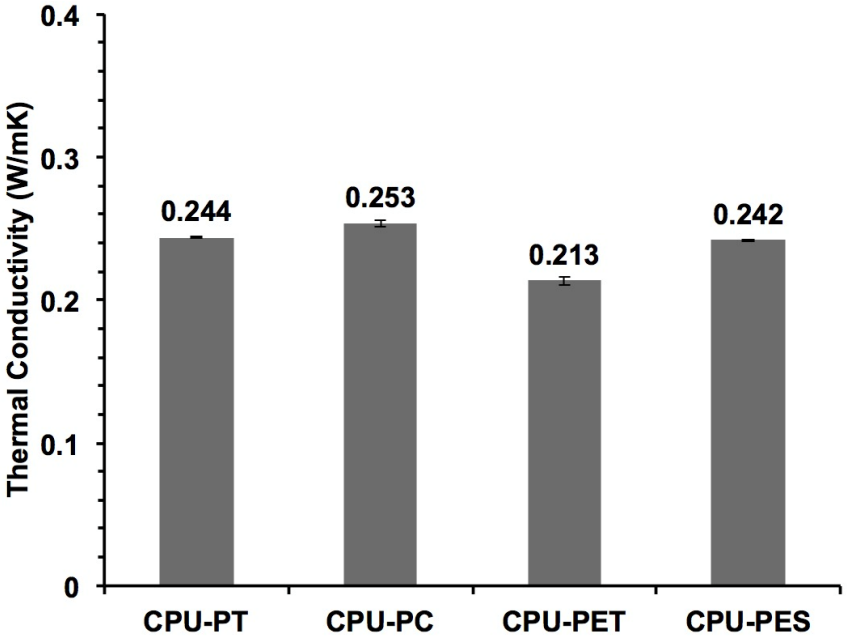

Figure 32. Thermal conductivities of the model CPU systems.

The results of some earlier wear studies have suggested that the polymeric system with a higher damping characteristic shows a higher temperature rise during wear [114, 115]. Some other studies have proposed that COF plays a more important role than thermal conductivity in wear temperature [116, 117]. The damping properties (loss tangents) of the model CPU systems have been investigated in the previous study by using dynamic mechanical analysis [88]. The tan δ curves of the model systems around room temperature, where the wear tests were carried out, are extracted and shown in Figure 33. Four model systems exhibit different magnitudes of damping near room temperature, and the ranking of damping matches well the ranking of temperature rise for the model systems during wear. This can be explained by the fact that as the polymer specimen undergoes deformation, larger amount of heat is dissipated for a polymer with a higher damping. Additionally, it has been shown that a higher damping is partially responsible for a higher COF for polymeric systems, since the larger amount of dissipated heat softens the surface and leads to an increase in surface friction [78-80]. The measured COF between the model CPU systems and stainless steel surface as listed in Table 6 follow the same trend with their damping characteristics as well as the temperature rises. Therefore, both damping characteristic and COF are likely to be more critical than thermal conductivity in determining the temperature rise of the model CPU systems during wear.

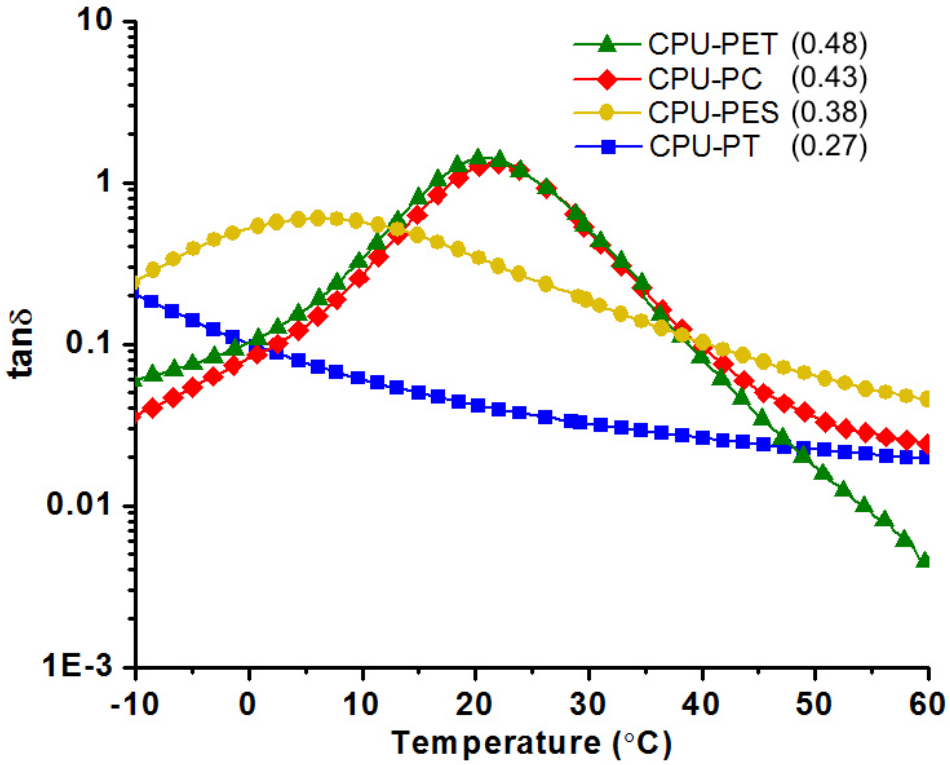

Figure 33. Loss tangent of the model CPU systems around room temperature (COF of each model system is shown in the legend).

4.3.5 Fretting Wear

The measured volumetric wear of the model CPU systems from the linear reciprocating fretting wear test are shown in Figure 34 as a comparison to the sliding wear results. Significantly different trends are observed between the volume loss during fretting wear and sliding wear tests. All the model systems completed the entire 300 m of fretting wear test and showed much lower wear volumes than those of the sliding wear test. All the model systems did not exhibit transfer film formation on the stainless steel counterface after the fretting wear tests. CPU-PET still showed the highest wear volume among the model systems. However, the other three model systems have quite

similar fretting wear volumes. As a result, no correlation can be found between the fretting wear volume and the scratch resistance against tensile tear induced cracking/material removal of the model systems. Comparison of these two sets of data suggests that different mechanisms are responsible for fretting wear and sliding wear behaviors of the model systems.

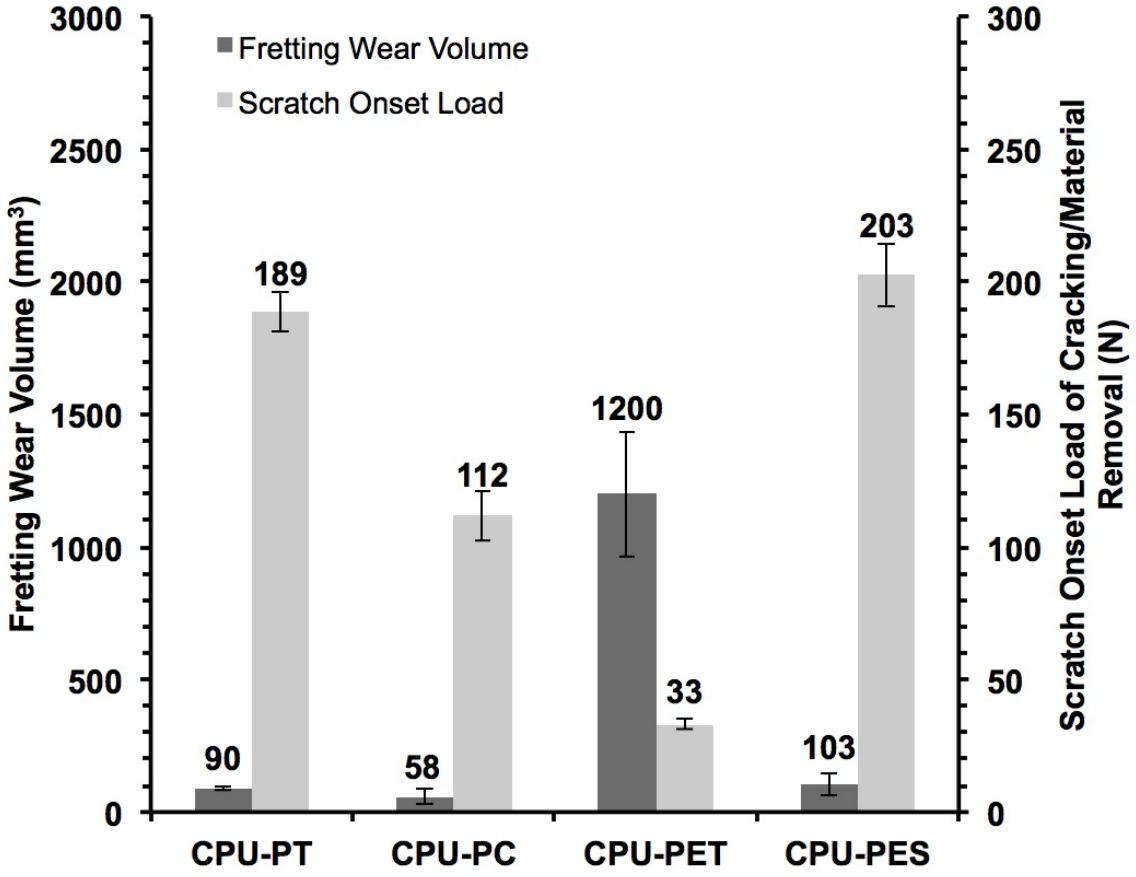

Figure 34. Fretting wear volume of the model CPU systems; the critical normal load for onset of tensile tear induced cracking/material removal of the model CPU systems during scratch.

Different from the long stroke distance during sliding wear, the stroke distance during fretting wear is short that only enough to break the adhesive sticking between the two surfaces at the two ends of reciprocation. As a result, the two mutually loaded surfaces do not have sufficient distance to continuously slide against each other and the abrasive wear mechanism is suppressed. On the contrary, the intermittent sticking and slipping become the predominant interaction between the two mutually loaded surfaces during fretting wear. This interaction can be described as adhesive wear. Adhesive wear is often discussed together with fatigue wear since adhesive damage induced by contact shearing often initiates cracks that propagate with repeated motions [29, 118]. Therefore, the fretting wear damage of the model systems is governed by adhesive-fatigue wear mechanism as illustrated in Figure 35, and as such, cannot be associated with the tensile strength of the model systems. Instead, shear strength and crack growth parameters might play more important roles in determining the adhesive-fatigue wear resistance of the model systems, i.e., a higher shear strength can resist the initiation of cracks contributed by the rupture of adhesive junctions between polymer and counterface during contact shearing, and a higher crack growth resistance can slow down the propagation of cracks resulted from repeated fretting motions [29, 118].

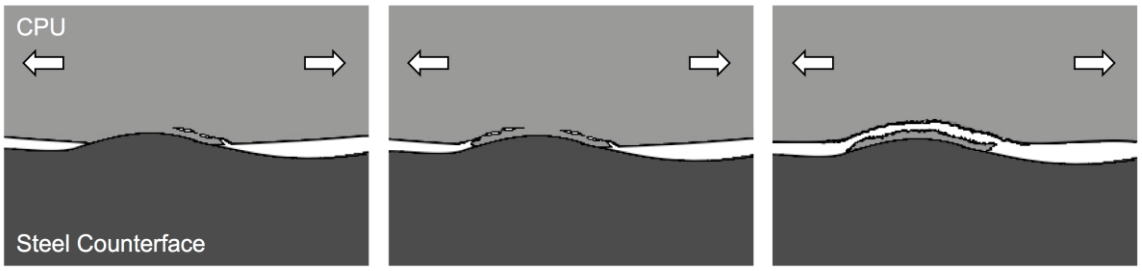

Figure 35. Adhesive-fatigue wear mechanism during fretting wear test.

The fretting wear surface images of the model CPU systems shown in Figure 36 are in agreement with the measured volume loss during fretting. The irregular cracking damage on the surface of CPU-PET sheds light on its highest fretting wear volume among the model systems. By contrast, the dominant damage feature of the other three model systems is the formation of parallel waves along with a few debris rolls. The accumulation of debris rolls on wear surface is commonly observed during fretting wear of polymers [119-121]. This can be due to the short stroke distance of fretting wear test that does not allow debris to be expelled from the contact efficiently. Even though the wear surface features of the model systems appear to be similar for fretting and sliding wears, it should be noted that the propagation of shear induced cracking requires repeated motions, while the formation of tensile tear induced cracking can happen during each cycle of sliding. Consequently, this might slow down the generation of wear debris during fretting wear than sliding wear and contribute to the lower fretting wear volumes than sliding wear volumes of the model systems.

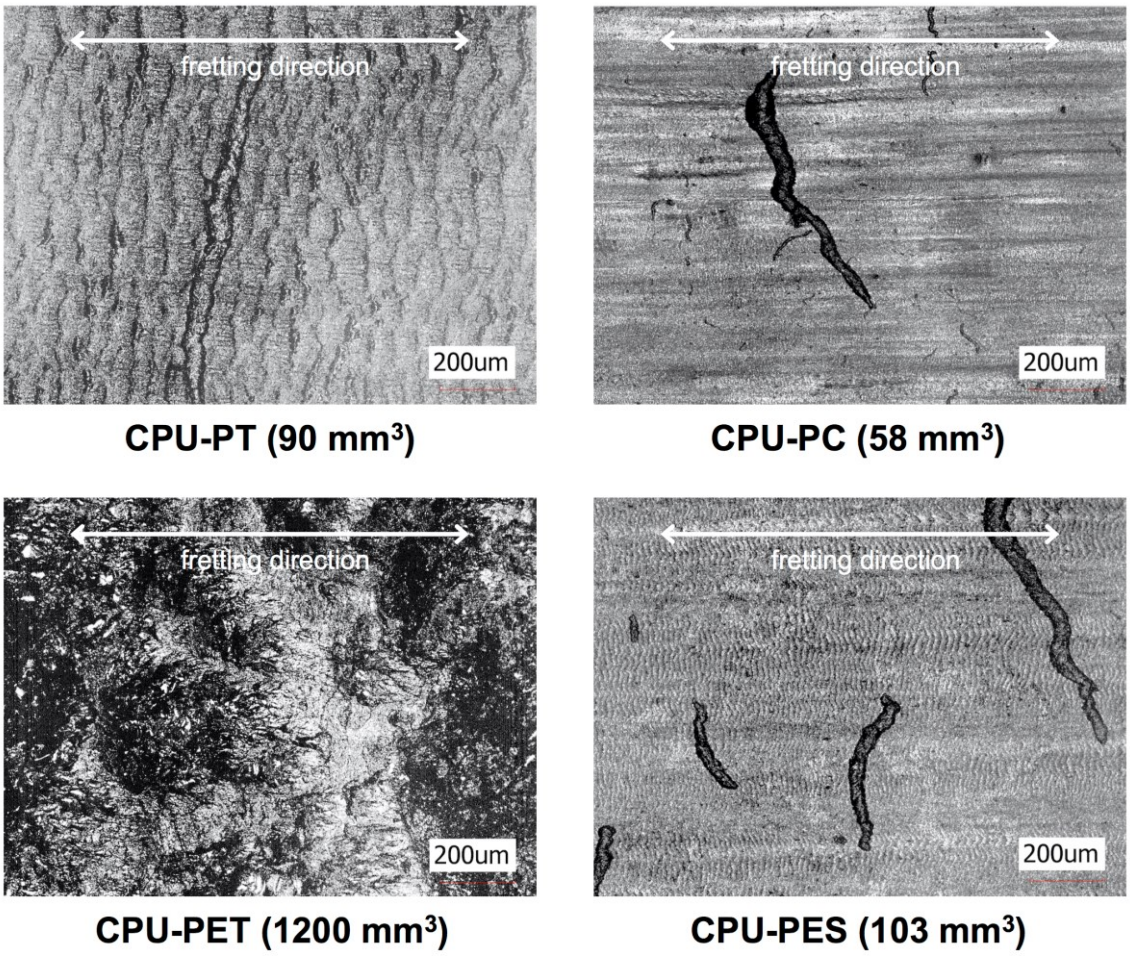

Figure 36. VLSCM images of the fretting wear surfaces of the model CPU systems (wear volume of each model system is shown in the legend).

The temperature rises of the model CPU systems versus travelling distance during fretting wear test follow the same trends with the temperature rises during sliding wear test, as shown in Figure 37. However, all the model systems exhibited lower temperature rises during fretting wear test compared with sliding wear test, even if the frequency of fretting wear test was high. Since the specimen experiences cyclic loading-unloading during the slide-stop reciprocating motion, a possible explanation can be due

to the long stroke distance of sliding wear test induces a high strain magnitude on the specimen and leads to a large hysteresis loop. As a result, more heat is generated from the specimen due to hysteresis loss during the long stroke sliding wear test. Moreover, the formation of tensile tear induced cracking damage during each cycle of sliding might generate additional heat and further increase the temperature. Therefore, lower temperature rises of the model systems were observed during fretting wear test compared with sliding wear test.

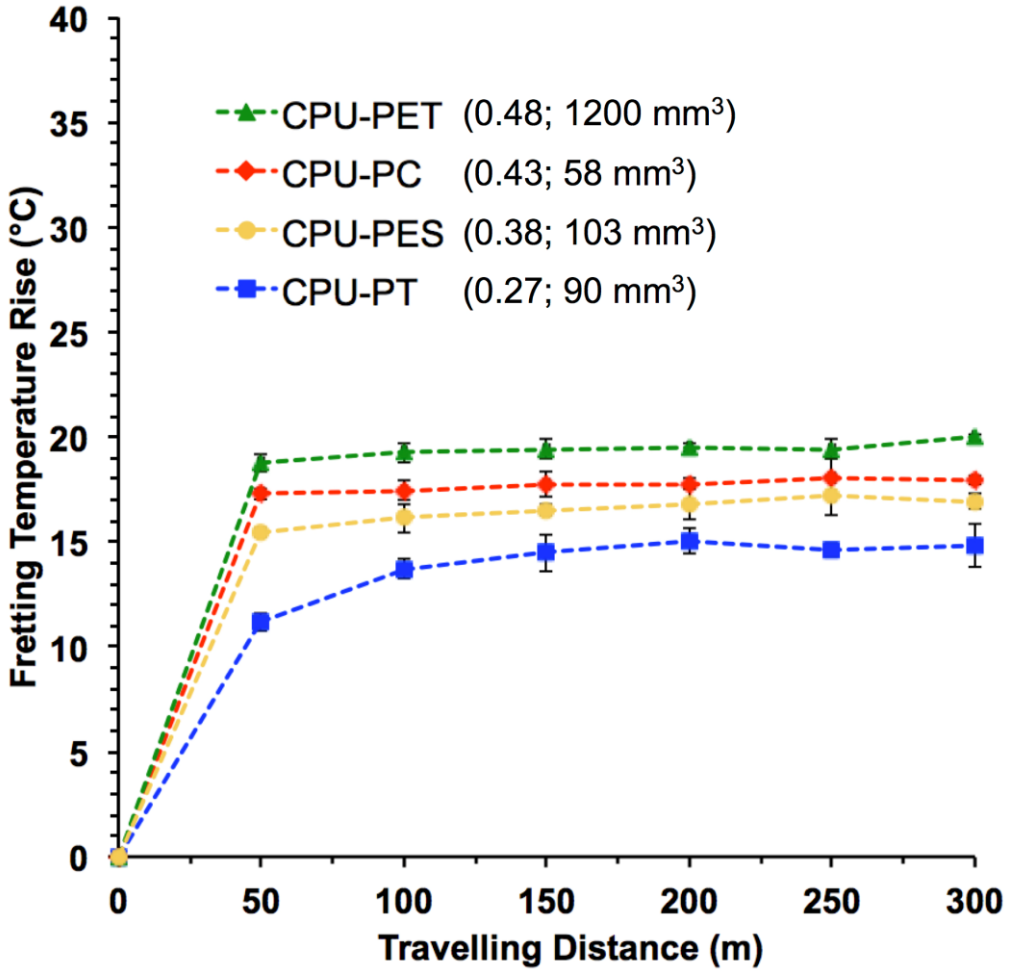

Figure 37. Fretting wear temperature rise of the model CPU systems versus travelling distance (COF and wear volume of each model system are shown in the legend).

As the scratch resistance against tensile tear induced cracking/material removal of the model CPU systems can be physically correlated with their abrasive wear performance, the present study provides fundamental insights into understanding of complex abrasive wear behavior of polymers through their corresponding simpler scratch behavior. As such, the key material property that is responsible for the scratch resistance against tensile tear induced cracking/material removal, i.e., tensile strength,

can then be extended to abrasive wear resistance of polymers. Thus, scratch test can be potentially employed to predict the abrasive wear performance of polymers and facilitate effective design of abrasive wear-resistant polymers.

4.4 Conclusions

Wear behaviors of a series of model CPU systems under linear reciprocating sliding and fretting conditions were investigated and physically compared with their corresponding scratch behavior. It is found that the sliding wear and scratch damages of the model systems are both governed by abrasive wear mechanism. The scratch resistance against tensile tear induced cracking/material removal of the model CPU systems correlates well with their abrasive wear performance, which can then be linked to their material properties. In contrast, the fretting wear damage of the model systems is found to be dominated by adhesive-fatigue wear mechanism, and thus cannot be correlated with the scratch performance. The influence of temperature rise of the model systems during wear on the observed wear behaviors was also discussed. The following conclusions can be drawn based on this study:

- The sliding wear and scratch damages are governed by abrasive wear mechanism. Increasing tensile strength improves resistance against tensile tear induced cracking on wear surface and reduces volume loss during abrasive wear.

- The fretting wear damage is governed by adhesive-fatigue wear mechanism. Shear strength and crack growth parameters can be the major properties that influence the adhesive-fatigue wear resistance.
- A higher temperature rise accelerates the wear damage. Damping characteristic and COF are more critical than thermal conductivity in determining temperature rise of the model CPU systems during wear.

CHAPTER V

EFFECT OF MOLECULAR WEIGHT ON SCRATCH AND ABRASIVE WEAR BEHAVIORS OF THERMOPLASTIC POLYURETHANE ELASTOMERS

As tensile strength has been determined as the key mechanical property that responsible for the resistance of PU elastomers against scratch onset of cracking/material removal and abrasive wear volume loss, in this chapter, research effort is performed to explore the possibility of improving the tensile strength, scratch and abrasive wear performances of PU elastomers by modifying the molecular weight. The model TPU systems considered in this chapter are synthesized to contain different molecular weights, but with the same type and ratio of hard and soft segments. The effect of molecular weight on morphology, tensile true stress-strain behavior, COF, scratch and abrasive wear behaviors of the model systems are investigated.

5.1 Introduction

PU elastomers are one kind of block copolymers that typically consist of two different chemical constituents, i.e., hard segment and soft segment. Each segment of PU elastomers can be designed to achieve a broad range of properties for many different applications. Still, for applications where aesthetic appearance and surface structural integrity are highly desired, PU elastomers have been shown to possess inadequate resistance against surface damages like scratch and wear [122].

Scratch behavior of PU elastomers [88, 102] has been recently studied using the ASTM D7027/ISO19252 standardized scratch test [7, 8], which has been widely utilized for investigating the scratch behaviors of different polymeric systems [14, 16, 22, 99, 123]. The results show that during the scratch process, PU elastomers exhibit tensile tear-induced cracking along with material removal on the surface when the scratching load is high. Tensile strength is found to be the key mechanical property related to the resistance of PU elastomers against this scratch damage.

Thereafter, abrasive wear behavior of PU elastomers [124] was examined using a custom built multi-axis tribometer in a pin-on-flat configuration, and the result was compared with the previous scratch test result. It is found that abrasive wear and scratch damages of PU elastomers are governed by the same damage mechanism, which involves tensile tear-induced cracking along with material removal on the surface. Abrasive wear volume of PU elastomers shows good correlation with the onset of cracking/material removal during scratch. Consequently, the key mechanical property related to scratch resistance of PU elastomers can also be extended to abrasive wear resistance of PU elastomers, i.e., a higher tensile strength improves the resistance against both scratch onset of cracking/material removal and abrasive wear volume loss.

It is well known that molecular weight has a significant influence on the tensile properties of polymers, especially on tensile strength. For many polymers, the effect of molecular weight on tensile strength reaches a plateau value above a sufficiently high molecular weight level, and then becomes less appreciable with further increase in molecular weight [41-46].

Limited research has been done about the molecular weight effect on tensile strength of PU elastomers. Schollenberger and Dinbergs [47] measured the tensile strength of a series of TPU over a M_w range from 47,900 to 366,800 g/mol. Their result showed the same trend with the above findings in other polymers. The tensile strength of the TPU increased with increasing molecular weight up to a limiting value, and then gradually leveled off.

Most of the other studies in the past [57, 125-128] only focused on the effect of soft segment molecular weight on tensile strength. For instance, Zdrahala et al. [125] and Ma et al. [126] studied TPU specimens with wide variations in soft segment molecular weight. Interestingly, they found that increasing soft segment molecular weight had similar effect to increasing final PU molecular weight on tensile strength. The tensile strength of their TPU specimens increased with initial increase in soft segment molecular weight, and then dropped off with further increase. They attributed this phenomenon to the changes in morphology, since research has shown that increasing soft segment molecular weight promotes the microphase separation between hard and soft segments [127]. A higher degree of microphase separation contributes to a better development of reinforcing hard domain in the soft matrix and increases the tensile strength, but an extremely microphase-separated system might exhibit sharp phase boundaries that result in stress concentration and reduce the tensile strength [52, 62].

To-date, the effect of molecular weight on tensile strength of TPU systems that contain different molecular weights but with the same type and ratio of hard and soft segments has not been investigated and should be explored. Moreover, numerous studies

have indicated that the molecular weight of other types of polymers might affect their resistance against scratch and abrasive wear [12, 29, 48-51].

In this study, one set of model TPU systems that contain different molecular weights but with the same type and ratio of hard and soft segments are chosen to determine how the molecular weight of PU elastomers affects the tensile strength, and thus the resistance against scratch and abrasive wear. To achieve this objective, the morphology, tensile true stress-strain behavior, COF, scratch and abrasive wear behaviors of the model systems were investigated and analyzed by various characterization techniques. The implications of the present study for the design of scratch and abrasive wear resistant PU elastomers by modifying the molecular weight are discussed.

5.2 Materials and Methods

5.2.1 Materials

The model TPU systems used in this study were provided by BASF Polyurethane Specialties (China) Co. Ltd. (Shanghai, China). The model systems were synthesized by the same type of hard and soft segments with the same content of each segment. However, the model systems were formulated with different molecular weights and labeled TPU-1, TPU-2 and TPU-3 in order of high to low molecular weight. Physical properties of the model systems were evaluated by BASF Polyurethane Specialties (China) Co. Ltd. and are summarized in Table 7. Gel permeation chromatography (GPC) was used to determine the molecular weight, and polydispersity index (PDI) is defined

as M_w/M_n, as usual. Melt flow rate (MFR) was measured based on ASTM D1238 (210 °C, 10 kg weight) [129]. Differential scanning calorimetry (DSC) was utilized to assess the percent crystallinity of the model systems, which was determined using the ratio of cold crystallization enthalpy to the enthalpy of crystallization for a perfect crystal (196.8 J/g) [130].

Table 7. Material information of the model TPU systems.

	TPU-1	**TPU-2**	**TPU-3**
Hard segment	4,4'-methylene diphenyl diisocyanate + 1,4-butane diol		
Soft segment	Polytetrahydrofuran		
Hard segment content (%)	39		
Molecular weight (g/mol)	110,800	102,510	91,673
PDI	1.79	1.77	1.99
MFR (g/10min)	33	64	129
Crystallinity (%)	7.1	8.3	8.2
RMS roughness (μm)	0.18	0.17	0.17

The specimens were injection-molded into plaques with a thickness of 10 mm by BASF. The surface finish of the plaques was smooth with similar root mean square (RMS) roughness measured on an area of 1.3 mm × 1 mm. Upon receipt, all the specimens were dried in a vacuum oven (30 mm Hg of vacuum pressure) in between two smooth glass plates at 80 ºC for 6 h and then left to slowly cool overnight to room temperature to remove pre-existing moisture and residual stresses in the as-received specimens. For wear testing, the specimen plaques were machined into pins with 25.4 mm in diameter and 10 mm in thickness.

5.2.2 AFM

The morphology of each model TPU system on the cross-section close to the specimen surface was characterized using AFM (Dimension Icon, Bruker) in PeakForce QNM (Quantitative Nanomechanical Property Mapping) imaging mode by BASF Material Physics & Analytics Lab (Shanghai, China). The height, modulus and adhesion maps of the TPU surfaces were collected using a probe (Tap150A, Bruker) with a nominal spring constant of 5 N/m. The modulus and adhesion maps were used to examine the morphology of each model system. The smooth cross-sections were prepared by cryo-microtome (EM UC7FC7, Leica) at -80 °C. The AFM measurements were done at room temperature.

5.2.3 Tensile True Stress-strain Curve Generation

Due to the large straining both in tensile and lateral directions of elastomeric materials during tensile test, true stress-strain behavior is necessary to accurately characterize the tensile behavior of elastomeric materials [88, 102]. Therefore, tensile true stress-strain curve generations of the model systems were conducted using a Digital Image Correlation (DIC) video setup.

Test specimens were injection-molded thin sheets with a thickness of 2 mm. A dumbbell shape was cut from the sheets using a cutting die that conforms to the geometry specified in the ASTM D1708 [131], and then the cutting edges were carefully polished by 4000 grit number polishing paper to remove any possible surface defects. A black ink permanent marker was used to apply random speckle patterns on the gauge section of the specimens, which are required for the DIC analysis.

A MTS Insight® universal testing machine was used to conduct the tensile tests at a crosshead speed of 15 mm/min. A Canon EOS Rebel T5i DSLR camera was utilized to track the variation of speckle patterns on the gauge section during the test, and then a VIC-2D™ DIC software package was employed to generate the true strains in both tensile and lateral directions. Afterwards, the true stress in tensile direction was calculated by dividing the applied load by the measured instantaneous cross-sectional area. The tangential intercept method that measures the stress value at the intersection of the extensions of initial linear region and plateau region was used to determine the yield stress of each model system [75, 76]. And the specimen was stretched to break to determine the tensile strength.

5.2.4 COF Measurement

The COF between the model TPU systems and stainless steel surface were measured using a commercial scratch machine designed according to the ASTM D7027/ISO 19252 standard (Scratch 5, Surface Machine Systems, LLC). To avoid excessive material deformation that will compromise the COF measurements, a stainless steel flat tip with a large surface area of 10 mm × 10 mm and a low constant normal load of 3 N (0.03 MPa) were applied for the tests. Before each test, compressed nitrogen gas was used to remove any possible contaminants on the stainless steel flat tip and specimen surfaces. Three measurements were conducted on each model system to obtain an average value of the COF.

5.2.5 Scratch Test

In accordance with the ASTM D7027/ISO 19252 standard, scratch tests were performed using a linearly increasing normal load of 1-200 N over a scratch length of 100 mm at a constant scratch speed of 200 mm/s. A stainless steel conical scratch tip [88, 102], which has a continuous tip geometry with a 1 mm diameter sphere attached to a cone, was used for the scratch tests. Before each test, compressed nitrogen gas was used to remove any possible contaminants on the scratch tip and specimen surfaces. After completion of scratch test, the onset point of tensile tear-induced cracking/material removal damage on the model systems was located by a Keyence® VK9700 violet laser scanning confocal microscope (VLSCM) under 20 × magnification, and then the corresponding critical normal load for the onset was determined through the applied

normal load-travel distance curve generated by the scratch machine. Three scratch tests were conducted on each model system to obtain an average value of the critical normal load for the onset of tensile tear-induced cracking/material removal damage.

5.2.6 Wear Test

To investigate the abrasive wear behavior of the model TPU systems, sliding wear tests were performed by a custom built multi-axis tribometer in a pin-on-flat configuration. The detailed descriptions of this setup can be found elsewhere [124]. Basically, by using this setup, the TPU pin specimens were pneumatically loaded against a planar counterface stage that was capable of making two axis of motions at a specified velocity. The TPU pin specimens remained stationary during the wear test, while the counterface stage moved according to the programmed wear path and velocity. Wear was generated through the relative motion between the pin specimen and the counterface stage. The counterface used in this study was a hot rolled 304 stainless steel sheet with a RMS roughness of 8.19 μm. Since the asperities on the stainless steel counterface are non-uniform without directionality, a linear reciprocating wear path is adequate and thus employed to conduct the sliding wear tests [124].

As abrasive wear is generated as the result of removal of material from the polymer surface through penetration and continuous sliding of asperities on the counterface [29], a 50 mm long stroke distance was used for the reciprocation to ensure the two mutually loaded surfaces have sufficient distance to continuously slide against each other. A long stroke distance also allows most debris to be expelled during the

reciprocation so that a fresh pin surface is always sliding across counterface asperities at each cycle. This sliding wear test configuration has been successfully applied to evaluate the abrasive wear behaviors of cast polyurethane elastomers [124] and polyaryletherketone family of thermoplastics [29, 37, 103]. A normal load of 500 N, which achieved a nominal contact pressure of 1 MPa for the 25.4 mm diameter pins, was utilized to perform the tests at a constant velocity of 200 mm/s. To generate measurable quantity of wear debris, each test was run for 300 m of total traveling distance. Before and after each test, compressed nitrogen gas was used to clean the specimen surface. The weight loss was measured by weighing the specimen before and after each test using an analytical balance with 0.01 mg resolution, and then the wear volume was calculated by the weight loss and density of each model TPU system. Three tests were conducted on each model system to obtain an average value of the abrasive wear volume.

During the wear test, frictional heat was generated, increasing the temperature of the specimen. A Fluke® Ti45FT IR camera was positioned 0.3 m from the specimen to track the temperature rise of the specimen from the beginning of the test. The detector of the IR camera had a high resolution 160 × 120 focal plane array with a temperature sensitivity down to 0.08 ºC. For each specimen, an IR image was first taken before the test started. After the test started, an IR image was taken at every 10 m of travelling distance for the first 50 m of the test, and then at every 50 m of travelling distance for the rest of the test. Automatic internal calibration was performed through the IR camera before taking every image, to maintain high quality of each captured image.

After the wear test, wear surface of each model system was inspected by the VLSCM under 20 × magnification. For each model system, multiple images were taken at different locations on the wear surface to check the consistency of wear damage feature throughout the wear surface. One image of each model system was selected and shown.

5.3 Results and Discussion

5.3.1 AFM

Tapping mode AFM has been widely used to investigate the morphology of multi-phase polymers. During the scanning of tapping mode AFM probe, a phase lag between the excitation and response oscillation of the cantilever can be induced by different material properties of the phases such as modulus and adhesion. This effect provides contrasts for different phases so that the microphase-separated morphology can be observed. However, this method cannot distinguish the individual contribution from the modulus and adhesion of different phases. The recently developed PeakForce QNM mode AFM tracks the instantaneous force on the probe rather than a time-average of the force over time, as is done in the tapping mode phase imaging [132]. This new method allows the measurement of modulus variation and adhesion variation over the multi-phases polymer surface separately, which gives a better observation of the microphase-separated morphology. Research has demonstrated that the modulus and adhesion maps captured by the PeakForce QNM mode AFM are in good agreement with the corresponding phase image captured by the tapping mode AFM [133].

The AFM modulus and adhesion maps of the model TPU systems are shown in Figure 38. Similar to the phase image of AFM, the bright region on these maps refers to the region with a higher modulus and a higher adhesion between probe and specimen, i.e., the hard segment domain. As shown in the figure, within the range of molecular weights examined, all the model systems exhibit alternating bright and dark regions throughout the scanned area. The model system with a lower molecular weight appears to have a slightly more distinct two-phase morphology. However, these differences are very subtle. Therefore, the influence of morphology on the tensile strength of the model systems is expected to be minimal, if any.

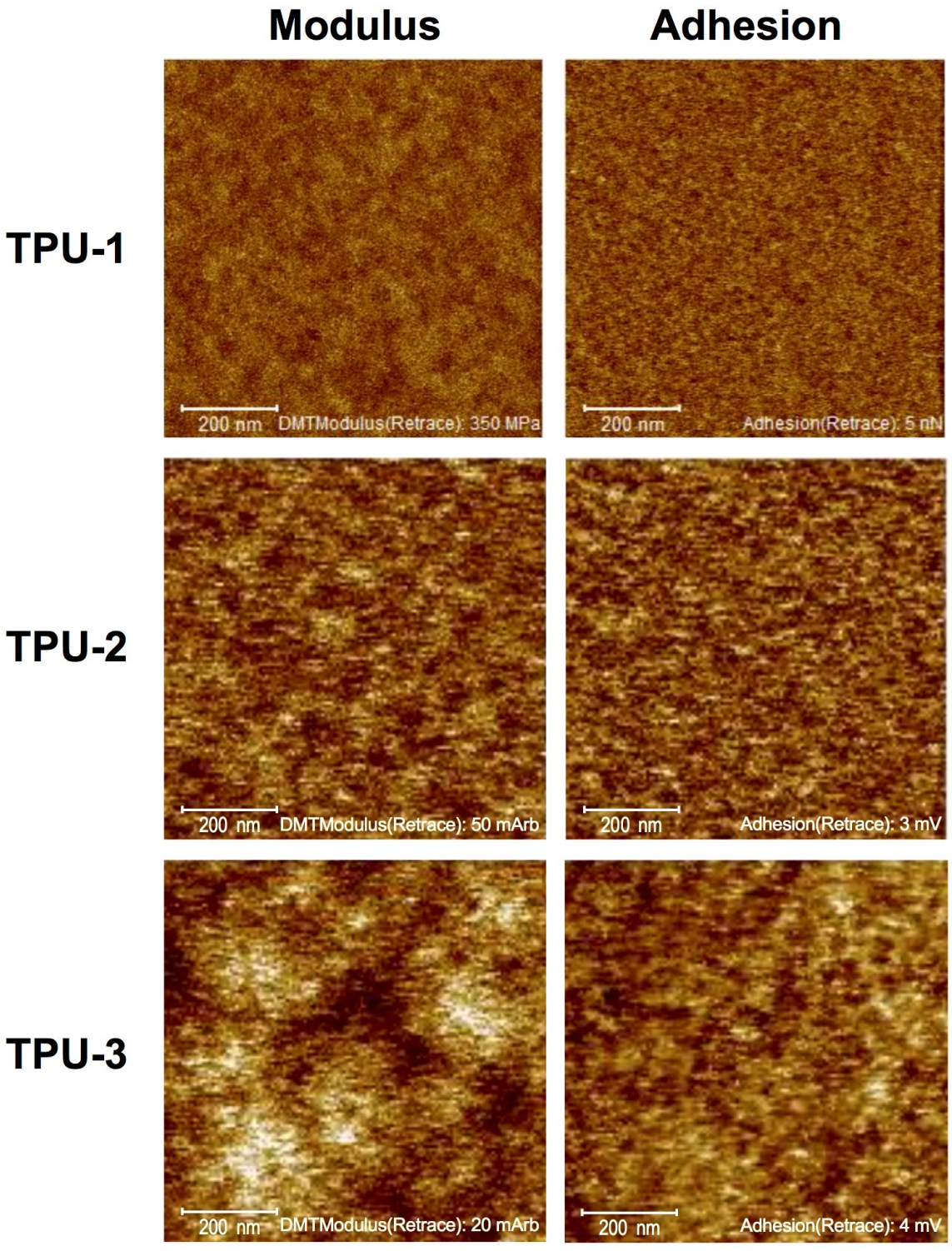

Figure 38. AFM modulus and adhesion maps of the model TPU systems.

5.3.2 Tensile True Stress-strain Behavior

The uniaxial tensile true stress-strain curves of the model TPU systems are shown in Figure 39 with key uniaxial tensile properties of the model systems summarized in Table 8. As shown in the figure and table, by changing the molecular weight of the model TPU systems, the tensile properties exhibit different degrees of changes. Within the range of molecular weights investigated in this study, the tensile strength of the model systems shows the most apparent changes, i.e., the model system with a higher molecular weight shows a higher tensile strength.

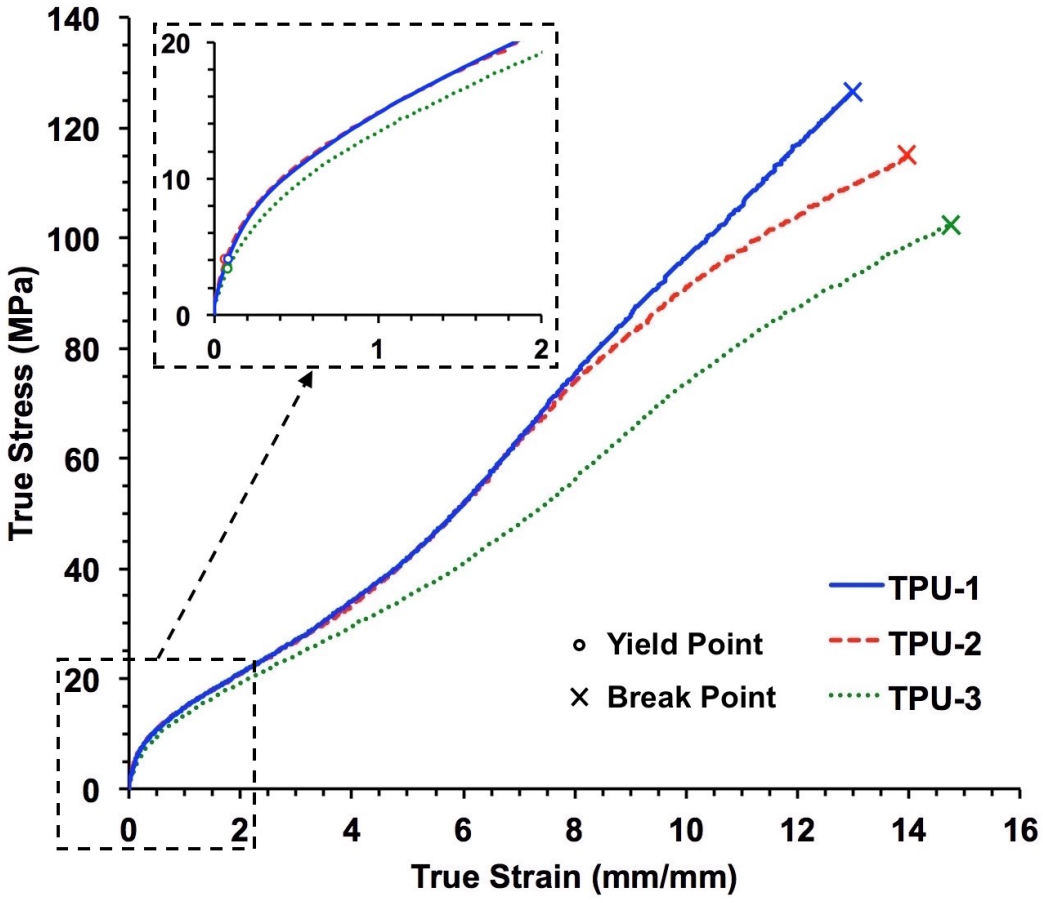

Figure 39. Tensile true stress-strain curves of the model TPU systems.

Table 8. Uniaxial tensile properties of the model TPU systems.

	TPU-1	TPU-2	TPU-3
Tensile modulus (MPa)	55.4 ± 5.1	55.1 ± 1.8	47.7 ± 2.9
Tensile yield stress (MPa)	4.1 ± 0.3	4.0 ± 0.4	3.5 ± 0.2
Tensile strain at break (%)	1369.2 ± 62.7	1404.8 ± 52.5	1482.0 ± 57.4
Tensile strength (MPa)	120.4 ± 5.6	111.6 ± 3.5	98.8 ± 4.0

Increasing molecular weight is known to increase the density of chain entanglements. Chain entanglements, which serve as physical crosslinks to reinforce the polymers, take place when the molecular weight of polymer exceeds the critical molecular weight for chain entanglements, and as such, the polymer can become strong enough to carry a load [134]. Polymers with a higher density of chain entanglements have more entangled molecular chains to support the tensile loading and a better resistance to the separation of molecular chains under tension [43, 135]. As a result, the tensile strength of the model TPU systems improves with increasing molecular weight. This finding is in good agreement with the results of previous studies about molecular weight effect on the tensile strength of TPU [47] and other polymeric systems [42-46].

However, these previous studies also pointed out that the positive effect of molecular weight on the tensile strength of polymers becomes less significant with further increase in molecular weight. As the molecular weight further increases to a

certain level, the chain mobility is reduced and the rearrangement of molecular chains is substantially inhibited prior to tensile breaking owing to the high density of chain entanglements and intermolecular forces [41, 47]. Consequently, the net effect is a reduction in tensile elongation at break, which limits the further increase in tensile strength with increasing molecular weight. Nevertheless, this phenomenon is not observed for the model TPU systems investigated in the present study, since the range of molecular weights examined might not high enough to induce considerable reduction in tensile elongation at break. This is evidenced by the minor changes in tensile elongation at break for the model TPU systems, i.e., the tensile elongation at break of the model TPU systems is insensitive to the changes in molecular weight if the standard deviation is taken into account.

Compared to the significant changes in tensile strength of the model TPU systems, the changes in modulus and yield stress appear to be independent of the variation in molecular weight over the range investigated. Because at low strains, the entangled molecular chains are not fully extended, and as a result, they do not have a chance to contribute to the modulus and yield stress of the model systems [42, 43].

5.3.3 COF Measurement

The increase in molecular weight for a polymer is known to reduce the flowability, as reflected by the MFR values of the model TPU systems listed in Table 7, and slow down the rate of crystallization, which may result in a lower crystallinity [29, 48]. It has been shown that for different polymeric systems, a decrease in crystallinity

leads to an increase in COF, which is attributed to the decrease in modulus of the surface layer resulted from the decrease in crystallinity [136-138]. However, in the present study, all the model TPU systems exhibit similar COF as shown in Figure 40. The COF of the model TPU systems is insensitive to the variation in molecular weight over the range investigated. This finding is supported by the comparable crystallinity and modulus of the model systems as listed in Table 7 and Table 8, respectively.

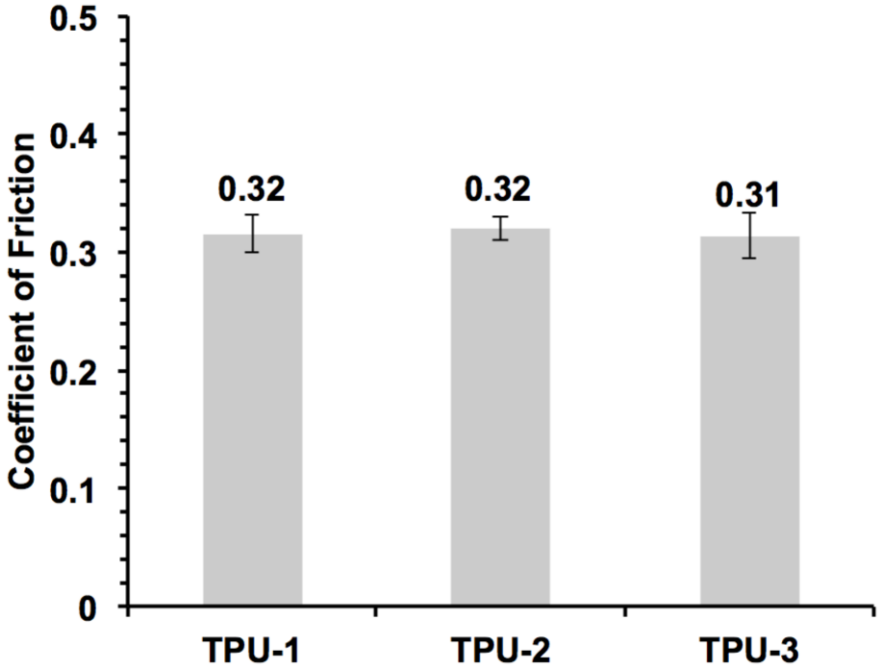

Figure 40. Coefficient of friction of the model TPU systems.

5.3.4 Scratch Behavior

The critical normal loads for the onset of tensile tear-induced cracking/material removal of the model TPU systems during scratch are plotted in Figure 41. The VLSCM images of the onset of tensile tear-induced cracking/material removal on the model TPU

systems are shown in Figure 42. As shown in the figure, all the model systems exhibit a clear onset of the cracking damage, and after the onset point, all of them show a similar type of continuous parabolic crack formation along the scratch path with small amount of materials removed from the middle portion of the cracks. However, each model system shows a different onset load for the damage. The model system with a higher molecular weight shows a higher onset load, which indicates a better resistance to this scratch damage.

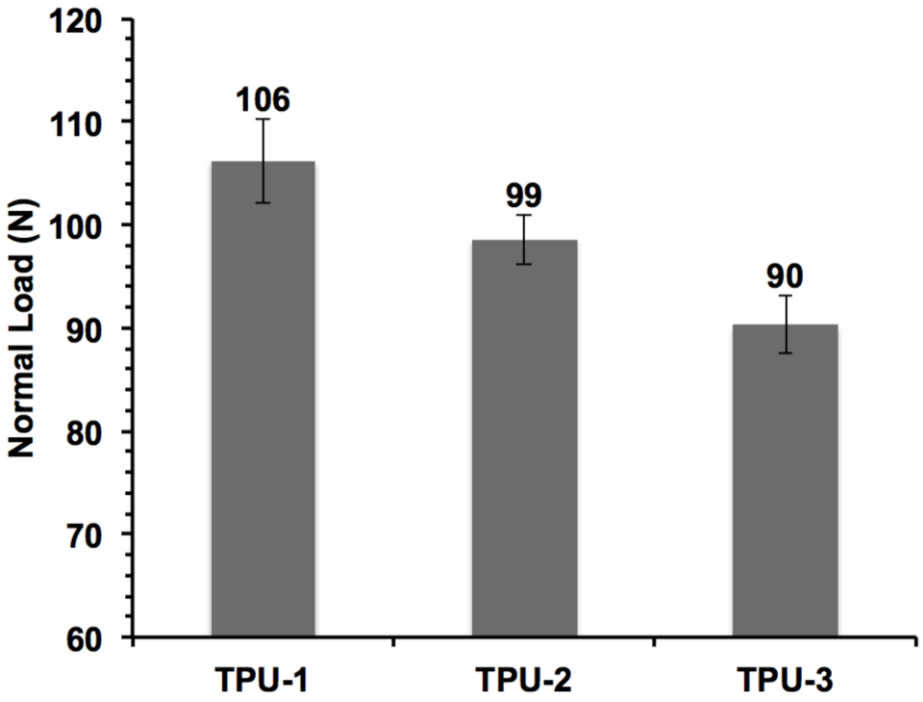

Figure 41. Critical normal loads for onset of tensile tear-induced cracking/material removal of the model TPU systems.

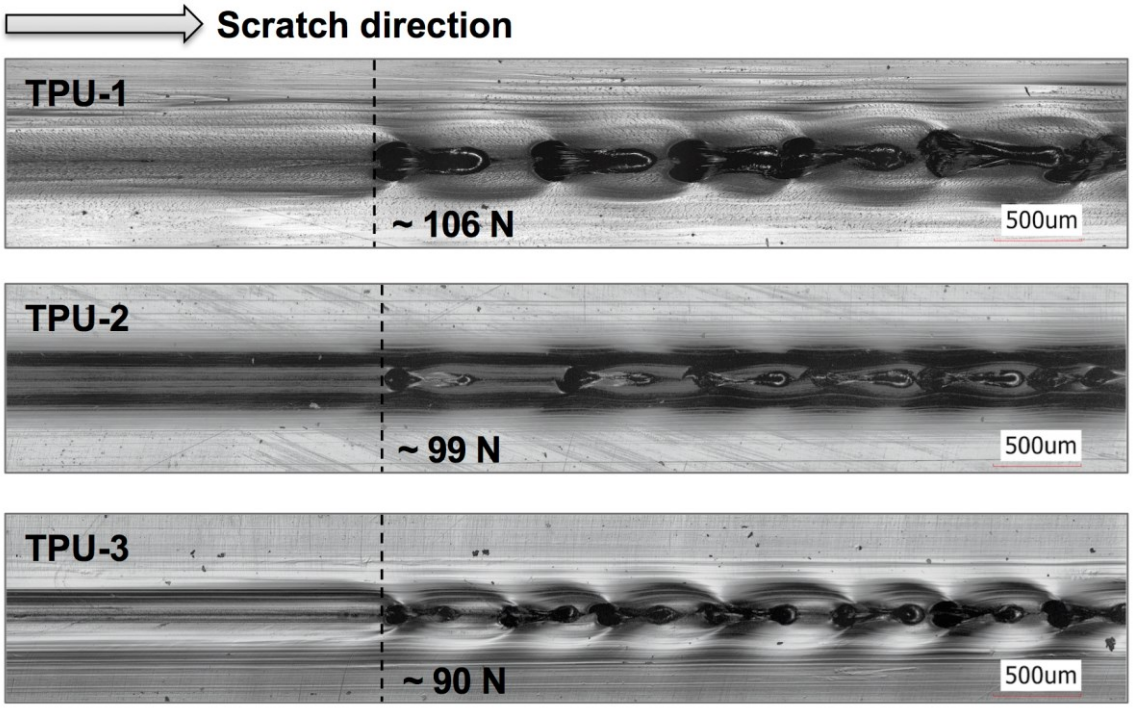

Figure 42. VLSCM images of onset of tensile tear-induced cracking/material removal on the model TPU systems.

As it has been demonstrated in previous experimental and numerical scratch studies using a linearly increasing normal load [16, 22, 88, 102], upon scratching, the scratch tip rubs against the specimen surface and penetrates through the material as the normal load increases, inducing a high magnitude of tensile stress nearly parallel to the scratch direction behind the scratch tip. As the scratching normal load further increases, the magnitude of the tensile stress will exceed the tensile strength of the specimen and lead to tensile tear-induced cracking/material removal along the scratch path. A higher tensile strength is found to be essential for a better resistance of polymers against this scratch damage. In addition, research has also shown that a higher COF intensifies the

stress gradient and magnitude on and underneath the specimen surface during scratching and has negative effect on the resistance of polymers against tensile tear-induced cracking/material removal [20, 139, 140].

Since the model TPU systems investigated in this study have comparable COF, the influence of COF can be ignored. The tensile strength would be the major material property that responsible for the observed scratch behavior of the model systems. As discussed earlier, within the range of molecular weights examined, the model system with a higher molecular weight shows a higher tensile strength. This finding is consistent with the scratch test result that the model system with a higher molecular weight shows a better resistance to tensile tear-induced cracking/material removal. Therefore, the scratch resistance of TPU against tensile tear-induced cracking/material removal can be improved by increasing the molecular weight.

5.3.5 Abrasive Wear Behavior

Scratch can be considered a single-pass sliding of a single-asperity under the influence of an applied normal load over the specimen surface, while abrasive wear typically involves multi-passes of multi-asperities over the same specimen surface [30]. As mentioned earlier, research efforts have been performed to establish physical correlation between scratch resistance and abrasive wear performance of PU elastomers [124]. It is found that both scratch and abrasive wear damages of PU elastomers involve tensile tear-induced cracking along with material removal on the surface. A PU

elastomer with a higher tensile strength shows better resistances against both scratch onset of tensile tear-induced cracking/material removal and abrasive wear volume loss.

The abrasive wear volume loss of the model TPU systems from the sliding wear test are plotted in Figure 43. As expected, within the range of molecular weights investigated, the model system with a higher molecular weight, i.e., a higher tensile strength, not only shows a latter onset of tensile tear-induced cracking/material removal during scratch but also shows a lower volume loss during abrasive wear. The difference in abrasive wear volumes among the model systems appears to be more pronounced than the difference in scratch onset loads. Since abrasive wear involves multi-passes of multi-asperities, the difference in the observed performance among the model systems is magnified. Consequently, the abrasive wear resistance of TPU can also be improved by increasing the molecular weight.

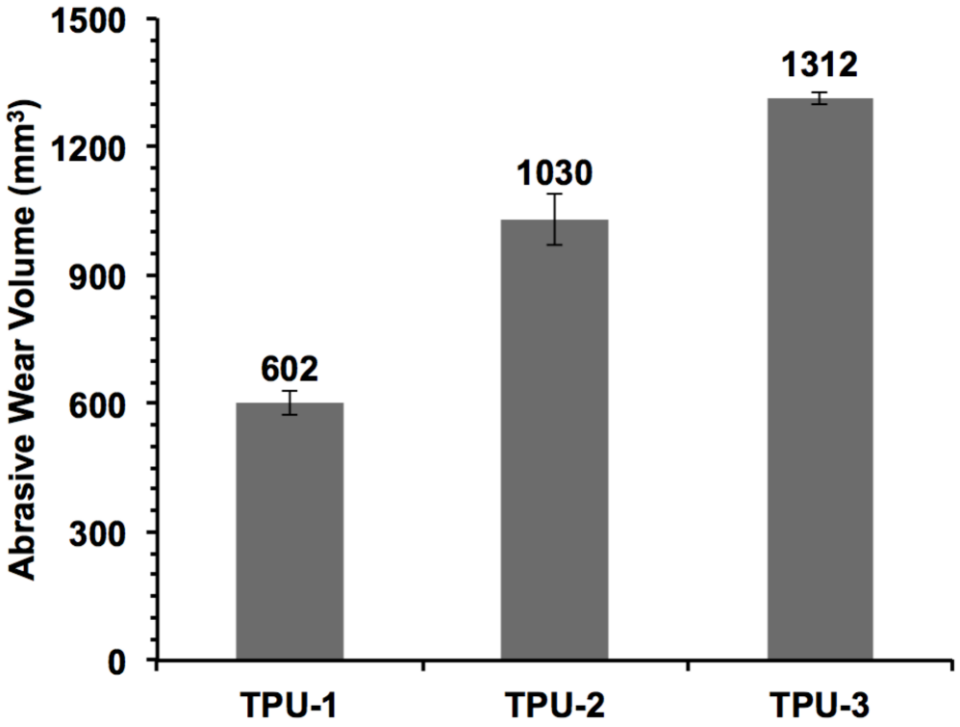

Figure 43. Abrasive wear volume of the model TPU systems.

The wear surface images of the model TPU systems taken by the VLSCM are shown in Figure 44. All the model systems exhibit a similar wear surface, which indicates the wear damage of the model systems occurred by the same mechanism. Material is removed from the specimen surface during the wear test due to the presence of numerous tiny asperities on the steel counterface, i.e., once the local stresses at these asperities resulted from the applied normal load exceed the tensile strength of the specimen, tensile tear-induced cracking occurs and material is removed from the cracks [124]. The parallel wave pattern on the wear surface that perpendicular to the sliding direction is commonly observed for polymers examined by a reciprocating wear test, which is a result of the accumulation of plastic deformation during the reciprocation

[105, 106]. Owing to the high tensile elongation at break of the model systems, several debris rolls have not been detached during the wear test and are still connected to the wear surface.

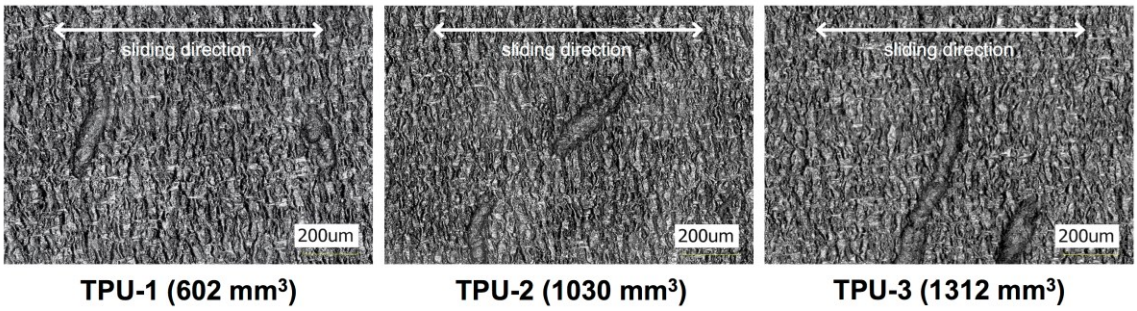

Figure 44. VLSCM images of wear surfaces on the model TPU systems (wear volume of each model system is shown in the legend).

The temperature rise of each model TPU system versus travelling distance during the wear test is plotted in Figure 45(a). The trend of the temperature rise in the model TPU systems is consistent with the finding in the previous study [124]. Since PU elastomers have low thermal conductivities, frictional heat accumulates quickly within the specimens and results in a fast temperature rise at the beginning of the test. However, due to the high thermal conductivity of stainless steel counterface, the accumulated heat reaches thermal equilibrium and the temperature rise gradually levels off for the rest of the test. The average temperature rise of each model TPU system in the plateau region (200 m, 250 m and 300 m) is summarized in Figure 45(b). All the model systems exhibit similar average temperature rise at the end of the wear test. It has been shown that COF is the key surface characteristic that determines the temperature rise of PU elastomers

during wear [124]. The average temperature rise of the model TPU systems in the plateau region is in good agreement with the measured COF that all the model TPU systems also have comparable COF. This finding, once again, confirms that the influence of surface friction on the observed scratch and abrasive wear behaviors of the model TPU systems can be ignored.

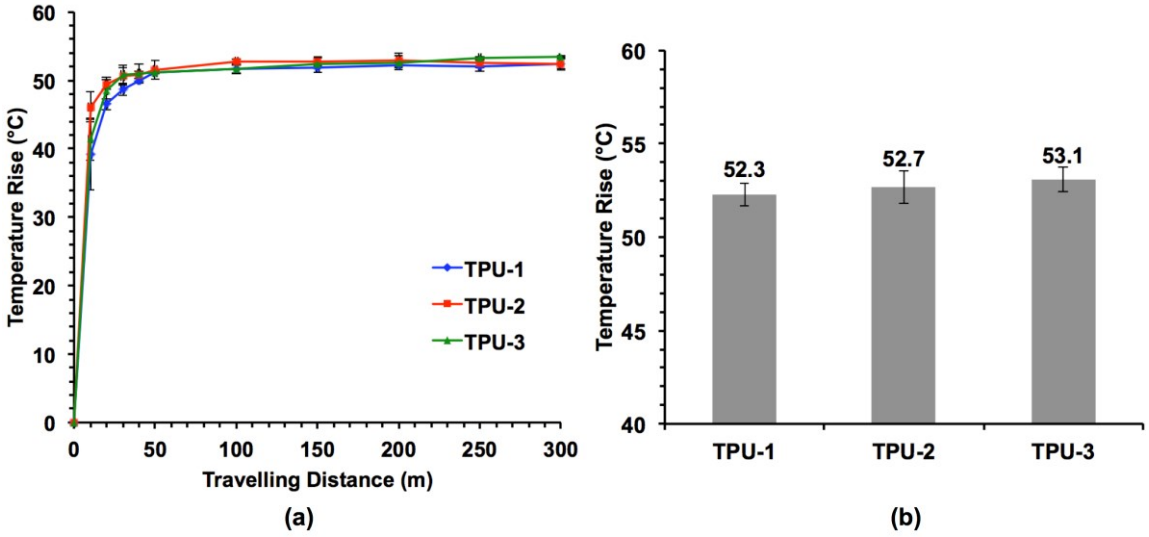

Figure 45. (a) Abrasive wear temperature rise of the model TPU systems versus travelling distance; (b) average temperature rise in the plateau region (200 m, 250 m and 300 m).

As tensile strength is responsible for the resistance of polymers against scratch onset of tensile tear-induced cracking/material removal and abrasive wear volume loss, the present study shows how the tensile strength, and thus the scratch and abrasive wear performance of polymers can be improved by increasing the molecular weight. The implication of the present study signifies that other means of increasing the tensile strength of polymers, such as incorporation of exfoliated nanoplatelets [141] or

introduction of crosslinking, can also be applied to improve the scratch and abrasive wear performance of polymers. This finding will be attractive to industries where aesthetic appearance and surface structural integrity of polymer products are highly desired.

5.4 Conclusions

Effect of molecular weight on scratch and abrasive wear behaviors of a series of model TPU systems was investigated. Within the range of molecular weights examined, it is found that the variation in molecular weight has considerable influence on the tensile strength of the model TPU systems. As a result, the scratch and abrasive wear performance of the model TPU systems are also significantly affected. The following conclusions can be drawn based on this study:

- Increasing the molecular weight improves the tensile strength of TPU.
- The variation in molecular weight has minimal influence on the morphology and COF of TPU.
- Increasing the molecular weight improves the resistance of TPU against scratch onset of tensile tear-induced cracking/material removal and abrasive wear volume loss.

CHAPTER VI

CONCLUSIONS AND CONSIDERATIONS FOR FUTURE RESEARCH

6.1 Summary and Conclusions

Extensive experimental works along with numerical analysis were carried out in this study to gain fundamental understanding of scratch and wear behaviors of PU elastomers. The focuses of this research effort were as follows:

- Determine the key mechanical properties and surface characteristics that are related to the scratch behavior of PU elastomers
- Investigate how environmental moisture affects the mechanical properties, surface characteristics and the corresponding scratch behavior of PU elastomers
- Establish physical correlation between scratch and abrasive wear behaviors of PU elastomers
- Explore the possibility of improving the resistance of PU elastomers against scratch and abrasive wear by modifying the molecular weight

Based on the experimental and numerical scratch studies, the mechanical properties and surface characteristics of PU elastomers have been quantitatively correlated with the observed scratch-induced deformation. It is found that PU elastomers with a higher degree of microphase separation, a more uniform domain size and distribution possess improved tensile and compressive properties. Increasing the compressive yield stress and/or decreasing the COF of PU elastomers delays the onset of

scratch groove formation. Increasing the tensile strength and/or decreasing the COF of PU elastomers enhances scratch resistance against tensile tear induced cracking/material removal. In addition, PU elastomers with a more pronounced damping characteristic exhibit a higher COF when sliding against stainless steel and tend to be more sensitive to speed of scratching.

Upon exposure to moisture, the absorption and diffusion of water in PU elastomers depend on the chemical constituents, e.g., different soft segment types. It is found that the water absorption and diffusion of the less polar polyether-based PU elastomers are dominated by the abundant of free volume in the matrix, while those of the more polar polyester-based PU elastomers are governed by the polar bonding sites in the matrix. For polyether-based PU elastomers, the homogeneously absorbed water molecules serve as plasticizer to degrade the tensile strength, and thus deteriorating the resistance against cracking/ material removal. The plasticization effect also contributes to an increase in COF and results in earlier onset of groove formation and cracking/material removal. However, for polyester-based PU elastomers, due to the interaction between water molecules and the polar bonding sites, clustering of water occurs on the surface and acts as lubricant to decrease the COF, and thus improving the resistance to groove formation and cracking/material removal.

The wear study of PU elastomers under different wear conditions shows that abrasive wear volume of PU elastomers has good correlation with the onset of cracking/material removal during scratch. Abrasive wear and scratch damages of PU elastomers are governed by the same damage mechanism, which involves tensile tear

induced cracking along with material removal on the surface. Consequently, the key mechanical property that responsible for scratch resistance of PU elastomers can be extended to abrasive wear resistance of PU elastomers, i.e., a higher tensile strength improves the resistance against both scratch onset of cracking/material removal and abrasive wear volume loss.

In order to improve the scratch and abrasive wear performance of PU elastomers, the key is to increase the tensile strength. It is found that increasing the molecular weight is an effective way to increase the tensile strength of PU elastomers. As a result, the resistance of PU elastomers against scratch onset of tensile tear induced cracking/material removal and abrasive wear volume loss is also improved significantly. The present research effort provides fundamental understanding on the scratch and abrasive wear behaviors of PU elastomers and offers fundamental insights into the design of scratch and abrasive wear resistant PU elastomers by modifying the molecular parameters.

6.2 Considerations for Future Research

The scratch and abrasive wear mechanisms of PU elastomers have been extensively investigated. The findings presented in this research work provide insights and directions for future research in the field.

6.2.1 Improving Tensile Strength by Heat Treatment

As tensile strength has been determined as the key mechanical property that responsible for the resistance of PU elastomers against scratch onset of cracking/material removal and abrasive wear volume loss, one direction of the future research can be focused on improving the tensile strength of PU elastomers. Heat treatment of polymers is considered one of the most effective methods for modifying the properties of polymers. Annealing is one of the most commonly used heat treatment process to improve the tensile properties of polymers.

For a semi-crystalline polymer, annealing at a temperature above the glass transition temperature of the polymer results in a higher degree of crystallinity. For a multiphase block copolymer, annealing is shown to promote the phase separation between different phases. Both of these will improve the tensile strength of the polymer. However, research on how annealing influences the tensile strength, and thus the scratch and abrasive wear behaviors of PU elastomers is still lacking. It would be interesting to learn if PU elastomers with improved scratch and abrasive wear resistances can be made simply by applying a post-processing heat treatment. This will be highly attractive to industries where the tribological performance of PU elastomers is of great importance.

6.2.2 Promoting Transfer Film Formation by the Incorporation of Nanoparticles

During the wear process of a polymer against a metal counterface, many polymers will deposit a thin layer of transfer film on the metal counterface. The formation of the transfer film will protect the polymer from wear damage by covering

the sharp asperities on the metal counterface. As a result, the wear resistance of a polymer is strongly influenced by its ability to form a transfer film on the counterface. However, as discussed earlier, during the wear process of PU elastomers, no transfer film formation is observed.

In order to promote the transfer film formation of PU elastomers during wear, nanoparticles can be incorporated into the PU matrix. Research has shown that during the wear process of a polymer nanocomposite, the nanoparticles can be released from the matrix and deposited on the counterface. These nanoparticles will then form a layer of transfer film to prevent the direct contact between the polymer matrix and counterface. Consequently, the wear performance of the polymer system can be improved. Moreover, the incorporation of well-dispersed nanoparticles in polymer has also been shown to increase the tensile strength of the polymer, which may further improve the abrasive wear resistance, as well as the scratch resistance. Future work to incorporate well-dispersed nanoparticles in PU elastomers would be highly beneficial.

6.2.3 FEM Simulation of Tensile Tear Induced Cracking

The experimental findings in this research work have shown that abrasive wear and scratch damages of PU elastomers are governed by the same damage mechanism, which involves tensile tear induced cracking along with material removal on the surface. To better understand the mechanics behind the crack formation, FEM simulation of the cracking process on the sample surface during scratch and wear is needed. As tensile strength has been determined as the key mechanical property that related to the

resistance against tensile tear induced cracking, strain rate dependent tensile behavior of PU elastomers would be important for a precise simulation. This simulation will allow the inspection of stress and strain field developed during crack formation, which provides a more comprehensive understanding on the damage mechanism. It will also allow the prediction of scratch and abrasive wear performance of PU elastomers based on the constitutive behavior.

REFERENCES

[1] J. Chu, L. Rumao, B. Coleman, Scratch and mar resistance of filled polypropylene materials, Polymer Engineering & Science 38(11) (1998) 1906-1914.

[2] J. Chu, C. Xiang, H.J. Sue, R.D. Hollis, Scratch resistance of mineral-filled polypropylene materials, Polymer Engineering & Science 40(4) (2000) 944-955.

[3] R.S. Kody, D.C. Martin, Quantitative characterization of surface deformation in polymer composites using digital image analysis, Polymer Engineering & Science 36(2) (1996) 298-304.

[4] B. Briscoe, A. Delfino, E. Pelillo, Single-pass pendulum scratching of poly (styrene) and poly (methylmethacrylate), Wear 225 (1999) 319-328.

[5] P. Guevin, State-of-the-art instruments to measure coating hardness, JCT, Journal of coatings technology 67(840) (1995) 61-65.

[6] M. Wong, G. Lim, A. Moyse, J. Reddy, H.-J. Sue, A new test methodology for evaluating scratch resistance of polymers, Wear 256(11-12) (2004) 1214-1227.

[7] ASTM, D7027-13 Standard Test Method for Evaluation of Scratch Resistance of Polymeric Coatings and Plastics Using an Instrumented Scratch Machine, ASTM International, Pennsylvania, 2013.

[8] ISO, 19252:2008 Plastics — Determination of scratch properties, International Organization for Standardization, 2008.

[9] M.M. Hossain, E. Moghbelli, E. Jahnke, P. Boeckmann, S. Guriyanova, R. Sander, R. Minkwitz, H.-J. Sue, Rubber particle size and type effects on scratch behavior of styrenic-based copolymers, Polymer 63 (2015) 71-81.

[10] Y.L. Liang, H.J. Sue, R. Minkwitz, Rubber content effect on scratch behavior in acrylonitrile-styrene-acrylate copolymers, Journal of Applied Polymer Science 126(3) (2012) 1088-1096.

[11] Y.-L. Liang, E. Moghbelli, H.-J. Sue, R. Minkwitz, R. Stark, Effect of high temperature annealing on scratch behavior of acrylonitrile styrene acrylate copolymers, Polymer 53(2) (2012) 604-612.

[12] R. Browning, H.J. Sue, R. Minkwitz, P. Charoensirisomboon, Effects of acrylonitrile content and molecular weight on the scratch behavior of styrene-

acrylonitrile random copolymers, Polymer Engineering & Science 51(11) (2011) 2282-2294.

[13] R. Browning, R. Minkwitz, P. Charoensirisomboon, H.-J. Sue, Influence of humidity on the scratch behavior of polystyrene–acrylonitrile random copolymers, Journal of materials science 46(17) (2011) 5790-5797.

[14] M.M. Hossain, E. Jahnke, P. Boeckmann, S. Guriyanova, R. Minkwitz, H.-J. Sue, Effect of thermal history on scratch behavior of multi-phase styrenic-based copolymers, Tribology International 99 (2016) 248-257.

[15] M. Hamdi, H.-J. Sue, Effect of color, gloss, and surface texture perception on scratch and mar visibility in polymers, Materials & Design 83 (2015) 528-535.

[16] M.M. Hossain, S. Xiao, H.-J. Sue, M. Kotaki, Scratch behavior of multilayer polymeric coating systems, Materials & Design 128 (2017) 143-149.

[17] H. Jiang, R. Browning, H.-J. Sue, Understanding of scratch-induced damage mechanisms in polymers, polymer 50(16) (2009) 4056-4065.

[18] M.M. Hossain, H. Jiang, H.-J. Sue, Effect of constitutive behavior on scratch visibility resistance of polymers—A finite element method parametric study, Wear 270(11-12) (2011) 751-759.

[19] M.M. Hossain, R. Browning, R. Minkwitz, H.-J. Sue, Effect of asymmetric constitutive behavior on scratch-induced deformation of polymers, Tribology Letters 47(1) (2012) 113-122.

[20] M.M. Hossain, R. Minkwitz, H.J. Sue, Minimization of surface friction effect on scratch-induced deformation in polymers, Polymer Engineering & Science 53(7) (2013) 1405-1413.

[21] M.M. Hossain, R. Minkwitz, P. Charoensirisomboon, H.-J. Sue, Quantitative modeling of scratch-induced deformation in amorphous polymers, Polymer 55(23) (2014) 6152-6166.

[22] E. Moghbelli, R. Banyay, H.-J. Sue, Effect of moisture exposure on scratch resistance of PMMA, Tribology International 69 (2014) 46-51.

[23] C.R. Dias, M.J. Rosa, M.N. de Pinho, Structure of water in asymmetric cellulose ester membranes—and ATR-FTIR study, Journal of membrane science 138(2) (1998) 259-267.

[24] H. Kitano, K. Ichikawa, M. Ide, M. Fukuda, W. Mizuno, Fourier transform infrared study on the state of water sorbed to poly (ethylene glycol) films, Langmuir 17(6) (2001) 1889-1895.

[25] K. Saijo, O. Arimoto, T. Hashimoto, M. Fukuda, H. Kawai, Moisture sorption mechanism of aromatic polyamide fibres: diffusion of moisture into regular Kevlar as observed by time-resolved small-angle X-ray scattering technique, Polymer 35(3) (1994) 496-503.

[26] M. Unemori, Y. Matsuya, S. Matsuya, A. Akashi, A. Akamine, Water absorption of poly (methyl methacrylate) containing 4-methacryloxyethyl trimellitic anhydride, Biomaterials 24(8) (2003) 1381-1387.

[27] A.M. Thomas, Moisture permeability, diffusion and sorption in organic film-forming materials, Journal of Applied Chemistry 1(4) (1951) 141-158.

[28] W. Drotning, E. Roth, Effects of moisture on the thermal expansion of poly (methylmethacrylate), Journal of materials science 24(9) (1989) 3137-3140.

[29] K. Laux, H. Sue, A. Montoya, T. Bremner, Wear behavior of polyaryletherketones under multi-directional sliding and fretting conditions, Tribology Letters 58(3) (2015) 41.

[30] K. Friedrich, H. Sue, P. Liu, A. Almajid, Scratch resistance of high performance polymers, Tribology International 44(9) (2011) 1032-1046.

[31] F. Martínez, M. Canales, J. Bielsa, M. Jiménez, Relationship between wear rate and mechanical fatigue in sliding TPU–metal contacts, Wear 268(3-4) (2010) 388-398.

[32] H. Kim, R.-U. Kim, K.-H. Chung, J.-H. An, H.-G. Jeon, B.-J. Kim, Effect of test parameters on degradation of polyurethane elastomer for accelerated life testing, Polymer Testing 40 (2014) 13-23.

[33] D. Xu, J. Karger-Kocsis, A. Schlarb, Rolling friction and wear of organoclay-modified thermoplastic polyurethane rubbers against steel, KAUTSCHUK UND GUMMI KUNSTSTOFFE 61(3) (2008) 98.

[34] M. Yahiaoui, J. Denape, J.-Y. Paris, A.G. Ural, N. Alcalà, F.J. Martinez, Wear dynamics of a TPU/steel contact under reciprocal sliding, Wear 315(1-2) (2014) 103-114.

[35] G. Zhang, C. Zhang, P. Nardin, W.-Y. Li, H. Liao, C. Coddet, Effects of sliding velocity and applied load on the tribological mechanism of amorphous poly-ether–ether–ketone (PEEK), Tribology international 41(2) (2008) 79-86.

[36] R. Elleuch, K. Elleuch, B. Salah, H. Zahouani, Tribological behavior of thermoplastic polyurethane elastomers, Materials & design 28(3) (2007) 824-830.

[37] K. Laux, C. Schwartz, Influence of linear reciprocating and multi-directional sliding on PEEK wear performance and transfer film formation, Wear 301(1-2) (2013) 727-734.

[38] H.-J. Song, Z.-Z. Zhang, X.-H. Men, The tribological behaviors of the polyurethane coating filled with nano-SiO2 under different lubrication conditions, Composites Part A: Applied Science and Manufacturing 39(2) (2008) 188-194.

[39] G. Zhao, T. Wang, Q. Wang, Friction and wear behavior of the polyurethane composites reinforced with potassium titanate whiskers under dry sliding and water lubrication, Journal of materials science 46(20) (2011) 6673-6681.

[40] R. Prehn, F. Haupert, K. Friedrich, Sliding wear performance of polymer composites under abrasive and water lubricated conditions for pump applications, Wear 259(1-6) (2005) 693-696.

[41] R.W. Nunes, J.R. Martin, J.F. Johnson, Influence of molecular weight and molecular weight distribution on mechanical properties of polymers, Polymer Engineering & Science 22(4) (1982) 205-228.

[42] H.W. McCormick, F.M. Brower, L. Kin, The effect of molecular weight distribution on the physical properties of polystyrene, Journal of Polymer Science 39(135) (1959) 87-100.

[43] W.G. Perkins, N.J. Capiati, R.S. Porter, The effect of molecular weight on the physical and mechanical properties of ultra-drawn high density polyethylene, Polymer Engineering & Science 16(3) (1976) 200-203.

[44] R.J. Gardner, J.R. Martin, Humid aging of plastics: effect of molecular weight on mechanical properties and fracture morphology of polycarbonate, Journal of Applied Polymer Science 24(5) (1979) 1269-1280.

[45] A. Gent, A. Thomas, Effect of molecular weight on the tensile strength of glassy plastics, Journal of Polymer Science Part A-2: Polymer Physics 10(3) (1972) 571-573.

[46] B. Bersted, T. Anderson, Influence of molecular weight and molecular weight distribution on the tensile properties of amorphous polymers, Journal of Applied Polymer Science 39(3) (1990) 499-514.

[47] C. Schollenberger, K. Dinbergs, Thermoplastic polyurethane elastomer molecular weight-property relations. further studies, Journal of Elastomers & Plastics 11(1) (1979) 58-91.

[48] E. Moghbelli, R. Browning, W.-J. Boo, S. Hahn, L. Feick, H.-J. Sue, Effects of molecular weight and thermal history on scratch behavior of polypropylene thin sheets, Tribology International 41(5) (2008) 425-433.

[49] T.A. Tervoort, J. Visjager, P. Smith, On abrasive wear of polyethylene, Macromolecules 35(22) (2002) 8467-8471.

[50] A.-M. Yang, T. Wu, Abrasive wear and craze breakdown in polystyrene, Journal of materials science 28(4) (1993) 955-962.

[51] Z. Lu, K. Friedrich, On sliding friction and wear of PEEK and its composites, Wear 181 (1995) 624-631.

[52] D.J. Martin, G.F. Meijs, G.M. Renwick, P.A. Gunatillake, S.J. Mccarthy, Effect of soft-segment CH2/O ratio on morphology and properties of a series of polyurethane elastomers, Journal of Applied Polymer Science 60(4) (1996) 557-571.

[53] L.T.J. Korley, B.D. Pate, E.L. Thomas, P.T. Hammond, Effect of the degree of soft and hard segment ordering on the morphology and mechanical behavior of semicrystalline segmented polyurethanes, Polymer 47(9) (2006) 3073-3082.

[54] M. Rogulska, A. Kultys, J. Lubczak, New thermoplastic polyurethane elastomers based on aliphatic–aromatic chain extenders with different content of sulfur atoms, Journal of Thermal Analysis and Calorimetry 121(1) (2015) 397-410.

[55] Y. Xu, Z. Petrovic, S. Das, G.L. Wilkes, Morphology and properties of thermoplastic polyurethanes with dangling chains in ricinoleate-based soft segments, Polymer 49(19) (2008) 4248-4258.

[56] J.W. Van Bogart, P.E. Gibson, S.L. Cooper, Structure-property relationships in polycaprolactone-polyurethanes, Journal of Polymer Science: Polymer Physics Edition 21(1) (1983) 65-95.

[57] D.J. Martin, G.F. Meijs, G.M. Renwick, S.J. Mccarthy, P.A. Gunatillake, The effect of average soft segment length on morphology and properties of a series of polyurethane elastomers. I. Characterization of the series, Journal of Applied Polymer Science 62(9) (1996) 1377-1386.

[58] S. Desai, I. Thakore, B. Sarawade, S. Devi, Effect of polyols and diisocyanates on thermo-mechanical and morphological properties of polyurethanes, European Polymer Journal 36(4) (2000) 711-725.

[59] G. Spathis, M. Niaounakis, E. Kontou, L. Apekis, P. Pissis, C. Christodoulides, Morphological changes in segmented polyurethane elastomers by varying the NCO/OH ratio, Journal of applied polymer science 54(7) (1994) 831-842.

[60] C.B. Wang, S.L. Cooper, Morphology and properties of segmented polyether polyurethaneureas, Macromolecules 16(5) (1983) 775-786.

[61] K. Madhavan, B. Reddy, Synthesis and characterization of poly (dimethylsiloxane-urethane) elastomers: Effect of hard segments of polyurethane on morphological and mechanical properties, Journal of Polymer Science Part A: Polymer Chemistry 44(9) (2006) 2980-2989.

[62] A. Eceiza, M. Martin, K. De La Caba, G. Kortaberria, N. Gabilondo, M. Corcuera, I. Mondragon, Thermoplastic polyurethane elastomers based on polycarbonate diols with different soft segment molecular weight and chemical structure: mechanical and thermal properties, Polymer Engineering & Science 48(2) (2008) 297-306.

[63] F. Grytten, H. Daiyan, M. Polanco-Loria, S. Dumoulin, Use of digital image correlation to measure large-strain tensile properties of ductile thermoplastics, Polymer Testing 28(6) (2009) 653-660.

[64] C.-F. Lee, H.-J. Sue, D.M. Fiscus, Refined fixture design for effective essential work of fracture toughness characterization of m-LLDPE thin films, Polymer Testing 32(2) (2013) 256-264.

[65] ASTM, D695-10 StandardTest Method for Compressive Properties of Rigid Plastics, ASTM International, Pennsylvania, 2010.

[66] D.Y. Wu, S. Meure, D. Solomon, Self-healing polymeric materials: a review of recent developments, Progress in Polymer Science 33(5) (2008) 479-522.

[67] Y. Chen, A.M. Kushner, G.A. Williams, Z. Guan, Multiphase design of autonomic self-healing thermoplastic elastomers, Nature chemistry 4(6) (2012) 467-472.

[68] S. Velankar, S.L. Cooper, Microphase separation and rheological properties of polyurethane melts. 2. Effect of block incompatibility on the microstructure, Macromolecules 33(2) (2000) 382-394.

[69] S. Oprea, The effect of chain extenders structure on properties of new polyurethane elastomers, Polymer bulletin 65(8) (2010) 753-766.

[70] H.D. Kim, T.J. Lee, J.H. Huh, D.J. Lee, Preparation and properties of segmented thermoplastic polyurethane elastomers with two different soft segments, Journal of applied polymer science 73(3) (1999) 345-352.

[71] A. Aneja, G.L. Wilkes, A systematic series of ‘model’PTMO based segmented polyurethanes reinvestigated using atomic force microscopy, Polymer 44(23) (2003) 7221-7228.

[72] K. Kojio, M. Furukawa, Y. Nonaka, S. Nakamura, Control of mechanical properties of thermoplastic polyurethane elastomers by restriction of crystallization of soft segment, Materials 3(12) (2010) 5097-5110.

[73] L. Morbitzer, H. Hespe, Correlations between chemical structure, stress-induced crystallization, and deformation behavior of polyurethane elastomers, Journal of Applied Polymer Science 16(10) (1972) 2697-2708.

[74] S. Liow, V. Lipik, L. Widjaja, S. Venkatraman, M. Abadie, Enhancing mechanical properties of thermoplastic polyurethane elastomers with 1, 3-trimethylene carbonate, epsilon-caprolactone and l-lactide copolymers via soft segment crystallization, eXPRESS Polym, Lett 5 (2011) 897-910.

[75] S. Rao, V. Shim, S. Quah, Dynamic mechanical properties of polyurethane elastomers using a nonmetallic Hopkinson bar, Journal of Applied Polymer Science 66(4) (1997) 619-631.

[76] M.E. Kabir, M. Saha, S. Jeelani, Effect of ultrasound sonication in carbon nanofibers/polyurethane foam composite, Materials Science and Engineering: A 459(1-2) (2007) 111-116.

[77] D.S. Huh, S.L. Cooper, Dynamic mechanical properties of polyurethane block polymers, Polymer Engineering & Science 11(5) (1971) 369-376.

[78] K. Ludema, D. Tabor, The friction and visco-elastic properties of polymeric solids, Wear 9(5) (1966) 329-348.

[79] A. Bueche, D. Flom, Surface friction and dynamic mechanical properties of polymers, Wear 2(3) (1959) 168-182.

[80] K. Grosch, The relation between the friction and visco-elastic properties of rubber, Proc. R. Soc. Lond. A 274(1356) (1963) 21-39.

[81] J.D. Liu, H.-J. Sue, Z.J. Thompson, F.S. Bates, M. Dettloff, G. Jacob, N. Verghese, H. Pham, Strain rate effect on toughening of nano-sized PEP–PEO block copolymer modified epoxy, Acta Materialia 57(9) (2009) 2691-2701.

[82] J. Huacuja-Sánchez, K. Müller, W. Possart, Water diffusion in a crosslinked polyether-based polyurethane adhesive, International Journal of Adhesion and Adhesives 66 (2016) 167-175.

[83] B. Yang, W. Huang, C. Li, L. Li, Effects of moisture on the thermomechanical properties of a polyurethane shape memory polymer, Polymer 47(4) (2006) 1348-1356.

[84] A. Boubakri, N. Haddar, K. Elleuch, Y. Bienvenu, Impact of aging conditions on mechanical properties of thermoplastic polyurethane, Materials & Design 31(9) (2010) 4194-4201.

[85] M. Shibaya, Y. Suzuki, M. Doro, H. Ishihara, N. Yoshihara, M. Enomoto, Effect of soft segment component on moisture-permeable polyurethane films, Journal of Polymer Science Part B: Polymer Physics 44(3) (2006) 573-583.

[86] F. De Candia, R. Russo, Effect of water vapour on the aging of a polyurethane elastomer, Journal of thermal analysis 30(6) (1985) 1325-1329.

[87] A. Boubakri, K. Elleuch, N. Guermazi, H. Ayedi, Investigations on hygrothermal aging of thermoplastic polyurethane material, Materials & Design 30(10) (2009) 3958-3965.

[88] S. Xiao, M.M. Hossain, P. Liu, H. Wang, F. Hu, H.-J. Sue, Scratch behavior of model polyurethane elastomers containing different soft segment types, Materials & Design 132 (2017) 419-429.

[89] A. Stalder, G. Kulik, D. Sage, L. Barbieri, P. Hoffmann, A snake-based approach to accurate determination of both contact points and contact angles, Colloids and surfaces A: physicochemical and engineering aspects 286(1-3) (2006) 92-103.

[90] C. Zhou, Bulk Preparation of Radiation Crosslinking Poly (Urethane-Imide), New Polymers for Special Applications, Intech2012.

[91] V. Thomas, M. Jayabalan, The effect of virtual cross linking on the oxidative stability and lipid uptake of aliphatic poly (urethane urea), Biomaterials 23(1) (2002) 273-282.

[92] N. Dolmaire, E. Espuche, F. Méchin, J.P. Pascault, Water transport properties of thermoplastic polyurethane films, Journal of Polymer Science Part B: Polymer Physics 42(3) (2004) 473-492.

[93] J. Barrie, A. Nunn, A. Sheer, The sorption and diffusion of water in polyurethane elastomers, Permeability of Plastic Films and Coatings, Springer1974, pp. 167-182.

[94] P. Pissis, L. Apekis, C. Christodoulides, M. Niaounakis, A. Kyritsis, J. Nedbal, Water effects in polyurethane block copolymers, Journal of Polymer Science Part B: Polymer Physics 34(9) (1996) 1529-1539.

[95] N. Schneider, L. Dusablon, L. Spano, H. Hopfenberg, F. Votta, Sorption and diffusion of water in a rubbery polyurethane, Journal of Applied Polymer Science 12(3) (1968) 527-532.

[96] A. Kanapitsas, P. Pissis, J.G. Ribelles, M.M. Pradas, E. Privalko, V. Privalko, Molecular mobility and hydration properties of segmented polyurethanes with varying structure of soft-and hard-chain segments, Journal of applied polymer science 71(8) (1999) 1209-1221.

[97] S. Mondal, J. Hu, Z. Yong, Free volume and water vapor permeability of dense segmented polyurethane membrane, Journal of Membrane Science 280(1-2) (2006) 427-432.

[98] ABAQUS, ABAQUS® Analysis User's Manual, Version 6.14, Dassault Systèmes.

[99] M. Hamdi, X. Zhang, H.-J. Sue, Fundamental understanding on scratch behavior of polymeric laminates, Wear 380 (2017) 203-216.

[100] M. Hamdi, M. Puopolo, H. Pham, H.-J. Sue, Experimental and FEM analysis of scratch behavior on polypropylene thin films: Effect of film orientation and ethylene monomer content, Tribology International 103 (2016) 412-422.

[101] H. Jiang, G. Lim, J. Reddy, J. Whitcomb, H.J. Sue, Finite element method parametric study on scratch behavior of polymers, Journal of Polymer Science Part B: Polymer Physics 45(12) (2007) 1435-1447.

[102] S. Xiao, H. Wang, F. Hu, H.-J. Sue, Effect of moisture exposure on scratch behavior of model polyurethane elastomers, Polymer 137 (2018) 209-221.

[103] K. Laux, H.-J. Sue, M. Hossain, T. Bremner, Influence of wet contact conditions on the multidirectional fretting behavior of Polyetheretherketone and composites, Polymer 108 (2017) 462-475.

[104] S. Xia, Y. Liu, L. Zhang, D. Wang, W. Zou, J. Peng, S. Cao, Tribological mechanism improving the wear resistance of polyurethane/epoxy interpenetrating polymer network via nanodiamond hybridization, Journal of Applied Polymer Science 131(10) (2014).

[105] K. Plumlee, C. Schwartz, Investigating UHMWPE wear mechanisms by decomposing wear debris distributions, Wear 271(9-10) (2011) 2208-2212.

[106] A. Wang, C. Stark, J. Dumbleton, Role of cyclic plastic deformation in the wear of UHMWPE acetabular cups, Journal of biomedical materials research 29(5) (1995) 619-626.

[107] B. Audoly, A. Boudaoud, Buckling of a stiff film bound to a compliant substrate—Part I:: Formulation, linear stability of cylindrical patterns, secondary bifurcations, Journal of the Mechanics and Physics of Solids 56(7) (2008) 2401-2421.

[108] K. Laux, A. Jean-Fulcrand, H. Sue, T. Bremner, J. Wong, The influence of surface properties on sliding contact temperature and friction for polyetheretherketone (PEEK), Polymer 103 (2016) 397-404.

[109] C. McC. Ettles, Polymer and elastomer friction in the thermal control regime, ASLE transactions 30(2) (1987) 149-159.

[110] K. Plumlee, C. Schwartz, Surface layer plastic deformation as a mechanism for UHMWPE wear, and its role in debris size, Wear 301(1-2) (2013) 257-263.

[111] A. Patnaik, M. Abdulla, A. Satapathy, S. Biswas, B.K. Satapathy, A study on a possible correlation between thermal conductivity and wear resistance of particulate filled polymer composites, Materials & Design 31(2) (2010) 837-849.

[112] M. Conte, B. Fernandez, A. Igartua, Effect of surface temperature on tribological behavior of PTFE composites, Proceedings of the Surface Effects and Contact Mechanics X, WIT press, UK (2011) 219-230.

[113] H. Düzcükoğlu, Ş. Ekinci, Ö.S. Şahin, A. Avci, M. Ekrem, M. Ünaldi, Enhancement of wear and friction characteristics of epoxy resin by multiwalled carbon nanotube and boron nitride nanoparticles, Tribology Transactions 58(4) (2015) 635-642.

[114] H. Hwang, S. Jung, K. Cho, Y. Kim, H. Jang, Tribological performance of brake friction materials containing carbon nanotubes, Wear 268(3-4) (2010) 519-525.

[115] B.K. Goriparthi, K. Suman, N.M. Rao, Effect of fiber surface treatments on mechanical and abrasive wear performance of polylactide/jute composites, Composites Part A: Applied Science and Manufacturing 43(10) (2012) 1800-1808.

[116] L. Mu, Y. Shi, X. Feng, J. Zhu, X. Lu, The effect of thermal conductivity and friction coefficient on the contact temperature of polyimide composites: Experimental and finite element simulation, Tribology International 53 (2012) 45-52.

[117] J. Karger-Kocsis, A. Mousa, Z. Major, N. Békési, Dry friction and sliding wear of EPDM rubbers against steel as a function of carbon black content, Wear 264(3-4) (2008) 359-367.

[118] M. Omar, A. Atkins, J. Lancaster, The role of crack resistance parameters in polymer wear, Journal of Physics D: Applied Physics 19(2) (1986) 177.

[119] A. Chateauminois, B. Briscoe, Nano-rheological properties of polymeric third bodies generated within fretting contacts, Surface and Coatings Technology 163 (2003) 435-443.

[120] A. Krichen, C. Bradai, A. Chateauminois, M. Kharrat, Surface damage of poly (methylmethacrylate) under fretting loading, Wear 230(2) (1999) 146-155.

[121] Q. Guo, W. Luo, Mechanisms of fretting wear resistance in terms of material structures for unfilled engineering polymers, Wear 249(10-11) (2001) 924-931.

[122] I. Clemitson, Castable polyurethane elastomers, CRC Press2008.

[123] J. Chrisman, S. Xiao, M. Hamdi, H. Pham, M.J. Mullins, H.-J. Sue, Testing and evaluation of mar visibility resistance for polymer films, Polymer Testing 69 (2018) 238-244.

[124] S. Xiao, K. Laux, H. Wang, F. Hu, H.-J. Sue, Physical Correlation between Abrasive Wear Performance and Scratch Resistance in Model Polyurethane Elastomers, Wear (2018) Under Review.

[125] R. Zdrahala, S. Hager, R. Gerkin, F. Critchfield, Polyether Based Thermoplastic Polyurethanes Effect of the Soft Segment Molecular Weight, Journal of Elastomers & Plastics 12(4) (1980) 225-244.

[126] Z. Ma, Y. Hong, D.M. Nelson, J.E. Pichamuthu, C.E. Leeson, W.R. Wagner, Biodegradable polyurethane ureas with variable polyester or polycarbonate soft segments: Effects of crystallinity, molecular weight, and composition on mechanical properties, Biomacromolecules 12(9) (2011) 3265-3274.

[127] A.M. Castagna, A. Pangon, T. Choi, G.P. Dillon, J. Runt, The role of soft segment molecular weight on microphase separation and dynamics of bulk polymerized polyureas, Macromolecules 45(20) (2012) 8438-8444.

[128] N. Liu, Y. Zhao, M. Kang, J. Wang, X. Wang, Y. Feng, N. Yin, Q. Li, The effects of the molecular weight and structure of polycarbonatediols on the properties of waterborne polyurethanes, Progress in Organic Coatings 82 (2015) 46-56.

[129] ASTM, D1238-13 Standard Test Method for Melt Flow Rates of Thermoplastics by Extrusion Plastometer, ASTM International, Pennsylvania, 2013.

[130] G. Vasquez, C. Majewski, B. Haworth, N. Hopkinson, A targeted material selection process for polymers in laser sintering, Additive Manufacturing 1 (2014) 127-138.

[131] ASTM, D1708-13 Standard Test Method for Tensile Properties of Plastics by Use of Microtensile Specimens, ASTM International, Pennsylvania, 2013.

[132] B. Pittenger, N. Erina, C. Su, Application Note #128 Quantitative Mechanical Property Mapping at the Nanoscale with PeakForce QNM, Bruker Corporation (2012).

[133] P. Schön, K. Bagdi, K. Molnár, P. Markus, B. Pukánszky, G.J. Vancso, Quantitative mapping of elastic moduli at the nanoscale in phase separated polyurethanes by AFM, European Polymer Journal 47(4) (2011) 692-698.

[134] R.F. Landel, L.E. Nielsen, Mechanical properties of polymers and composites, CRC press1993.

[135] B. Bersted, Entanglement network model relating tensile impact strength and the ductile-brittle transition to molecular structure in amorphous polymers, Journal of Applied Polymer Science 24(1) (1979) 37-50.

[136] S.P. Ho, P.F. Joseph, M.J. Drews, T. Boland, M. LaBerge, Experimental and numerical modeling of variable friction between nanoregions in conventional and crosslinked UHMWPE, Journal of biomechanical engineering 126(1) (2004) 111-119.

[137] J. Li, H. Liao, C. Coddet, Friction and wear behavior of flame-sprayed PEEK coatings, Wear 252(9-10) (2002) 824-831.

[138] K.K. Karuppiah, A.L. Bruck, S. Sundararajan, J. Wang, Z. Lin, Z.-H. Xu, X. Li, Friction and wear behavior of ultra-high molecular weight polyethylene as a function of polymer crystallinity, Acta Biomaterialia 4(5) (2008) 1401-1410.

[139] G. Hamilton, L. Goodman, The stress field created by a circular sliding contact, Journal of Applied Mechanics 33(2) (1966) 371-376.

[140] G.M. Hamilton, Explicit equations for the stresses beneath a sliding spherical contact, Proceedings of the Institution of Mechanical Engineers, Part C: Journal of Mechanical Engineering Science 197(1) (1983) 53-59.

[141] W.J. Boo, L. Sun, J. Liu, E. Moghbelli, A. Clearfield, H.J. Sue, H. Pham, N. Verghese, Effect of nanoplatelet dispersion on mechanical behavior of polymer nanocomposites, Journal of Polymer Science Part B: Polymer Physics 45(12) (2007) 1459-1469.